

Integral pumping tests for the characterization of groundwater contamination

Dissertation

zur Erlangung des Grades eines Doktors der Naturwissenschaften

der Geowissenschaftlichen Fakultät der
Eberhard-Karls-Universität Tübingen

vorgelegt von
Martí Bayer-Raich
aus Barcelona

2004

Tag der mündlichen Prüfung: 29. Oktober 2004

Dekan: Prof. Klaus G. Nickel, Ph.D.

1. Berichterstatter: Dr. Thomas Ptak

2. Berichterstatter: Dr. Rudolf Liedl

Summary

Where cities are located above productive aquifers and are far from surface water supplies, groundwater is usually the primary freshwater source. However, groundwater pollution in industrialized sites is a general problem in a variety of European cities. Most of them are located at river basins and use groundwater for water supply from local aquifer systems. The investigation of groundwater contamination, given the relative inaccessibility of the subsurface, is typically restricted by the number of monitoring wells and therefore detailed characterization, using conventional approaches, is economically not feasible at many sites.

A new integral approach for the investigation of groundwater contamination has been recently developed at the Center of Applied Geosciences, University of Tübingen. Using this integral approach, the concentration in a pumping well is measured as a function of time. This procedure increases the sampling volume and reduces the effect of small scale variability that may bias point measurements. This method is therefore capable of reaching the aquifer volume located between monitoring wells, avoiding the risk of missing narrow contaminant plumes. Average concentrations and total mass flow rates are obtained through an inversion procedure, providing reliable estimates of water quality and source strength, respectively.

This thesis is entirely focused on the development and application of analytical and numerical tools for the inversion of data obtained through integral pumping tests. A derivation of the fundamental equation, partially based on previous results, is provided here and generalized to account for advective transport and linear retardation within 3D heterogeneous aquifers. Both existing analytical and numerical approaches have been further developed, tested and applied to a wide range of field scale conditions. Within the analytical approach, the existing solutions have been generalized to fully account for the groundwater velocity, i. e. without assuming perfect radial flow during pumping. Additionally, the integral approach is further analysed through the classical theory of integral equations by means of Abel's integral transform providing a new closed-form solution. The novel results are then compared, yielding a general methodology for dimensioning the optimal pumping duration. Within the numerical framework, less restrictive conditions are considered (e. g. heterogeneous aquifers, multiple-well pumping tests). A new numerical algorithm (an updated version of the original code C1, extensively rewritten) is developed, implemented (in the code CSTREAM), tested and applied to real data. A number of field-scale applications have been evaluated, in cooperation with our partners in the projects SAFIRA and INCORE yielding consistent results. Within the project SAFIRA, the integral approach is applied for the first time to a multi-layer aquifer system. In a more theoretical framework, CSTREAM is also used to quantify the effects of heterogeneity and variability of boundary conditions.

The results of this Thesis show that this approach has a great potential within both applied framework for evaluation and investigation of real contaminated aquifers and theoretical or basic research to further develop conceptual models for the evaluation of concentration-time data obtained in pumping wells.

Zusammenfassung

Städte, die keinen unmittelbaren Zugang zu oberflächigen Wasserreservoirs haben, decken häufig einen erheblichen Teil ihres Bedarfs an Trink- und Gebrauchswasser mit Grundwasser, das lokal von meist ergiebigen Aquiferen gefördert wird. Ein typisches Problem an urbanen industriellen Standorten in Europa bilden jedoch Verunreinigungen im Grundwasser. Davon sind besonders oberflächennahe Aquifere betroffen, die vorrangig für die Wassergewinnung in Frage kommen. Die Untersuchung von Grundwasserverunreinigungen erfolgt wegen der Unzugänglichkeit des gesamten Untergrunds konventionell nur grob über lokale Messungen an wenigen Überwachungsbrunnen. Detaillierte Untersuchungen allein mithilfe von Punktmessungen sind an vielen Standorten ökonomisch oder technisch nicht durchführbar. Als Alternative zur gängigen punktuellen Probennahme wurde vor kurzem am Zentrum für Angewandte Geowissenschaften (ZAG) der Universität Tübingen ein neues integrales Verfahren entwickelt. Dabei wird an einem Brunnen kurze Zeit Grundwasser gefördert und währenddessen die Veränderung der Schadstoffkonzentration über die Zeit gemessen. Verglichen mit Punktmessungen beprobt man mit diesem Verfahren ein deutlich größeres Volumen des Untergrunds. Zudem verliert die kleinmaßstäbliche Variabilität von Schadstoffkonzentrationen, die an Punktmessungen schwer zu interpretieren ist, durch die räumliche Betrachtung an Bedeutung. Während bei ausschließlich punktuellen Messungen Schadstofffahnen bei grobem Beprobungsraaster leicht übersehen werden können, werden nun auch kleinräumliche Schadstoffausdehnungen im Untergrund erreicht.

Bei der integralen Probenahme erhält man über ein Inversionsverfahren Durchschnittskonzentrationen und Massenflussraten. Sowohl Wasserqualität als auch Schadstoff-Quellstärke lassen sich verlässlich abschätzen. Die vorliegende Dissertation widmet sich der Entwicklung und Anwendung analytischer und numerischer Werkzeuge für die Invertierung der durch die integrale Probenahme gewonnenen Daten. Der hierzu grundlegende Algorithmus wird erläutert und zur Anwendung auf advektiven Transport unter Berücksichtigung von Schadstoffretardation in dreidimensionalen heterogenen Aquiferen umformuliert. Sowohl bestehende analytische als auch numerische Ansätze werden weiterentwickelt und in einer Reihe von Untersuchungen unter Feldbedingungen getestet. Das analytische Lösungsverfahren wird zur Berücksichtigung von Hintergrundströmung erweitert. Zusätzlich wird mithilfe der Integraltransformation nach Abel eine neue Lösung in geschlossener Form ermittelt. Die neuentwickelten analytischen Lösungen werden gegenübergestellt und liefern zusammen eine allgemeine Methodik zur Abschätzung der optimalen Pumpdauer beim Pumpversuch.

Für das numerischen Verfahren werden weniger restriktive (Rand-)Bedingungen angenommen, so zum Beispiel ein heterogener Grundwasserleiter und Pumptests mit mehreren Brunnen. Ausgehend von dem numerischen Verfahren im bisher bestehenden Programm „C1“ wurde ein neuer Algorithmus entwickelt, dieser als Software implementiert („CSTREAM“) und getestet. Die Anwendung des Programms auf Felddaten aus einer Reihe von Anwendungen zeigte Konsistenz mit den bisherigen Ergebnissen von Projektpartnern (SAFIRA, INCORE). Innerhalb des SAFIRA-Projektes wurde der integrale Ansatz erstmals auf einen mehrschichtigen Aquifer angewandt. Schließlich dienten theoretische Studien mit CSTREAM zu Sensitivitätsanalysen der Ergebnisse bei variabler Aquiferheterogenität und veränderlichen Randbedingungen. Die Ergebnisse deuten auf eine breite Anwendbarkeit der entwickelten Verfahren hin, sowohl zum Feldeinsatz als auch zur Grundlagenforschung konzeptioneller Modelle für die Bewertung zeitlich variabler Konzentrationen, die bei Pumptests gemessen werden.

1. INTRODUCTION

1.1 Motivation	1
1.2 Objective	1
1.3 Structure	2

2. THE INTEGRAL GROUNDWATER INVESTIGATION APPROACH

2.1. Relationship to previous work	3
2.2. Governing equations	5
2.2.1. Contaminant mass flow rate across a control plane	5
2.2.2. Mass flux integral equation	7
2.2.3. Mathematical statement of the inversion problem: Analytical and numerical approaches	9
2.2.4. Accounting for linear retardation: a simplified formulation	11
2.3 Numerical simulation and discussion of methodology	11
2.3.1. Forward simulation: plume development and integral pumping tests	11
2.3.2. Inverse problem: Analytical and numerical approaches	13

3. ANALYTICAL APPROACH FOR HOMOGENEOUS AQUIFERS

3.1. Introduction	16
3.2. Problem formulation for homogeneous aquifers: Volterra integral equation	16
3.3. Solution for the Volterra integral equation by numerical integration	19
3.3.1. Discrete solution	
3.3.2. Numerical implementation in CSTREAM.	20
3.4. Approximate solution: Abel's integral transform	24
3.4.1. Problem formulation: simplifying assumptions	24
3.4.2. Discrete solution, Schwarz et. al. (1998)	26
3.4.3. Continuous solution: Abel's transform	27
3.5. Verification and comparison of approaches	29
3.5.1 A trivial case: $C_w(t) = C_{plume}$	29
3.5.2 Simple plumes	31

3.5.3	Applicability of the simplified approach	35
3.6	Applicability in heterogeneous aquifers: effective parameters of the equivalent homogeneous aquifer	36
3.6.1.	Plume development in heterogeneous conditions and integral pumping tests	36
3.6.2.	Effective parameters of the equivalent homogeneous aquifer	37
3.6.3.	Mass flow rate estimates	39
3.7	Depth differentiated vs. depth integrated approaches	40
3.7.1.	Numerical model and forward simulations	40
3.7.2.	Depth integrated approach	42
3.7.3.	Depth differentiated approach	43
3.7.4.	Comparison of depth differentiated and integrated approaches	44
3.8.	Dimensioning of integral pumping tests	45
3.8.1.	Analytical solution for indefinitely long pumping tests	45
3.8.1.1.	Average concentration	45
3.8.1.2.	Mass flow rate	47
3.8.2.	Simple analytical solutions versus exact solution	48
3.8.3	Analytical expressions versus field test conditions	
3.8.4.	Dimensioning the duration of integral pumping tests	50
4.	NUMERICAL APPROACH FOR HETEROGENEOUS AQUIFERS	
4.1.	Groundwater modeling with MODFLOW and MODPATH	52
4.2.	Code CSTREAM	52
4.2.1.	History of the code: code C1	54
4.2.2.	Initialization	54
4.2.3.	Isochrone definition	56
4.2.4.	Streamtube definition	59
4.2.5.	Concentration inversion	63
4.2.6.	Mass flow rate integration	65
4.3.	2D verification in homogeneous media	66
4.3.1.	Verification for short pumping tests	66
4.3.2.	Verification for long pumping tests	69
4.4.	2D verification in heterogeneous media	72
4.4.1.	Verification through a Multigaussian K-field	72

4.4.2. Neckar Valley model, high variance: the new flow weighted averaged approach.	74
4.4.3. Bitterfeld, multi-layered approach	78
4.5. Application example: Depth integrated application in the Neckar valley in Stuttgart (Germany): Quantifying model uncertainties	81
4.5.1. Direct integral measurement predictions: left-right uncertainty	82
4.5.2. Complex integral measurement predictions: model uncertainty and possible source locations	83
4.5.3. Results of site application, analyses of real IPT	84
4.6. Application example: Depth integrated application in Linz (Austria)	87
4.6.1. Performance of the integral pumping tests	87
4.6.2. Interpretation of the integral pumping tests	89
4.7. Application example: Depth differentiated application in Bitterfeld (Germany).	93
4.7.1. Update and model cut of the regional SAFIRA MODFLOW model	93
4.7.2. Numerical evaluation of the integral pump tests	96

5. SUMMARY AND CONCLUSIONS

5.1. Integral approach, integral equation	103
5.2. Analytical solutions: averaging measured data and dimensioning integral pumping tests.	104
5.3. Numerical algorithm: CSTREAM	105
References	107

List of symbols:

∇	Nabla operator
$b(x, y)$ [L]	Saturated thickness of the aquifer layer
$C_0(x, y, z)$ [M L ⁻³]	Initial concentration distribution before pumping
$\bar{C}_0(x)$ [M L ⁻³]	Initial concentration distribution, left-right arithmetic average
$C_w(t)$ [M L ⁻³]	Time-dependant concentration measured at the pumping well
$\vec{j}(x, y, z)$ [M T ⁻¹ L ⁻²]	Contaminant mass flux
$K(x, y, z)$ [L T ⁻¹]	Hydraulic conductivity
ℓ_{CP}	Length of the control plane (width of the capture zone)
ℓ_{CPm}	Width of the capture zone considering linear retardation R_m
$\ell_I(t)$	Isochrone length assuming 2D-flow fields
$\ell^+_I(t)$	The half of the isochrone $\ell_I(t)$ located at $x > 0$
$\ell_Y(x, t)$ [L]	Distance separating upstream and downstream intersections of the isochrone and a straight line at x parallel to the y axis.
M_{CP} [M T ⁻¹]	Mass flow rate across the control plane
\vec{n}	Outward unit normal vector.
$n_e(x, y, z)$	Effective porosity
Q [L ³ T ⁻¹]	Pumping rate
$\vec{q}_0(x, y, z)$ [L T ⁻¹]	Initial Darcy's flow field before pumping
$\vec{q}_w(x, y, z)$ [L T ⁻¹]	Convergent Darcy's flow field during pumping
R_m [-]	Linear retardation, $R_m = 1$ indicates advective transport
$R(t)$	Half of the width of capture zone volume at time t
$r(t)$	Radius of the well capture zone (assuming perfect radial flow)
$r_m(t)$	Radius of the "contaminant mass capture zone" considering R_m
S_{CP}	Lateral surface of the control plane
$S_I(t)$	Lateral surface of the isochrone
t [T]	Pumping time, $t = 0$ is the beginning of the pumping test

t_D [-]	Dimensionless pumping time
$\bar{v}_w(x, y, z)$ [L T ⁻¹]	Particle velocity during pumping
$V_I(t)$	Volume of the well capture zone at time t
$V_R(t)$	Initial location of the volume of the <i>contaminant</i> mass captured at the pumping well up to time t
x, y [L]	Cartesian spatial coordinates
x_D, y_D [-]	Cartesian spatial dimensionless coordinates

Chapter 1

INTRODUCTION

This thesis is entirely focused on the Integral Approach (IA) (Teutsch et al., 2000; Ptak et al., 2000; Schwarz, 2002), a new approach for cost-effective reliable investigation of groundwater contamination.

1.1. Motivation

The rapid shift of populations to urban areas is causing great demands on groundwater resources, particularly in the developing world. Where cities are located above productive aquifers and are far from surface water supplies, groundwater is usually the primary freshwater source (United Nations Environment Programme, 2002)

The UN have expressed their concern about three principal gaps in groundwater management, which have enormous implications for sustainable development (International Water and Sanitation Centre, 2003). These are:

-The accelerated degradation of groundwater systems, through pollution of aquifers.

-The lack of both professional and public awareness about the sustainable use and economic importance of groundwater resources generally.

-The economic implications of not resolving groundwater demand and supply management.

In particular, groundwater pollution in industrialized sites is a general problem in a variety of European cities. Most of them

are located in river basins and use groundwater for water supply from local aquifer systems. Within the last decades changes in land use and ownership have resulted in complex contamination patterns, such as heterogeneous distribution of contaminants, different contaminants and large subsurface areas. Industrial development and the need for groundwater conservation are in acute conflict (INCORE, **IN**tegrated **CO**ncept for Groundwater **RE**mediation, 5th Framework Programme of the European Community for Research, Technological Development and Demonstration activities)

1.2. Objectives

The major objective of this thesis is to further extend the concepts originally developed in Teutsch et al. (2000), Ptak et al. (2000) and Schwarz (2002), for systematical application of the Integral Approach under a variety of field scale conditions, using both analytical and numerical approaches. Specifically, three objectives are addressed within this thesis:

1- Provide a formal derivation of the governing equations describing the Integral Approach, extending the results given in (Teutsch et al., 2000; Ptak et al., 2000; Schwarz, 2002).

2- Develop an analytical solution to fully account for the natural groundwater flow, by coupling the integral approach with the formulation given by Bear & Jacobs (1965).

3- Test and develop the numerical algorithm originally described in Ptak et al. (2000) and Schwarz (2002) for application in highly heterogeneous environments and additionally in multi-layered systems.

1.3 Structure

This thesis describes the Integral Approach, from a conceptual model to site-specific field-scale applications at contaminated sites. The basics of the Integral Approach are described in chapter 2, providing a derivation of the fundamental equations, extending the results given in Teutsch et al. (2000); Ptak et al. (2000) and Schwarz (2002). First, in section 2.1, a description of the previous work is given. In Section 2.2 the mathematical derivation of the fundamental equation is presented and finally, section 2.3 gives a discussion on the methodology employed in the Integral Approach, by using a numerically simulated example of an Integral Pumping Test (IPT) in a virtual aquifer.

Chapter 3 describes the analytical solutions for the basic equations. Two novel solutions are presented and compared to the results given in previous work.

In sections 3.1 and 3.2 the basic equations are particularized for the case of homogeneous media expressing Volterra integral equations of the first type and the basic assumptions of the analytical approach are presented. In section 3.3, a new analytical solution (following ideas of Bear & Jacobs, 1965) is derived, giving also a detailed algorithm for performing the numerical integration. Section 3.4 gives a new *non-recursive* approximate solution derived through Abel's integral transform. Both solutions are compared in section 3.5, and the range of validity of the approximate solution is established.

Sections 3.6 and 3.7 discuss how to apply the analytical approach in 2D-heterogeneous aquifers and in multi-

layered systems, respectively. Verification examples developed through numerical simulations are described to test the accuracy of the solutions presented in sections 3.3 and 3.4. Finally, section 3.8 further analyses the analytical solutions for investigating the issue of dimensioning IPT. A methodology for dimensioning pumping durations and distances between wells is given, based on data from IPTs already conducted within the projects SAFIRA (**S**Anierungs**F**orschung **I**n **R**egional kontaminierten **A**quiferen, framework of the German Ministry of Education and Science, BMBF), and INCORE (**I**Ntegrated **C**Oncept for Groundwater **R**emediation, 5th Framework Programme of the European Community for Research, Technological Development and Demonstration activities).

Chapter 4 describes the numerical algorithm implemented in the code CSTREAM, and gives test verification examples as well as real field scale applications developed in the context of this thesis and within the framework of the projects SAFIRA and INCORE.

Section 4.1 gives a brief description of the codes MODFLOW (McDonald & Harbaugh, 1988) and MODPATH (Pollock, 1994), used within the numerical inversion algorithm CSTREAM. In section 4.2, a detailed description of the algorithm is given, including all steps of the computation: streamtube discretization, isochrone definition, concentration inversion and mass flow rate integration. In Sections 4.3 and 4.4 provide verification test examples, in homogeneous and heterogeneous aquifers, respectively. Finally the last three sections describe application examples developed in cooperation with partners in the SAFIRA and INCORE projects.

In chapter 5, the conclusions of this research are presented, as well as a discussion of possible lines of future work.

Chapter 2

THE INTEGRAL GROUNDWATER INVESTIGATION APPROACH

The integral groundwater investigation approach (IGIA) provides a new methodology to quantify the impact of groundwater contamination based on sampling large volumes of groundwater through integral pumping tests. The IGIA, was originally developed by Teutsch et al. (2000), Ptak et al. (2000) and Schwarz (2002). After the first field demonstration application in the Rhine Valley (Schwarz et al., 1997) the IGIA has been applied to several sites, both before (e.g. Schwarz et al., 1998; Holder et al., 1998; Bockelmann et al., 2001) and during the framework of this thesis (e. g. Bayer-Raich et al., 2001; Jarsjö et al., 2002; Bauer et al., 2002). This chapter explains the basis of the IGIA providing a detailed derivation of the governing equations and discussing the methodology through a numerically simulated synthetic example.

2.1. Relationship to previous work

Groundwater risk assessment is generally performed on the basis of point-scale contaminant concentration measurements. Recent protocols however (LfU, 1996; EPA OSWER Directive, 1999) propose to quantify the impact of a source through the contaminant mass flow rate (i. e. contaminant mass leaving the source zone per unit of time) rather than the contaminant concentration. It has been shown through a field scale experiment with DNAPL that narrow plumes might be easily missed or poorly delineated by conventional groundwater monitoring well spacing (Rivett et al., 2001). The goal of the IGIA is to capture the total contaminant mass flow rate across a given control plane without the requirement of regionalising point concentration measurements (Teutsch et al., 2000).

Figure 2.1 illustrates the problem of source zone characterization within a heterogeneous aquifer environment. It is assumed that the exact position of the “hot spot” cannot be identified *a priori*. Consequently, the plume position and extent cannot be identified with sufficient certainty using groundwater samples from a few unpumped monitoring wells or point measurements (Holder et al., 1998).

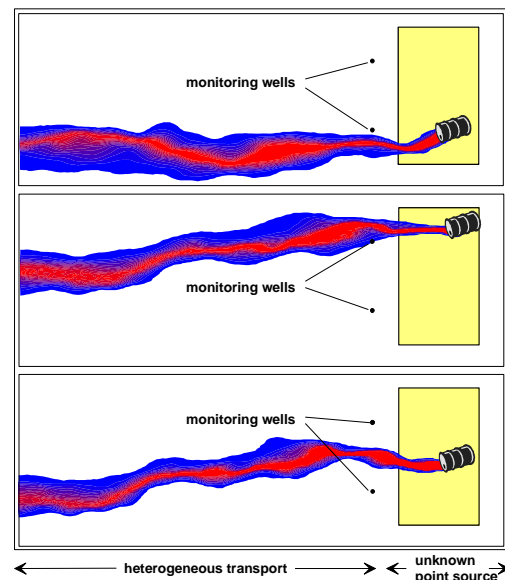


Figure 2.1: Concentration distribution in a heterogeneous aquifer with random position of the “hot spot” (Holder et al., 1998).

When using the IGIA, one or more pumping wells are installed along a control plane perpendicular to the mean groundwater flow direction and operated simultaneously or sequentially. Well positions, pumping rates, and pumping times are optimised to allow the well capture zones to cover the entire groundwater flow downstream of the (potentially) contaminated site. During well operation, concentrations of target

substances are measured as a function of time in the discharge of each of the pumping wells. Four typical contaminant scenarios are displayed in Figure 2.2 showing the concentration–time series at a pumping well and the interpreted subsurface plume location (Holder & Teutsch, 1999).

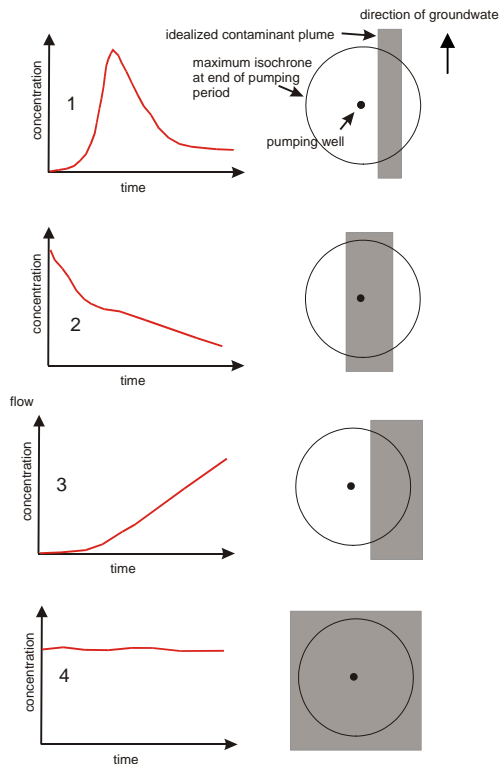


Figure 2.2: Four characteristic plume scenarios together with the expected concentration – time series (Holder & Teutsch, 1999).

The interpretation (or inversion) of the concentration-time signal obtained at the pumping well can be performed using an analytical solution (for homogeneous aquifers) or a numerical algorithm based on particle back-tracking (considering heterogeneity through a numerical groundwater model). Both analytical and numerical approaches were proposed in Teutsch et al. (2000) and Ptak et al. (2000). The development of the analytical solution

and the numerical implementation of the particle tracking algorithm were described in Schwarz et al. (1998) and have been expanded in the framework of this thesis as will be shown in chapters 3 and 4 respectively.

The analytical approach, described in detail in chapter 3, is based on a discrete formula derived for (1) homogeneous and confined aquifers, (2) perfect radial flow during the pumping test, and (3) no gradient of concentration in the flow direction within the capture zone (Schwarz et al., 1998). This solution has been applied at several sites, e. g. the Neckar Valley in Stuttgart by Holder et al. (1998) and Bockelmann et al. (2001). A new solution that does not require assumption (2) will be given in chapter 3.

The numerical approach, described in chapter 4, is based on the geometrical definition of streamlines and isochrones with particle tracking through the potentially heterogeneous model domain. In this case, assumptions (1) and (2) are not necessary, as opposed to the analytical approach, but (3) (i. e. the absence of concentration gradient along the flow direction) is still required. The basics of the numerical inversion were given in Ptak et al. (2000) and implemented in a C++ code called C1 (Schwarz, 2002). The numerical approach was evaluated at the well instrumented demonstration site of the Landesanstalt für Umweltschutz (LfU) – the state environmental protection agency – in Eppelheim (Baden Württemberg, Germany) by Schwarz et al. (1997). The existing code C1 was verified, modified and expanded in a new C++ code: CSTREAM, enabling the interpretation of integral pumping tests in highly heterogeneous environments and multi-layered aquifers.

2.2. Governing equations

The basic equations necessary for the formulation of the integral groundwater investigation approach are derived in this section. The expressions given in chapter 2 of Schwarz (2002) for perfect radial flow are generalized for heterogeneous conditions. These general equations are solved analytically in chapter 3 (for the particular case of homogeneous media) and numerically in chapter 4 (for the general case of heterogeneous aquifers).

2.2.1. Contaminant mass flow rate across a control plane

A variable of interest for characterizing the impact of a source zone or for quantifying natural attenuation is the mass flow rate across a given control plane M_{CP} [$M T^{-1}$].

When only one control plane is used, the mass flow rate gives the total contaminant mass passing the control plane per unit of time (source strength). When more than one control plane is used, the differences in mass flow rates let us quantify the occurrence of Natural Attenuation (e.g. the Neckar Valley study performed in Bockelmann et al., 2001, where two control planes at 140 m and 280 m downstream of the source were used). Figure 2.3 illustrates the problem of plume characterization through mass flow rate.

The mass flow rate may be obtained by integrating the contaminant mass flux \vec{j} [$M T^{-1} L^{-2}$] over the surface area of a control plane. The initial concentration distribution $C_0 = C_0(x, y, z)$ [$M L^{-3}$] in combination with the Darcian flow field $\vec{q}_0 = \vec{q}_0(x, y, z)$ [$L^3 T^{-1}$] (fixed by the regional boundary conditions and the heterogeneous transmissivity field) give the contaminant mass flux $\vec{j}_0 = C_0 \vec{q}_0$ [$M T^{-1} L^{-2}$].

Setting the y -coordinate parallel to the mean flow direction and defining the control plane by $y=0$, we get

$$M_{CP} = \int_{S_{CP}} C_0(x, 0, z) \vec{q}_0(x, 0, z) \cdot \vec{n} dS \quad (2.1)$$

with S_{CP} being the surface of the control plane, and \vec{n} the unit vector perpendicular to the control plane (i. e. parallel to the y -axis).

In 2D problems or multilayered aquifers where the vertical components of the flow velocities may be neglected, equation (2.1) may be formulated as

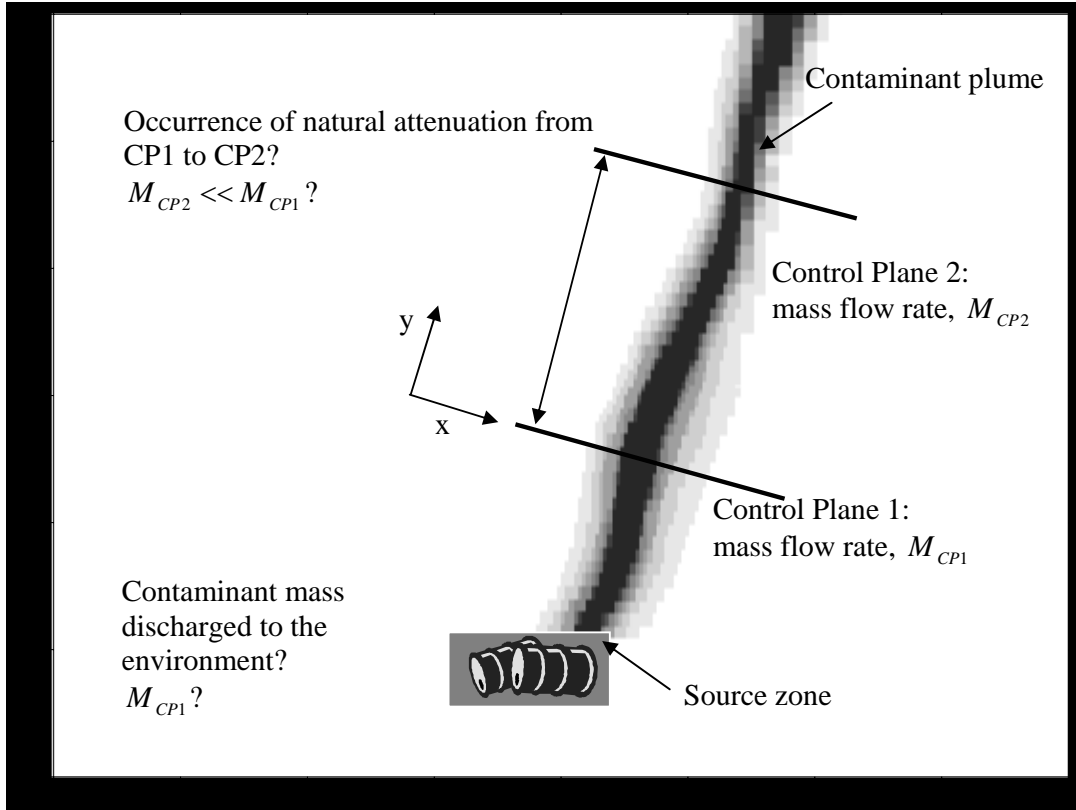
$$M_{CP} = \int_{l_{CP}} C_0(x, 0) q_{0y}(x, 0) b(x, 0) dx \quad (2.2)$$

where $b(x, y)$ [L] is the saturated thickness of the aquifer, and $q_{0y}(x, y)$ [$L T^{-1}$] is the y component of the Darcy velocity.

In general, the mass flow rate is time dependant if \vec{q}_0 or C_0 depend on time. However, if the initial concentration C_0 is the solution of the transport equation under steady-state flow conditions \vec{q}_0 (and the contaminant plume had sufficient time to develop), then both C_0 and M_{CP} become independent of time (steady-state plumes).

If dispersion and degradation are small in the vicinity of the control plane (advection dominated transport), C_0 also satisfies the condition $\vec{q}_0 \cdot \vec{\nabla} C_0 = 0$ (i. e., the concentration is constant along a streamline).

[m]



[m]

Figure 2.3: Plume characterization through the mass flow rate.

2.2.2. Mass Flux Integral Equation

The main goal of the IGIA is to obtain information on the spatial variability of the initial concentration distribution $C_0(x, y, z)$ through the temporal variability of concentrations at the pumping well $C_w(t)$.

The integral pumping test (operating at constant rate Q [$L^3 T^{-1}$]) temporarily changes the (steady-state) natural flow conditions leading to a transient convergent flow towards the pumping well. In confined aquifers, neglecting elastic storativity, the time-dependent concentration $C_w(t)$ measured at the

pumping well is related to the initial spatial concentration distribution $C_0(x, y, z)$ through the integral equation:

$$Q C_w(t) = - \oint_{S_I(t)} C_0(x, y, z) \vec{q}_w(x, y, z) \cdot \vec{n} dS \quad (2.3)$$

where integration is along the lateral surface of the isochrone $S_I(t)$ (i. e. the boundary of the capture zone at time t), $Q = - \oint_{S_I(t)} \vec{q}_w(x, y, z) \cdot \vec{n} dS$ is the pumping rate and \vec{n} is the outward unit normal vector. Equation (2.3) expresses a Volterra Integral Equation.

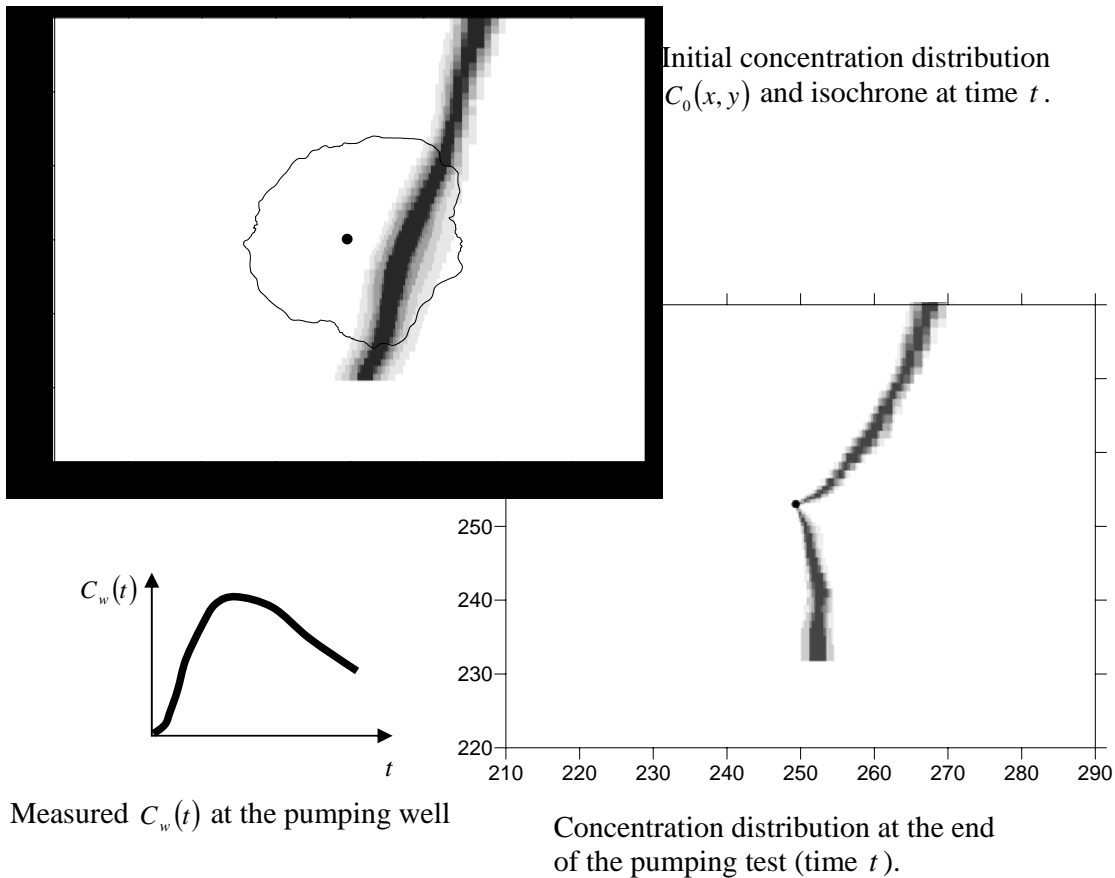


Figure 2.4: Concentration distribution before, and at the end of, an integral pumping test

In 2D problems or multilayered aquifers where the vertical components of the flow velocities may be neglected, equation (2.3) may be formulated as:

$$Q C_w(t) = - \oint_{\ell_i(t)} C_0(x, y) \bar{q}_w(x, y) \cdot \bar{n} b(x, y) d\ell \quad (2.4)$$

where integration is along the isochrone length $\ell_i(t)$. Equation (2.4) may be further simplified under the assumption of homogeneous conditions and radially convergent flow (equation 2.18 in Schwarz, 2002).

To prove equation (2.3), let m [M] be the total mass of contaminant discharged at the well up to time t (pumping test started at $t = 0$), which may be expressed as:

$$m = Q \int_0^t C_w(\tau) d\tau \quad (2.5)$$

On the other hand, m can be also computed as

$$m = \int_{V_i(t)} C_0(x, y, z) n_e(x, y, z) dV \quad (2.6)$$

which is the total mass of contaminant located within the capture zone volume $V_i(t)$ limited by the surface $S_i(t)$. $n_e(x, y, z) = n_e$ is the effective porosity. Equalling the right-hand sides of the above relationships and differentiating with respect to time, we get

$$\begin{aligned} \frac{\partial m}{\partial t} &= Q C_w(t) = \\ &= \frac{\partial}{\partial t} \int_{V_i(t)} C_0(x, y, z) n_e(x, y, z) dV = \\ &= - \oint_{S_i(t)} C_0(x, y, z) n_e(x, y, z) \bar{v}_w(x, y, z) \cdot \bar{n} dS + \\ &+ \int_{V_i(t)} \frac{\partial}{\partial t} [C_0(x, y, z) n_e(x, y, z)] dV \end{aligned} \quad (2.7)$$

where $\bar{v}_w(x, y, z)$ is the particle velocity during pumping at location (x, y, z) (independent of time if elastic storativity is neglected) ds is the surface boundary of the capture zone and \bar{n} is the outward unit normal vector. In this step we have used the general conservation law (also known as the Reynolds Transport Theorem, e.g. equation 1.11 Kolditz, 2002) particularized for the capture zone volume $V_i(t)$.

Since both $C_0(x, y, z)$ and $n_e(x, y, z)$ are independent of time, the last integral in (2.7) is zero, and using $\bar{q}_w = n_e \bar{v}_w$ we get (2.3).

It should be noted that (2.3) gives a relationship between “the concentration distribution *before* the pumping test started: $C_0(x, y, z)$ ” and “the concentration observed *during* the pumping test $C_w(t)$ ”. As indicated in Figure 2.4, the concentration distribution at the end of the pumping test will generally be different from the initial concentration $C_0(x, y, z)$.

However, under the same steady-state boundary conditions, the concentration distribution will lead to the same steady-state solution and, eventually, $C_0(x, y, z)$ will be reached again.

2.2.3. Mathematical statement of the inversion problem: Analytical and numerical approaches

The interpretation (or inversion) of an integral pumping test may be formulated as:

We seek the mass flow rate M_{CP} [M T⁻¹] across the control plane ℓ_{CP} , given the equations

$$\begin{cases} M_{CP} = \int_{\ell_{CP}} C_0(x,0) q_{0y}(x,0) b(x,0) dx \\ Q C_w(t) = - \oint_{\ell_I(t)} C_0(x,y) \bar{q}_w(x,y) \cdot \bar{n} b(x,y) d\ell \end{cases} \quad (2.8)$$

where

$\bar{q}_0(x,y)$ [L T⁻¹] is the Darcy flow field under natural conditions

$b(x,y)$ [L] is the saturated thickness

$\bar{q}_w(x,y)$ [L T⁻¹] is the convergent flow field during the pumping test,

$C_w(t)$ [M L⁻³] is the observed concentration during pumping

Q [L³ T⁻¹] is the pumping rate

$\ell_I(t)$ is the isochrone location at time t

\bar{n} is the outward unit normal vector

ℓ_{CP} is the length of the control plane (defined by the capture zone, and perpendicular to the mean flow direction).

and $C_0(x,y)$ being the initial concentration distribution, assumed to fulfil the condition $\bar{q}_0 \cdot \bar{\nabla} C_0 = 0$ (i. e. constant in the flow direction).

In homogeneous aquifers, assuming a perfect radial flow during pumping $\bar{q}_w(x,y)$, the equations in (2.8) simplify to:

$$\begin{cases} M_{CP} = q_0 b \int_{\ell_{CP}} C_0(x,0) dx \\ C_w(t) = \oint_{\ell_I(t)} C_0(x,y) d\ell \end{cases} \quad (2.9)$$

with the isochrone $\ell_I(t)$ defined by the cylinder of radius $r(t) = \sqrt{Qt/\pi b n_e}$.

Equation (2.9) is a simplified version of equation (2.8) where the term $\bar{q}_w(x,y) \cdot \bar{n} b(x,y)/Q$ is one. A recursive solution of (2.9) was derived by Schwarz et al. (1998; 2002), furthermore a closed-form solution (i. e. non recursive) for (2.9) is given in chapter 3.

The resolution of (2.8) may also be approached analytically (without the assumption of perfect radial flow) using superposition of the radial flow solution and the parallel flow solution (after Bear & Jacobs, 1965), leading to a more general analytical expression, derived in chapter 3.

In the general case, heterogeneous flow fields are not known through analytical expressions but through discrete solutions over the model grid (e. g. finite differences or finite elements). In this case, isochrone geometry $\ell_I(t)$ may be defined by particle back tracking to obtain an interpretation of the integral pumping test (Ptak et al., 2000). The numerical resolution of the equation (2.9) using particle locations was implemented in the C++ code C1 (Schwarz, 2002). The numerical algorithm was expanded and modified in order to consider the additional term $\bar{q}_w(x,y) \cdot \bar{n} b(x,y)$ in the numerical integration along the isochrone, in the C++ code CSTREAM (see further details in chapter 4).

In general, analytical approaches are only possible for simple parametrizations of the problem domain while numerical approaches can be applied to more arbitrary geometries. However, when the

explicit analytical expressions are known, they provide valuable information on the behaviour of the solutions (while numerical approaches require series of simulations to display the influence of variations within the input parameters). Advantages and disadvantages of both approaches as summarized in Tab. 2.1.

	ANALYTICAL APPROACH	NUMERICAL APPROACH
ADVANTAGES	<p>It does not require a numerical model of the aquifer, only effective values of q_0, b and n_e (confined conditions and small storativity)</p> <p>The analytical expression of the solution informs about the influence of the input parameters (e. g. linear dependencies)</p>	<p>Permits to consider heterogeneous aquifers explicitly.</p> <p>Permits to consider the influence of multiple well interpretations.</p>
DISADVANTAGES	<p>Can not consider heterogeneity.</p> <p>When using multiple wells, sufficient time lag is necessary between successive pumping.</p>	<p>Requires a numerical model.</p> <p>Does not provide qualitative information on the behaviour of the solutions.</p>

Table 2.1: Analytical and numerical approaches: advantages and disadvantages.

2.2.4. Accounting for linear retardation: simplified formulation

The assumption of purely advective transport is known not to be appropriate for some compounds (which may be significantly retarded). A relatively simple way for expanding the governing equation is to account for linear retardation (i. e. the mass velocity is assumed to be linearly related to the groundwater velocity through a constant factor R_m [-]). With

$$R_m = 1 + \frac{\rho_b}{n_e} k_d = 1 + \frac{\rho_b}{n_e} \frac{S_0}{C_0} \quad (2.10)$$

where $k_d = S_0/C_0$ is the sorption or distribution coefficient, S_0 is the contaminant mass sorbed per unit of mass of aquifer material and ρ_b is the bulk density. Under these conditions, the velocity of a specific particle of contaminant $v_m(x, y)$ and the velocity of a specific particle of water $v_w(x, y)$ are related through

$$R_m = \frac{v_w(x, y)}{v_m(x, y)} \quad (2.11)$$

A consequence of (2.11) is that after pumping for time t the aquifer volume of water removed is $V_I(t)$ but the aquifer volume of mass removed is $V_I(t/R_m)$. To generalize equation (2.6) for the case of linearly retarded transport, the total contaminant mass within the volume $V_I(t/R_m)$ is the sum of the mass dissolved in the water and the mass sorbed in the aquifer material, that is

$$m = \int_{V_I(t/R_m)} C_0(x, y, z) n_e(x, y, z) + S_0(x, y, z) \rho_b(x, y, z) dV \quad (2.12)$$

Equation (2.10) yields

$$(R_m - 1) \frac{n_e}{\rho_b} C_0 = S_0 \quad (2.13)$$

And introducing (2.13) in (2.12)

$$\begin{aligned} m &= \int_{V_I(t/R_m)} C_0(x, y, z) n_e(x, y, z) + \\ &(R_m - 1) n_e(x, y, z) C_0(x, y, z) dV = \\ &= R_m \int_{V_I(t/R_m)} C_0(x, y, z) n_e(x, y, z) dV \end{aligned} \quad (2.14)$$

Finally we can compute the derivative with respect time using equation (2.7) and applying the chain rule leading to

$$\begin{aligned} \frac{\partial m}{\partial t} &= Q C_w(t) = \\ &= \frac{\partial}{\partial t} R_m \int_{V_I(t/R_m)} C_0(x, y, z) n_e(x, y, z) dV = \\ &= - \oint_{S_I(t/R_m)} C_0(x, y, z) \bar{q}_w(x, y, z) \cdot \bar{n} dS \end{aligned} \quad (2.15)$$

And the generalized form for equation (2.4) is therefore

$$Q C_w(t) = - \oint_{\ell_I(t/R_m)} C_0(x, y) \bar{q}_w(x, y) \cdot \bar{n} b(x, y) d\ell \quad (2.16)$$

The problem statement defined in section 2.2.3. provides the methodology to estimate both mass flow rate M_{CP} and average concentration C_{av} , given $C_w(t)$, $\bar{q}_w(x, y)$, $\bar{q}_0(x, y)$, $b(x, y)$ and $n_e(x, y)$, i. e. mass flow rate and average concentration can be computed as $C_{av} = C_{av}(C_w, t, \bar{q}_0, \bar{q}_w, b, n_e)$ and $M_{CP} = M_{CP}(C_w, t, \bar{q}_0, \bar{q}_w, b, n_e)$. To obtain the estimates accounting for linear retardation the same problem 2.2.3 is to be solved (through the analytical or numerical approaches described in chapters 3 and 4) but using the following transformation

$$\begin{aligned} C_{av}^R &= C_{av}(C_w, t/R_m, \bar{q}_0, \bar{q}_w, b, n_e) \\ M_{CP}^R &= M_{CP}(C_w, t/R_m, \bar{q}_0, \bar{q}_w, b, n_e) \end{aligned} \quad (2.17)$$

where C_{av}^R and M_{CP}^R are the average concentration and mass flow rate accounting for linear retardation.

Retardation can be accounted for, within both the numerical and analytical approaches, by simply transforming the input measured data $C_w(t)$ to $C_w(t/R_m)$.

2.3 Numerical simulation and discussion of methodology

A numerically simulated verification example was developed in (Bayer-Raich et al. 2001) to discuss the methodology of the IGIA and to point out the differences between the analytical and the numerical approaches.

2.3.1. Forward simulation: plume development and integral pumping tests

The development of a contaminant plume in a heterogeneous $500 \times 500 \text{ m}^2$ domain is simulated using the code MT3D (Zheng, 1999). Figure 2.5 shows the heterogeneous K-field, generated using the Turning Bands Method with the code TUBA (Zimmerman & Wilson, 1990): geometric mean $K_G = 0.001 \text{ m/s}$, variance $\sigma_{LnK}^2 = 0.25$, correlation length $\lambda = 20 \text{ m}$, porosity $\phi = 0.1$ and thickness $b = 5 \text{ m}$.

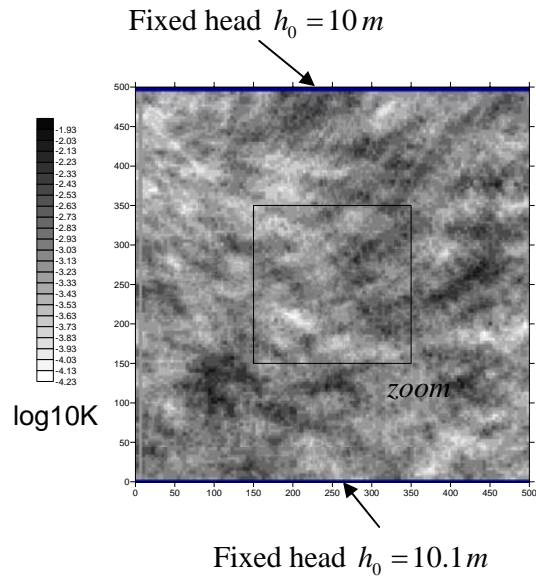


Figure 2.5: Heterogeneous K-field.

After a 1 year forward simulation under steady-state flow conditions, a 60 m long plume was obtained downstream of the source zone, shown in figure 2.6.

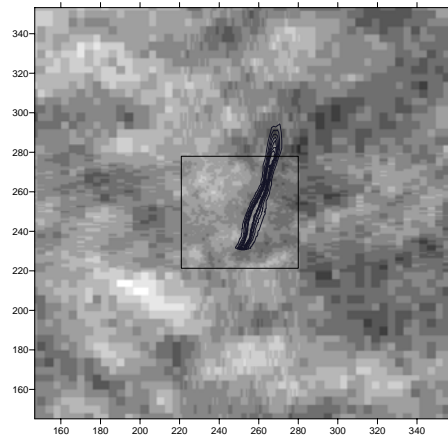


Figure 2.6: Contaminant plume. Contour lines for concentrations 0.1, 0.2, 0.3, 0.4, 0.5, 0.6, 0.7 and 0.8.

At this stage the plume is fully developed around the pumping well, i. e. concentrations remain constant in time. Then a (numerically simulated) integral pumping test is performed in wells 1 and 2, as indicated in Figure 2.7.

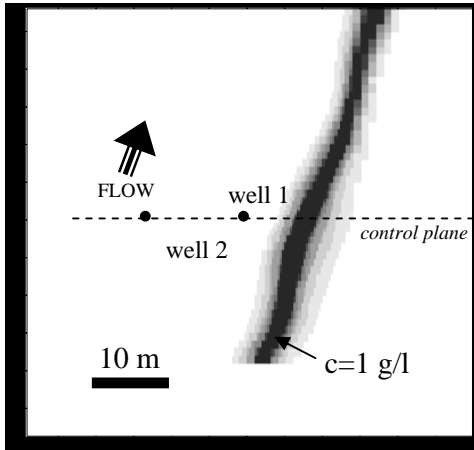


Figure 2.7 Location of the pumping wells and control plane.

In pumping well 1, at a constant rate of $Q=2$ l/s during 43h, 7 samples were taken at different times. Figure 2.8 shows the obtained concentration-time series in well 1 and the plume position after the pumping.

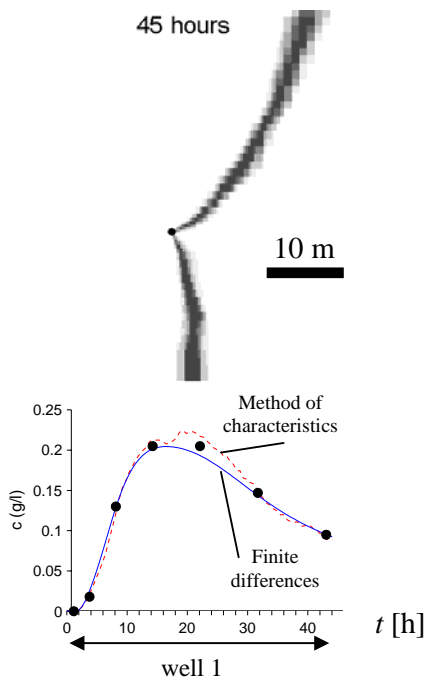


Figure 2.8: Plume position and concentration-time data after integral test in well 1.

55 h after the end of this first test, pumping well 2 operated at a constant rate of $Q=4$ l/s for a period of 10,2h. Figure 2.9 shows

the obtained concentration-time series in well 2 and the plume position after the pumping.

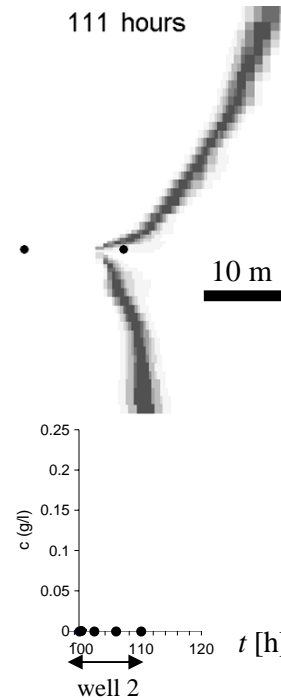


Figure 2.9: Plume position and concentration-time data after integral test in well 2.

2.3.2. Inverse problem: Analytical and numerical approaches

The analytical and numerical inversion methods are now applied to the data obtained in the numerical experiment performed in the previous section, pointing out the differences between both methods.

In the analytical interpretation a homogeneous equivalent aquifer is used, obtained by applying a constant estimate of the average conductivity, porosity and thickness throughout the domain. In general, the analytical solution is a simplified estimation tool, which can be applied to homogeneous or moderately heterogeneous field sites to estimate contaminant mass flow rates using a relatively small number of monitoring wells and without the need for a detailed

groundwater flow and transport model (Teutsch et al. 2000).

The forward transport simulation results (see previous section) on concentration-time data for well 1 are used to obtain the mass flow rate with the analytical formula derived by Schwarz et al. (1998), further explained and expanded in chapter 3. Through the analytical formula, several possible plume positions are obtained as shown in Figure 2.10.

The final estimation of the mass flow rate is obtained by multiplying the average concentration times the groundwater flow rate. Several estimations of the equivalent transmissivity were used for this example leading to errors in mass flow rate estimates varying from -16% to 32% depending on the estimate of equivalent hydraulic conductivity.

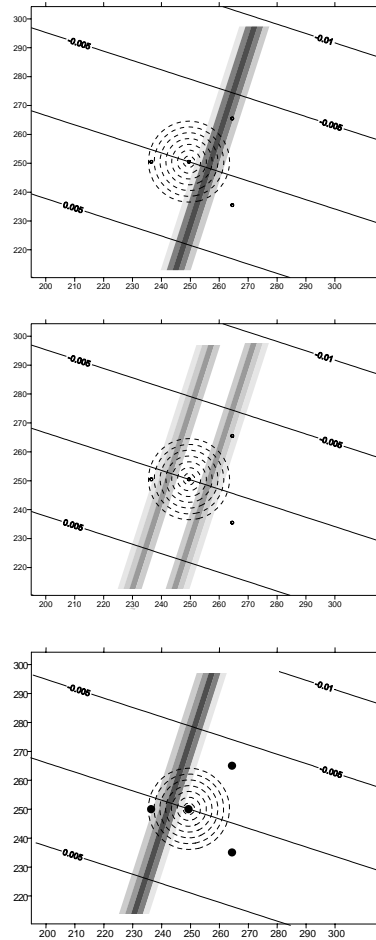


Figure 2.10: Possible plume positions obtained analytically (after Bayer-Raich et al., 2001).

The main limitations of the analytical interpretation are: (1) We can only use it if there is no perturbation of the plume position previous to the integral pumping test, caused for instance by other pumping tests, (2) we have to assume homogeneous conditions, and (3) unique solutions cannot be obtained for the plume position (a consequence of limitation (1) above that multiple pumping tests cannot be evaluated). The numerical interpretation overcomes these limitations using data from both pumping wells 1 and 2. In addition to the concentration-time data observed in the two different pumping wells, both natural (no pumping) and convergent (during pumping) flow fields in

the heterogeneous aquifer are used as input.

When using multiple pumping wells, the isochrones described by the second and successive wells can not be approximated by circles anymore because of the influence of the previous pumping wells, unless there is a sufficient time lag between the pumping tests. The particle tracking algorithm CSTREAM (originally developed in the code C1 by Schwarz, 2002 and expanded in Bayer-Raich et al. 2002b; see chapter 4) is used to define the isochrones and streamtubes through particle backtracking. The influence of heterogeneity and boundary conditions is taken into account through the flow model used for the particle tracking. Streamlines and isochrones are shown in Figure 2.11

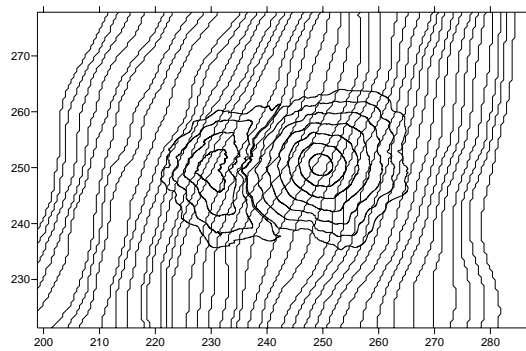


Figure 2.11: Streamlines and isochrones defined numerically through particle tracking.

Figures 2.10 and 2.12 show how the simplifications performed for the analytical inversion lead to straight streamlines and circular isochrones, while the numerical algorithm considers the heterogeneity of the flow field.

The concentration distribution is computed numerically for well 1 considering several possible plume positions, as shown in Figure 2.12.

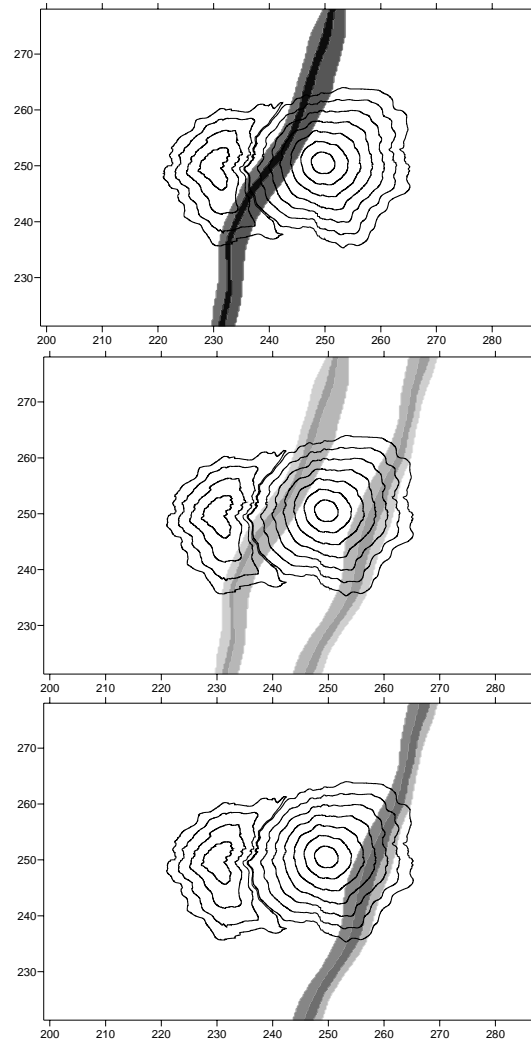


Figure 2.12: Possible plume positions obtained numerically (after Bayer-Raich et al., 2001).

Since well 2 detected no contaminant (figure 2.9), we can conclude that the region captured by well 2 was clean at the beginning of the pumping tests. Hence, one can reject the scenarios in which the plume intersects the well 2 isochrones (two upper graphs in figure 2.12). This indicates that no contaminant was present at the left hand side of well 1, leading to a unique solution for the plume position (figure 2.13). In general, more than two wells may be needed to obtain a unique solution. For instance, at least one more pumping well is needed when the plume is located in between the two first pumped wells.

Numerical evaluation methods are generally needed for relevant multiple well interpretations, as well as for a more detailed consideration of heterogeneity in aquifer properties and field-scale transient flow conditions.

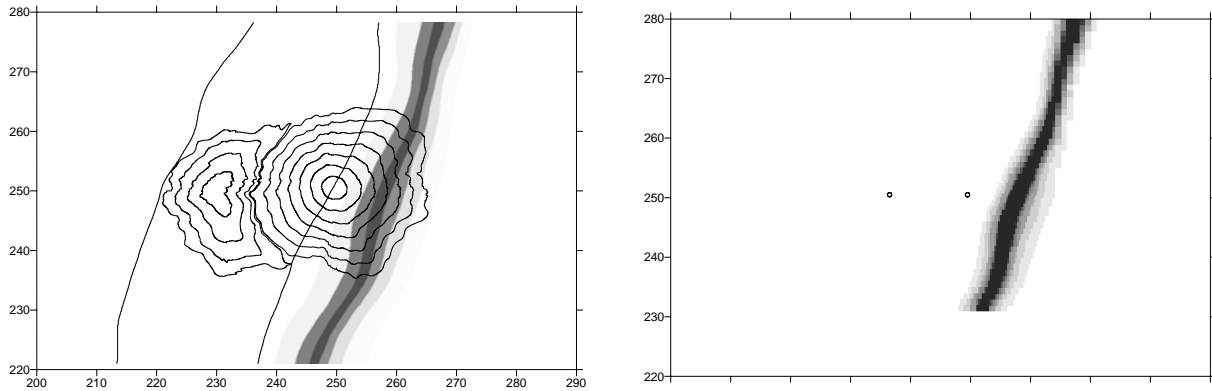


Figure 2.13: Unique plume position obtained numerically (left) and actual plume (right). Open lines in the left figure indicate the region where well 2 detected no contaminants Error in mass flow rate estimate: 14% (after Bayer-Raich et al., 2001)

Chapter 3

ANALYTICAL APPROACH FOR HOMOGENEOUS AQUIFERS

3.1 Introduction

This chapter further expands the analytical work presented in Teutsch et al. (2000) and Schwartz (2002) for the inversion of integral pumping tests. The previous analytical solution, based on the assumption of radial flow during pumping is generalized to account for the effect of the natural velocity field q_0 during the pumping test. Both approaches are compared in a homogeneous aquifer as a function of the (dimensionless) duration of the pumping test t_D , using the definition given in Bear & Jacobs (1965). The results show that, under the condition $t < Q n_e / 2\pi b q_0^2$ (where t is the duration of the pumping test), both approaches lead to similar estimates of the mass flow rate M_{CP} (relative errors $< 10\%$). Further, the simplified approach (i. e. based on the cylinder formula) is studied using the classical theory of Volterra integral equations, providing a closed-form solution for the computation of the mass flow rate. Both approaches are tested under heterogeneous conditions (using the concept of the equivalent homogeneous aquifer). The analytical approach is expanded and tested in a multi-layered aquifer, providing depth-differentiated estimates of the mass flow rate. Finally, the analytical solutions are used for investigating the issue of dimensioning IPTs. A methodology for dimensioning pumping durations and distances between wells is given, based on data from IPTs already conducted within the projects SAFIRA and INCORE.

3.2. Problem formulation for homogeneous aquifers: Volterra integral equation

In homogeneous aquifers (i. e. hydraulic conductivity $K(x, y) = K$, porosity $n_e(x, y) = n_e$ and thickness $b(x, y) = b$ for all (x, y)) a parallel flow field in the y direction is given by Darcy's equation $q_0 = K |\bar{\nabla} h|$. The natural parallel flow field is therefore:

$$\bar{q}_0(x, y) = \begin{pmatrix} 0 \\ q_0 \end{pmatrix} \quad (3.1)$$

Because the concentration, by assumption, is constant along streamtubes that are parallel to the y -axis (i.e. constant in the flow direction), the initial concentration distribution for homogeneous conditions becomes a function of x only, i. e. $C_0(x, y) = C_0(x)$. We then introduce

$$\bar{C}_0(x) = \frac{C_0(x) + C_0(-x)}{2} \quad (3.2)$$

and consider only $x > 0$. The reason for considering such an average concentration is physical - during a pumping test in a homogeneous aquifer, equal proportions of the sampled water will be drawn from the left ($x < 0$) and the right ($x > 0$) of the well. Introducing the definition of $\bar{C}_0(x)$ into equation (2.2) we get

$$\begin{aligned}
M_{CP} &= \int_{-R}^R C_0(x,0) q_{0y}(x,0) b(x,0) dx = \\
&= 2 q_0 b \int_0^R \bar{C}_0(x) dx
\end{aligned} \tag{3.3}$$

Equation (3.3) shows that the mass flow rate M_{CP} may be uniquely identified from $\bar{C}_0(x)$ (i. e. the mass flow rate may be precisely computed from $\bar{C}_0(x)$, even if $C_0(x)$ is unknown). In a homogeneous aquifer the mass flow rate is independent of the plume position (Teutsch et al., 2000).

We may introduce the definition of $\bar{C}_0(x)$ in the integral equation (2.4), and then perform the integration along $\ell^+_I(t)$ (the half of the isochrone $\ell_I(t)$ located at $x > 0$).

$$C_w(t) = -\frac{2b}{Q} \oint_{\ell^+_I(t)} \bar{C}_0(x) \bar{q}_w(x,y) \cdot \bar{n} d\ell \tag{3.4}$$

The equation of the convergent flow field during pumping $\bar{q}_w(x,y)$ may be obtained by superposition of radial flow and parallel flow. Using the (dimensionless) coordinates defined in Bear & Jacobs (1965), the Darcy flow during pumping can be expressed as:

$$\bar{q}_w(x,y) = \begin{pmatrix} -\frac{q_0 x_D}{x_D^2 + y_D^2} \\ q_0 - \frac{q_0 y_D}{x_D^2 + y_D^2} \end{pmatrix}$$

$$\text{with } x_D = \frac{2\pi b q_0}{Q} x ; \quad y_D = \frac{2\pi b q_0}{Q} y \tag{3.5}$$

From equation (3.5) the parametric equation of the isochrones $\ell_I(t)$ at time t_D

was derived by Bear & Jacobs (1965), providing the result

$$t_D = -y_D - \ln \left[\cos(x_D) - \frac{y_D}{x_D} \sin(x_D) \right]$$

with $t_D = \frac{2\pi b q_0^2}{Q n_e} t$ (3.6)

and the equation of the steady-state water divide (as indicated in Figure 3.1):

$$y_D = \frac{x_D}{\tan(x_D)} \tag{3.7}$$

Figure 3.1 show the solutions to equation (3.6) for $t_D = 1, 2, 3, 4, 5$ in dimensionless coordinates, when the groundwater flow moves in the direction of the y axis.

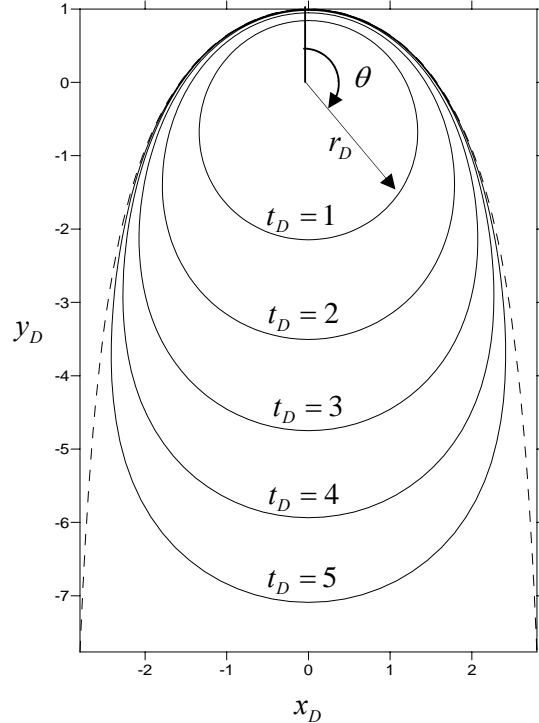


Figure 3.1: Isochrone geometry (dimensionless coordinates) with groundwater flow moving in the direction of the y axis. Water divide at the discontinuous line (Bear & Jacobs, 1965).

To express equation (3.4) in Cartesian coordinates, we introduce the function $\ell_Y(x,t)$ as the distance between the upstream and the downstream intersections of the isochrone and a straight line located at x and parallel to the y axis (Fig 3.2).

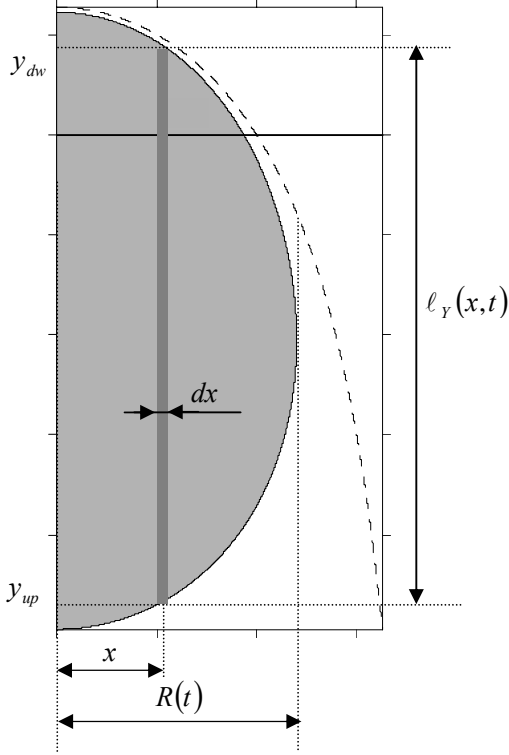


Figure 3.2: Integration of the volume limited by the isochrone: definition of $\ell_Y(x,t)$

Although the function $\ell_Y(x,t)$ is not known explicitly, it is given implicitly by the equation of the isochrone (equation 3.6), by setting $\ell_Y(x,t) = y_{dw} - y_{up}$ where y_{dw} and y_{up} are the two solutions of equation (3.6) for a given (x,t) pair.

The total volume captured by the isochrone up to time t can be obtained by integrating:

$$Qt = 2 \int_0^{R(t)} n_e b \ell_Y(x,t) dx \quad (3.8)$$

In figure 3.3. the capture width $R(t)$ is introduced as (half) the width of the set of streamtubes captured by the isochrone t . Developing equation (3.6) in cartesian coordinates and finding the location where the isochrone is parallel to the y axis leads to:

$$t_D = 1 - \frac{R_D}{\tan R_D} + \ln \left(\frac{R_D}{\sin R_D} \right)$$

with $t_D = \frac{2\pi b q_0^2}{Q n_e} t$; $R_D = \frac{2\pi b q_0}{Q} R$ (3.9)

Further, the total mass captured at the pumping well up to time t equals the total mass of contaminant within the volume limited by the isochrone of time t .

$$\frac{Q}{2} \int_0^t C_w(t) dt = \int_0^{R(t)} \bar{C}_0(x) n_e b \ell_Y(x,t) dx \quad (3.10)$$

Differentiating with respect to time leads to

$$\begin{aligned} \frac{Q}{2 n_e b} C_w(t) &= \frac{\partial}{\partial t} \int_0^{R(t)} \bar{C}_0(x) \ell_Y(x,t) dx = \\ &= \int_0^{R(t)} \bar{C}_0(x) \frac{\partial \ell_Y(x,t)}{\partial t} dx + \ell_Y(R(t),t) \frac{\partial R(t)}{\partial t} \end{aligned} \quad (3.11)$$

Where $\ell_Y(R(t),t) = 0$, therefore equation (3.11) may be written in the usual notation of the Volterra integral equations, in Cartesian coordinates (x,y) , as

$$C_w(t) = \frac{2 n_e b}{Q} \int_0^{R(t)} \bar{C}_0(x) \frac{\partial \ell_Y(x,t)}{\partial t} dx \quad (3.12)$$

which gives an alternative expression for equation (3.4), where the integration is performed along the x direction (while in (3.4) the integration is along the isochrone length). Combining both equations leads to the identity

$$n_e \int_0^{R(t)} \bar{C}_0(x) \frac{\partial \ell_y(x,t)}{\partial t} dx = \int_{\ell^*(t)} \bar{C}_0(x) \vec{q}_w(x,y) \cdot \vec{n} d\ell \quad (3.13)$$

Equation (3.13) gives two alternative expressions for the Volterra integral equation. Analytical solutions are usually formulated in Cartesian coordinates (left hand side of equation (3.13), or equation (3.12)) however, equation (3.12) is a weakly singular integral (the function within the integral is not bounded) and the numerical integration of equation (3.12) is performed by using the right hand side of equation (3.13), i. e. using the more general expression (3.4) (in which the integrand is bounded and therefore is easier to evaluate numerically).

The solution for the general case expressed by equation (3.12) is obtained by numerical integration of equation (3.4) (method of quadratures). The description of this methodology may be found, for example, in Polyanin & Manzhirov (1998) pages 487-488.

3.3. Solution for the Volterra Integral equation by numerical integration

3.3.1. Discrete solution

The discretization of a Volterra integral equation leads to a linear system of equations with a lower triangular matrix (Polyanin & Manzhirov, 1998). In order to apply the “method of quadratures” we assume that a limited number of samples $(t_i, C_w(t_i))$ for $i=1,2,..,n$ are taken during

the pumping test, and use these isochrones to define N streamtubes as indicated in Figure 3.3.

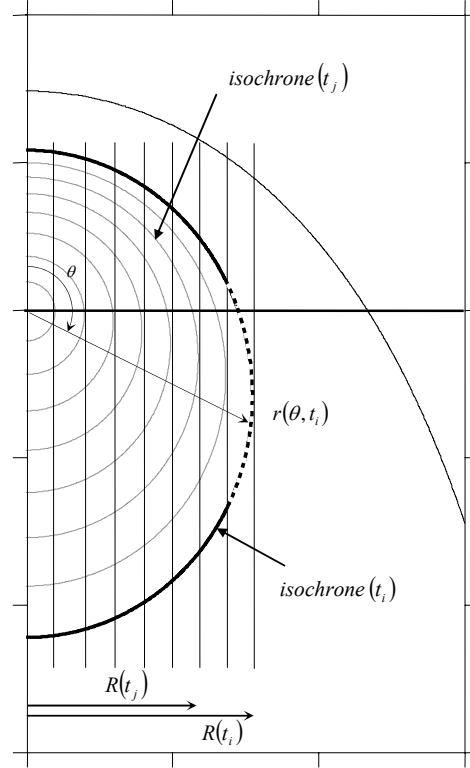


Figure 3.3: Discretization of 8 streamtubes based on the geometry of 8 isochrones.

Now we can discretize equation (3.12) by assuming that the initial concentration $\bar{C}_0(x)$ is constant within a streamtube.

Then $\bar{C}_0(x)$ can be written as:

$$\bar{C}_0(x) = \sum_{j=1}^N \bar{C}_j \xi_j(x) \quad (3.14)$$

$$\text{with } \xi_j(x) = \begin{cases} 1 & x \in (R_{i-1}, R_i) \\ 0 & x \notin (R_{i-1}, R_i) \end{cases}$$

with \bar{C}_j being the concentration of the j -th streamtube, N the number of samples and $R_j = R(t_j)$ the maximum width of the j -th isochrone in the x direction, as shown in

Figure 3.3. Introducing the definition (3.14) into (3.12) we get

$$\begin{aligned} C_w(t_i) &= \\ &= \sum_{j=1}^N \bar{C}_j \frac{2n_e b}{Q} \int_{R_{j-1}}^{R_j} \frac{\partial \ell_Y(x,t)}{\partial t} \Big|_{t=t_i} dx = \\ &= \sum_{j=1}^N \bar{C}_j g_{ij} \end{aligned} \quad (3.15)$$

From the previous expression we get recursive formula to obtain the concentration \bar{C}_i at the streamtubes and the mass flow rate M_{CP}

$$M_{CP} = 2q_0 b \sum_{i=1}^N \bar{C}_i (R_i - R_{i-1}) \quad (3.16)$$

$$\begin{aligned} \text{with } \bar{C}_i &= \frac{C_w(t_i) - \sum_{j=1}^{i-1} \bar{C}_j g_{ij}}{g_{ii}} \\ g_{ij} &= \frac{2n_e b}{Q} \int_{R_{j-1}}^{R_j} \frac{\partial \ell_Y(x,t)}{\partial t} \Big|_{t=t_i} dx \end{aligned}$$

$R_i = R(t_i)$ is given by the (non-linear) equation (3.9).

3.3.2. Numerical implementation in CSTREAM

The computation of the matrix g_{ij} through equation (3.16) involves the evaluation of a weakly singular integral (that is the area limited by a function that tends to infinity within the integration interval). To simplify the numerical integration we introduce a change of variables to perform the integration along the isochrone length, using constant increments of the angle θ .

We seek to introduce the expressions given by (3.5) and (3.6) in (3.4). Since the vector \vec{n} is perpendicular to the isochrone, we

may describe it as $\vec{n} = \vec{\nabla}t / |\vec{\nabla}t|$, where t is given by equation (3.6). The geometrical relationships shown in Figure 3.4 lead to $d\ell = |\vec{\nabla}t| r^2 d\theta / (\vec{\nabla}t \cdot \vec{r})$. Then the integral equation in (3.4) may be particularized as:

$$C_w(t) = \int_0^\pi \bar{C}_0(r(\theta,t) \sin \theta) g(r(\theta,t), \theta, t) d\theta$$

with

$$g(r, \theta, t) = \frac{2r^2 b}{-Q} \frac{\bar{q}_w(r, \theta) \cdot \vec{\nabla}t}{\vec{r} \cdot \vec{\nabla}t} \quad (3.17)$$

where $r = r(\theta, t)$ is given implicitly by equation (3.6) transformed to polar coordinates:

$$\begin{aligned} t_D &= -r_D \cos \theta - \\ &- \ln[\cos(r_D \sin \theta) - \cotan \theta \sin(r_D \sin \theta)] \end{aligned}$$

$$\text{with } r_D = \frac{2\pi b q_0}{Q} r. \quad (3.18)$$

Using these equations, g_{ij} is computed by numerical integration using the formula

$$g_{ij} = \int_0^\pi \xi_j(r(\theta, t_i) \sin \theta) g(r(\theta, t_i), \theta, t_i) d\theta \quad (3.19)$$

The integral appearing in the term g_{ij} is evaluated by numerical integration performed along the i -th isochrone. The quadrature of Newton-Cotes (trapezoidal rule) is used along the isochrone with a constant increment of the angle θ . The evaluation of the function $g(r(\theta, t), \theta, t_i)$ at each ‘‘base point’’ $(r(\theta, t), \theta)$ of the numerical integration requires solving the non-linear equations (3.6) for $r(\theta, t)$ and (3.9) for $R(t)$. Therefore a zero-finding Newton-Raphson algorithm has been implemented. The algorithm used to

evaluate g_{ij} and produce the graphical output with the geometry of the isochrones is detailed in figure 3.5.

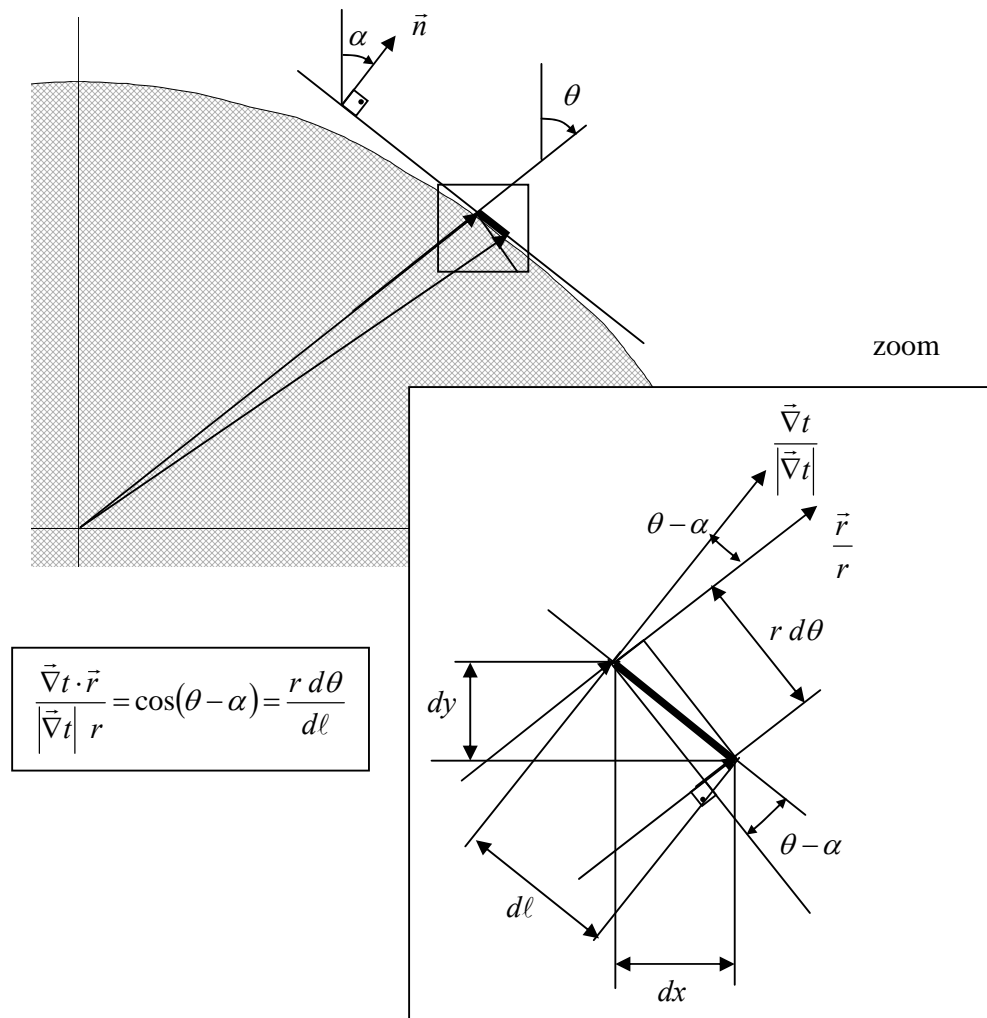
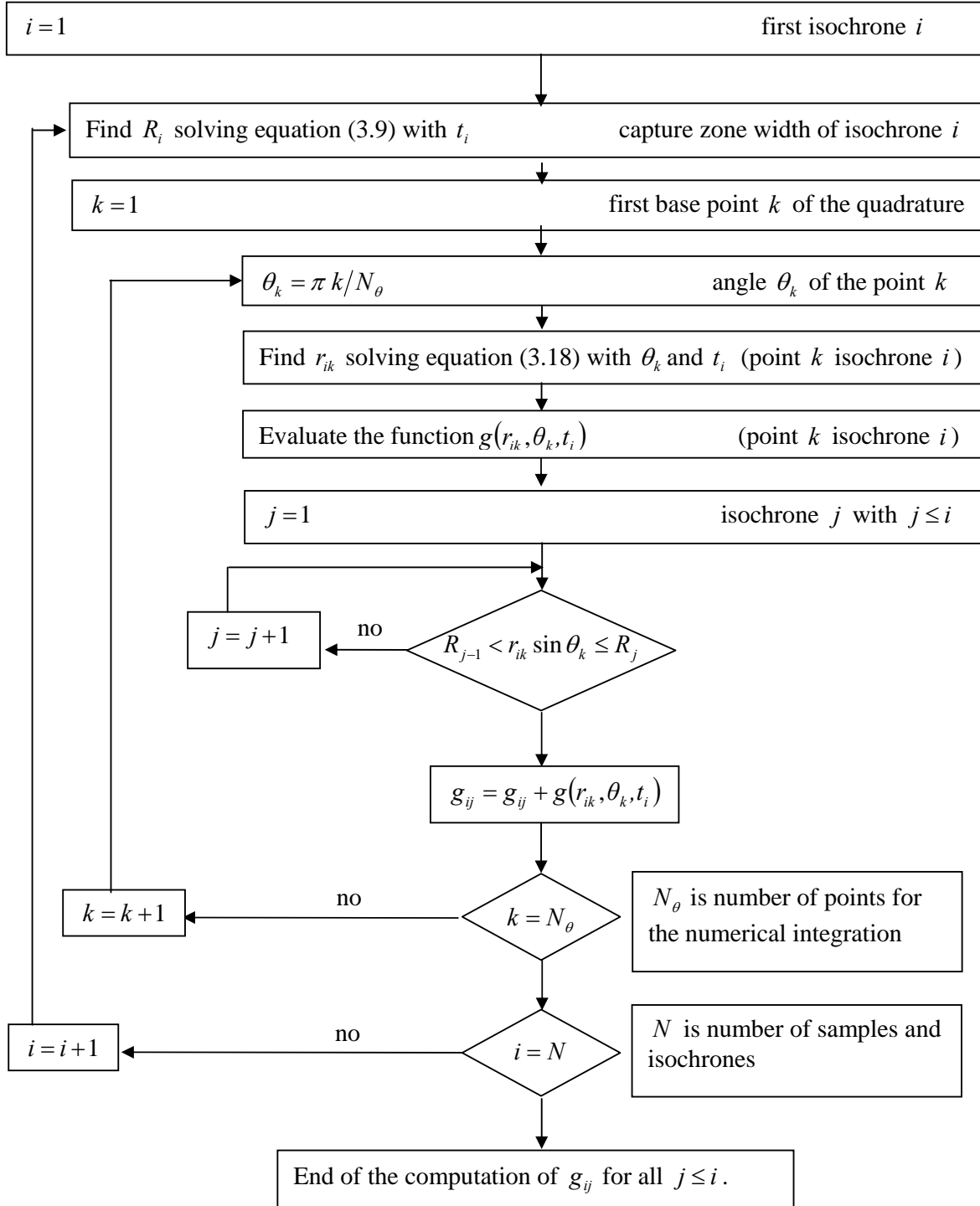


Figure 3.4: Detail of the relative position of the isochrone length $d\ell$ and vector $\vec{n} = \vec{\nabla}t / |\vec{\nabla}t|$ perpendicular to the isochrone.

Figure 3.5: Algorithm for the computation of g_{ij}

The Newton-Raphson iterative algorithms for solving the non-linear equations (3.18) and (3.9) (for $r(\theta, t)$ and $R(t)$) require the definition of objective functions and their derivatives.

For equation (3.6), we seek to find the solutions of the objective function $F(r_D)=0$ with derivative $F'(r_D)$:

$$\begin{aligned}
 F(r_D) &= t + r_D \cos \theta_k + \\
 &+ \ln[\cos(r_D \sin \theta_k) - \cotan \theta_k \sin(r_D \sin \theta_k)] = 0 \\
 F'(r_D) &= \cos \theta_k - \\
 &- \frac{\cos(r_D \sin \theta_k - \theta_k)}{\cos(r_D \sin \theta_k) - \frac{\sin(r_D \sin \theta_k)}{\tan \theta_k}}
 \end{aligned}
 \tag{3.20}$$

And for equation (3.9), the objective function is:

$$\begin{aligned}
 F(R_D) &= 1 - \frac{R_D}{\tan R_D} + \log\left(\frac{R_D}{\sin R_D}\right) - t_D = 0 \\
 F'(R_D) &= \frac{R_D}{\sin^2 R_D} - \frac{2}{\tan R_D} + \frac{1}{R_D}
 \end{aligned}
 \tag{3.21}$$

In both cases, the iterative algorithm for finding the iteration m as a function of the iteration $m-1$ is given by

$$r^{(m)} = r^{(m-1)} - \frac{F(r^{(m-1)})}{F'(r^{(m-1)})}
 \tag{3.22}$$

Since the solutions of both (3.20) and (3.21) are simple, the Newton-Raphson algorithm converges with order 2.

In the equation of the water divide, equation (3.7), given the angle θ , the radius location is obtained explicitly (no iterations are necessary)

3.4. Approximate solution: Abel's integral transform

Although the closed-form solution to the general Volterra equation (3.12) is not known (only a discrete solution was obtained by the method of quadratures) some simplifications allow us to derive a closed-form solution for a simplified version of equation (3.12). This solution is based on a generalized Abel integral transform, and is simpler (i. e. non recursive) than the previous existing solution derived by Schwarz et al. (1998).

3.4.1. Problem formulation: simplifying assumptions

The natural groundwater velocities before the (integral) pumping test q_0 influences the shape of the isochrones as shown in Figure 3.6: as the (dimensionless) duration of the pumping test increases, the isochrones extend to infinity in the upstream direction but are limited in the downstream direction by the water divide. Early isochrones are (almost) circular while late isochrones are extended in the upstream direction.

If the natural velocity is zero ($q_0 = 0$) the flux towards the well is given by Thiem's equation (Moragas, 1896; Thiem, 1906)

$$q_w = -Q / (2 \pi b r) \quad (3.23)$$

In the problem that we are studying, the natural groundwater flow is never zero, however in some cases we may use equation (3.23) to give an approximate description of the isochrone geometry.

The equation of the isochrones for the Thiem problem described above is given by the cylinder formula:

$$r(t) = \sqrt{\frac{Q t}{\pi b n_e}} \quad (3.24)$$

which may be written in dimensionless coordinates as (see equation (3.6) for the definition of t_D and r_D):

$$t_D = \frac{r_D^2}{2} \quad (3.25)$$

We will use equation (3.25) as an approximation to equations (3.6) and (3.9) (i. e. under this approximation $r(\theta, t) = r(t) = R(t)$).

Figure 3.6 shows both the geometry of the isochrones (equation 3.6) and the approximation given by the cylinder formula for dimensionless times $t_D = 0.02, 0.04, 0.06, 0.08, 0.1$ (with larger isochrones corresponding to higher t_D).

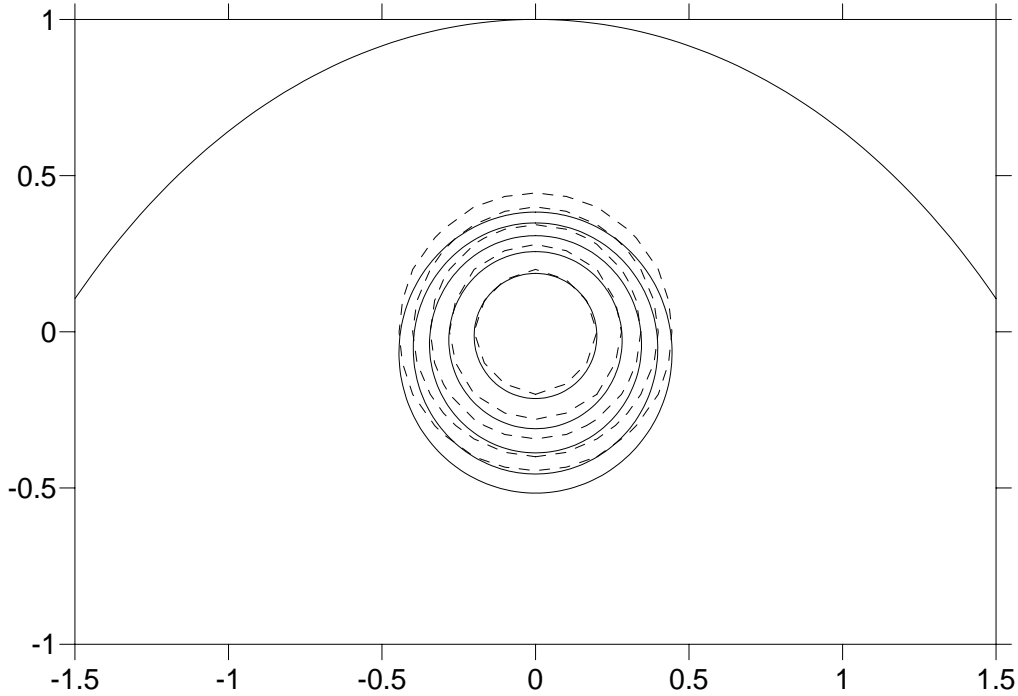


Figure 3.6: Influence of the natural gradient on the shape of the isochrones.
Solid line: actual isochrone, Dotted line: approximation (cylinder formula)

As shown in Figure 3.6 the isochrone geometry becomes (almost) circular for early (dimensionless) times, therefore considering perfect radial flow during the pumping test is justified for small values of t_D . This approximate solution corresponds to the solution of the problem summarized by equation (2.6); its range of validity is quantified in section 3.4.3.

To particularize the Volterra integral equation for this simplified approach we introduce $\ell_Y(x,t) = 2\sqrt{r(t)^2 - x^2}$ in equation (3.12) obtaining

$$C_w(t) = \frac{2}{\pi} \int_0^{r(t)} \frac{\overline{C_0}(x)}{\sqrt{r(t)^2 - x^2}} dx \quad (3.26)$$

Which may be also found from the more general equation (3.4) particularized by $\vec{q}_w \cdot \vec{n} = -Q/(2\pi br)$ and transforming coordinates to $x = r(t)\sin\theta$.

This equation has appeared before in the literature of integral equations (e.g. Volterra, 1894) and an exact solution may be formulated by means of the Abel inverse transform (Abel, 1823). A discrete solution based on the method of quadratures was also provided in Schwarz et al. (1998) and Teutsch et al. (2000).

3.4.2. Discrete solution, Schwarz et al. (1998)

A solution based on the discretization of equation (3.26) was provided by Schwarz et al. (1998) and Schwarz (2002). This solution may be obtained from equation (3.19) or (3.16) where g_{ij} is integrated for $r(\theta, t_i) = r(t_i) = r_i$ given by the cylinder formula and $g(r(\theta, t), \theta, t_i) = 1/\pi$. In this case,

$$\begin{aligned} g_{ij} &= \frac{2}{\pi} \int_0^{\pi/2} \xi_j (r_i \sin \theta) d\theta = \\ &= \frac{2}{\pi} \left[\arccos \left(\sqrt{\frac{t_{j-1}}{t_i}} \right) - \arccos \left(\sqrt{\frac{t_j}{t_i}} \right) \right] \end{aligned} \quad (3.27)$$

which may be also derived by particularizing equation (3.16) for $\ell_y(x, t) = 2\sqrt{r(t)^2 - x^2}$. Therefore, equation (3.16) leads to the result provided in Schwarz et al., (1998)

$$M_{CP} = 2q_0 b \sum_{i=1}^N \bar{C}_i (r_i - r_{i-1})$$

with

$$\bar{C}_i = \frac{\frac{\pi}{2} C_w(t_i) - \sum_{j=1}^{i-1} \bar{C}_j \left(\arccos \frac{r_{j-1}}{r_i} - \arccos \frac{r_j}{r_i} \right)}{\arccos \frac{r_{i-1}}{r_i}} \quad (3.28)$$

This solution is the first equation that was used in field investigations for estimation of the mass flow rate from an integral pumping test. All integral pumping tests performed in Holder et al. (1998), Bockelmann et al., (2001;2003), Bayer-Raich et al. (2002) and Béland-Pelletier et al. (2003) where interpreted using this solution.

Figure 3.7 shows the graph of $C_w(t)$ for a single plume $\bar{C}_0(x)$.

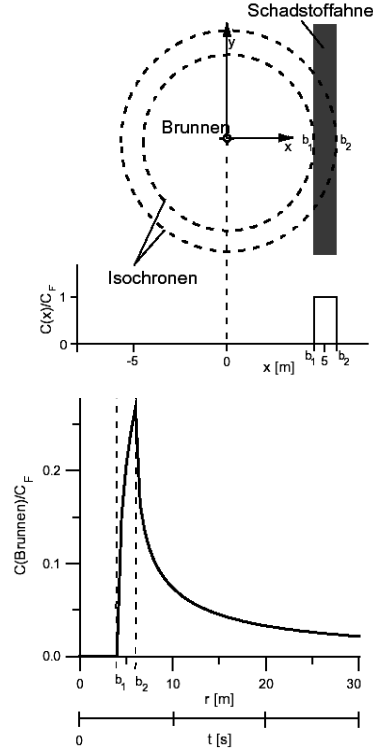


Figure 3.7. Discrete solution obtained by analytical integration (Schwarz, 2002)

3.4.3. Continuous solution: Abel's transform

Exact (closed-form) solutions of integral equations play an important role in the proper understanding of features of many phenomena and processes in various areas of natural science (Polyanin & Manzhirov, 1998). The Norwegian mathematician Niels Henrik Abel (1802-1829) discovered integral equations in his third paper *Solutions of some problems by means of definite integrals* (Abel, 1823). A generalized form of Abel's integral transform is (Porter & Stirling, 1990):

$$f(r) = \int_0^r \frac{g(x)}{(h(r) - h(x))^\alpha} dx \quad (3.29a)$$

for given functions $g(x)$, $h(x)$ and $0 < \alpha < 1$. If $f(r)$, $h(x)$ are given in the above equation, the function $g(x)$ is obtained by the inverse transform as

$$g(x) = \frac{\sin \alpha \pi}{\pi} \frac{d}{dx} \int_0^x \frac{h'(r) f(r)}{(h(x) - h(r))^{1-\alpha}} dr \quad (3.29b)$$

Abel (1823) derived these relationships for the particular case of $h(x) = x$. The solution (3.29) for the case $\alpha = 0.5$ and $h(x) = x^2$ was given in Volterra (1894). Equation (3.29) applies to the integral equation (3.26), therefore the interpretation of an integral pumping test may be formulated by means of the generalized Abel integral transform with $g(x) = 2\overline{C}_0(x)/\pi$, $f(r) = C_w(t(r))$, $\alpha = 0.5$ and $h(x) = x^2$:

$$C_w(t(r)) = \frac{2}{\pi} \int_0^r \frac{\overline{C}_0(x)}{\sqrt{r^2 - x^2}} dx$$

which is exactly (3.26), therefore the inverse transform is then given by equation (3.29) as

$$\overline{C}_0(x) = \frac{d}{dx} \int_0^x \frac{r C_w(t(r))}{\sqrt{x^2 - r^2}} dr \quad (3.30)$$

Using this result within equation (3.3) we integrate the mass flow rate as

$$\begin{aligned} M_{CP} &= 2 q_0 b \int_0^R \overline{C}_0(x) dx = \\ &= 2 q_0 b \int_0^R \frac{d}{dx} \int_0^x \frac{r C_w(t(r))}{\sqrt{x^2 - r^2}} dr dx = \\ &= 2 q_0 b \int_0^R \frac{r C_w(t(r))}{\sqrt{R^2 - r^2}} dr \end{aligned} \quad (3.31)$$

Performing the integration along $\xi = r^2 \pi b n_e / (Q t_{\max}) = t(r) / t_{\max}$ with $d\xi = 2 r \pi b n_e dr / (Q t_{\max})$, yields:

$$M_{CP} = q_0 b R \int_0^1 \frac{C_w(\xi t_{\max})}{\sqrt{1 - \xi}} d\xi \quad (3.32)$$

Equation (3.32) provides a simple explicit solution for the computation of the mass flow rate, which may also be written in the form $M_{CP} = 2 q_0 b R C_{av}$ with

$$C_{av} = \int_0^1 \frac{C_w(\xi t_{\max})}{2 \sqrt{1 - \xi}} d\xi \quad (3.33)$$

Note that (3.33) is independent of aquifer thickness, porosity and pumping rate. Assuming perfectly radial flow, the average concentration C_{av} is determined by a weighted average of $C_w(t)$ along the time. As shown in Figure 3.8, the later times give a higher contribution. This equation is valid only for $t_D \ll 1$. In general, the weighting function shown in Figure 3.8 depends on the (dimensionless) duration of the integral pumping test. Porosity and thickness only affect the mass

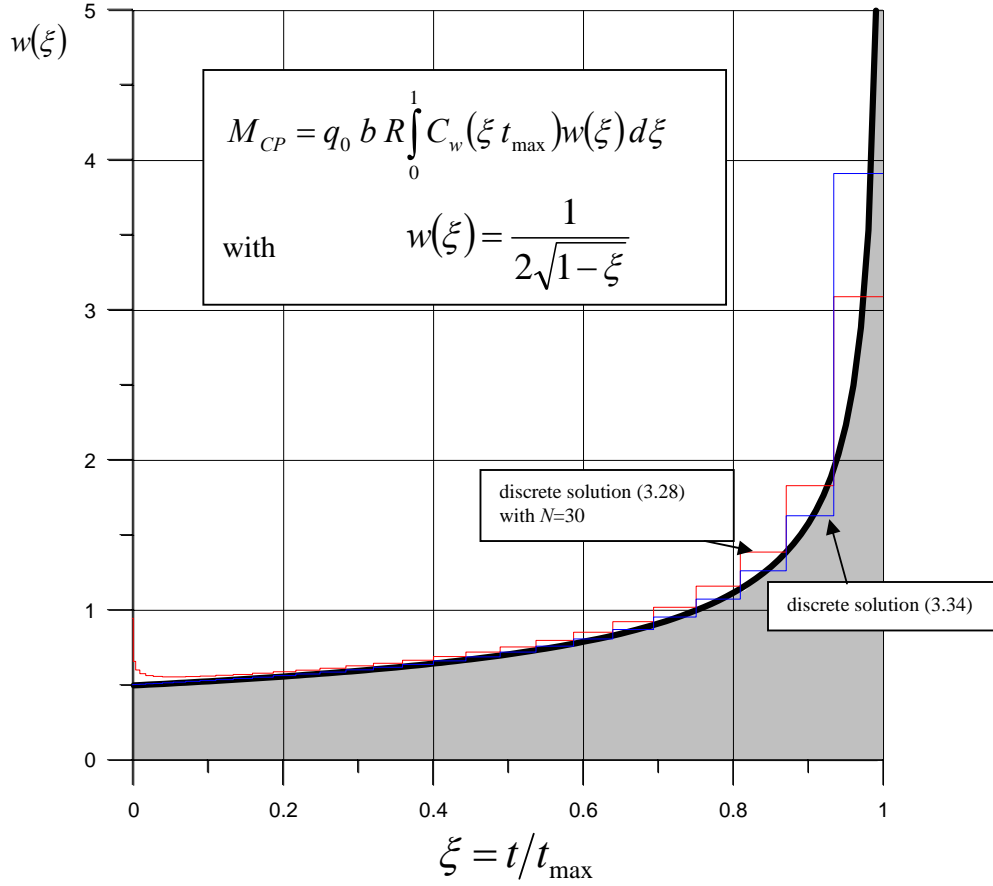


Figure 3.8 Averaging of the concentration at the pumping well. Area of the shaded region = 1.

flow rate because of their influence on the area of the control plane (given by the term $2bR$) and they do not influence the average mass flux or the average concentration C_{av} .

Taking as an approximation $C_w(t) = C_w(t_i)$ for all t within $t_{i-1} < t < t_i$ we may integrate the previous expression yielding

$$M_{CP} = q_0 2Rb \sum_{i=1}^N C_w(t_i) \left[\sqrt{1 - \frac{t_{i-1}}{t_n}} - \sqrt{1 - \frac{t_i}{t_n}} \right] \quad (3.34)$$

which may be used as an alternative to the recursive solution (3.28).

Equations (3.28) and (3.34) may be compared to equation (3.16) to test the effect of the simplifying assumptions. The mass flow rate is expressed in all cases, as a weighted sum of the concentration values sampled at the well, in general defining the normalized time $\xi = t/t_{\max}$ and with t_D being the dimensionless duration of the pumping test we may write

$$M_{CP} = q_0 b 2R \int_0^1 C_w(\xi t_{\max}) w(\xi, t_D) d\xi \quad (3.35)$$

which, for short pumping tests, simplifies to

$$w(\xi, t_D \rightarrow 0) = w(\xi) = \frac{1}{2\sqrt{1-\xi}} \quad (3.36)$$

yielding to the closed-form solution (3.32).

3.5. Verification and comparison of approaches

In this section I address the question: “When may we use the approximate solutions (3.28) or (3.34) for the interpretation of integral pumping tests?”. I show this question can be reduced to check the inequality $t < Q n_e / 2\pi b q_0^2$, leads to errors $< 10\%$ in the mass flow rate estimate. For integral tests longer than $Q n_e / 2\pi b q_0^2$, the more general solution (3.16) should be used. The effect of heterogeneity and depth integration will be quantified in sections 3.6 and 3.7 respectively. This section quantifies the errors due to the influence of the natural gradient during pumping.

3.5.1 A trivial case: $C_w(t) = C_{plume}$

At first, we consider the (trivial) case of an aquifer with constant concentration $\overline{C_0}(x) = C_{plume}$. Under these conditions the concentration obtained at the pumping well is also constant $C_w(t) = C_{plume}$ and the mass flow rate reduces to $M_{CP} = q_0 b 2 R(t) C_{plume}$.

In Figure 3.9, the isochrones given by Bear & Jacobs (1965) (equation (3.6) and the cylinder formula (3.25)) are compared for increasing (dimensionless) time. Furthermore, the figure shows the size of the control plane obtained from $R(t)$ in equations (3.9) and (3.25). The simplified approach leads to an overestimation of the mass flow rate because the width of the control plane $r(t)$ is always greater than the actual width $R(t)$ (as shown in Figure

3.9). The captured radius predicted by the cylinder formula is 6% larger than the actual radius for $t_D > 1$ and is 100% larger if $t_D > 17$. Figure 3.10 gives the error (overestimation) of the cylinder formula in terms of mass flow rates for several values of t_D .

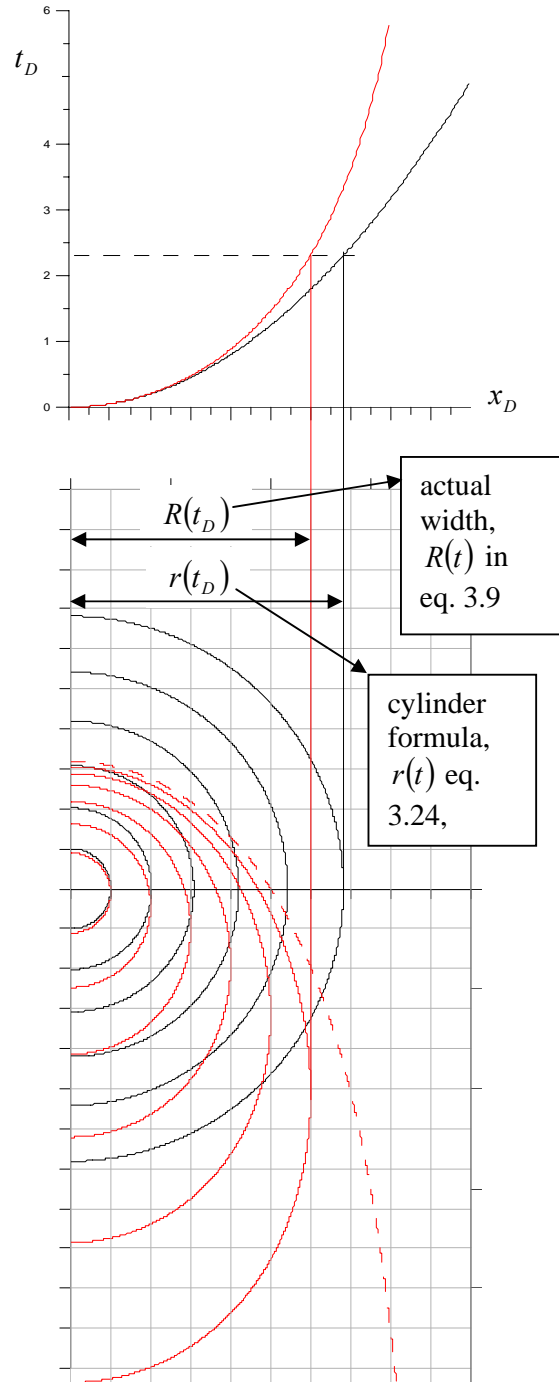


Figure 3.9 Width of the capture zone.

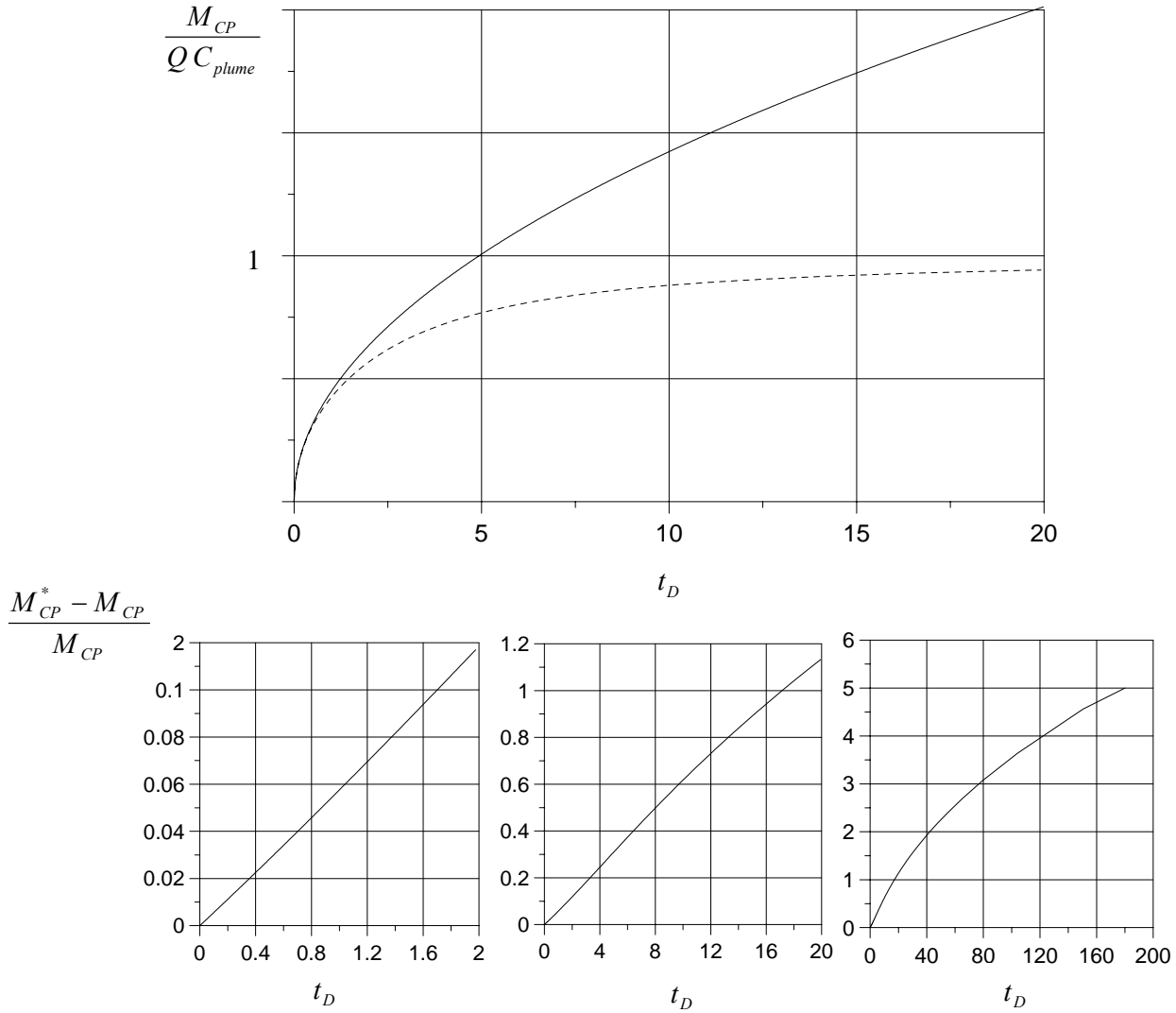


Figure 3.10: Top: Estimation of the mass flow rate using the simplified approach (cylinder formula) dotted line: actual mass flow rate. Bottom: relative error of the cylinder formula: M_{CP}^* estimate based on the cylinder formula; M_{CP} actual value

It is remarkable that the actual mass flow rate is bounded by $Q C_{plume}$ but the estimation provided by the cylinder formula never reaches a limit (may grow infinitely with increasing duration of the integral pumping test).

Those errors are quantified for the trivial case $\overline{C_0}(x) = C_{plume}$; $C_w(t) = C_{plume}$. In the next section we check some simple distributions of $\overline{C_0}(x)$ to estimate the errors of the cylinder formula for variable $C_w(t)$.

3.5.2 Simple plumes

A simplified scenario with several plume distributions was used to perform an integral pumping test of duration $t_D = 2.3$. Six different plumes at different (dimensionless) distances from the well are considered as shown in figure 3.11.

The concentration at the pumping well $C_w(t)$ was obtained by numerical integration of equation (3.17), with 600 isochrones and 10000 “base points” along each isochrone using the trapezoidal rule and constant increments of the angle $\Delta\theta = \pi/10000$ (quadrature of Newton-Cotes).

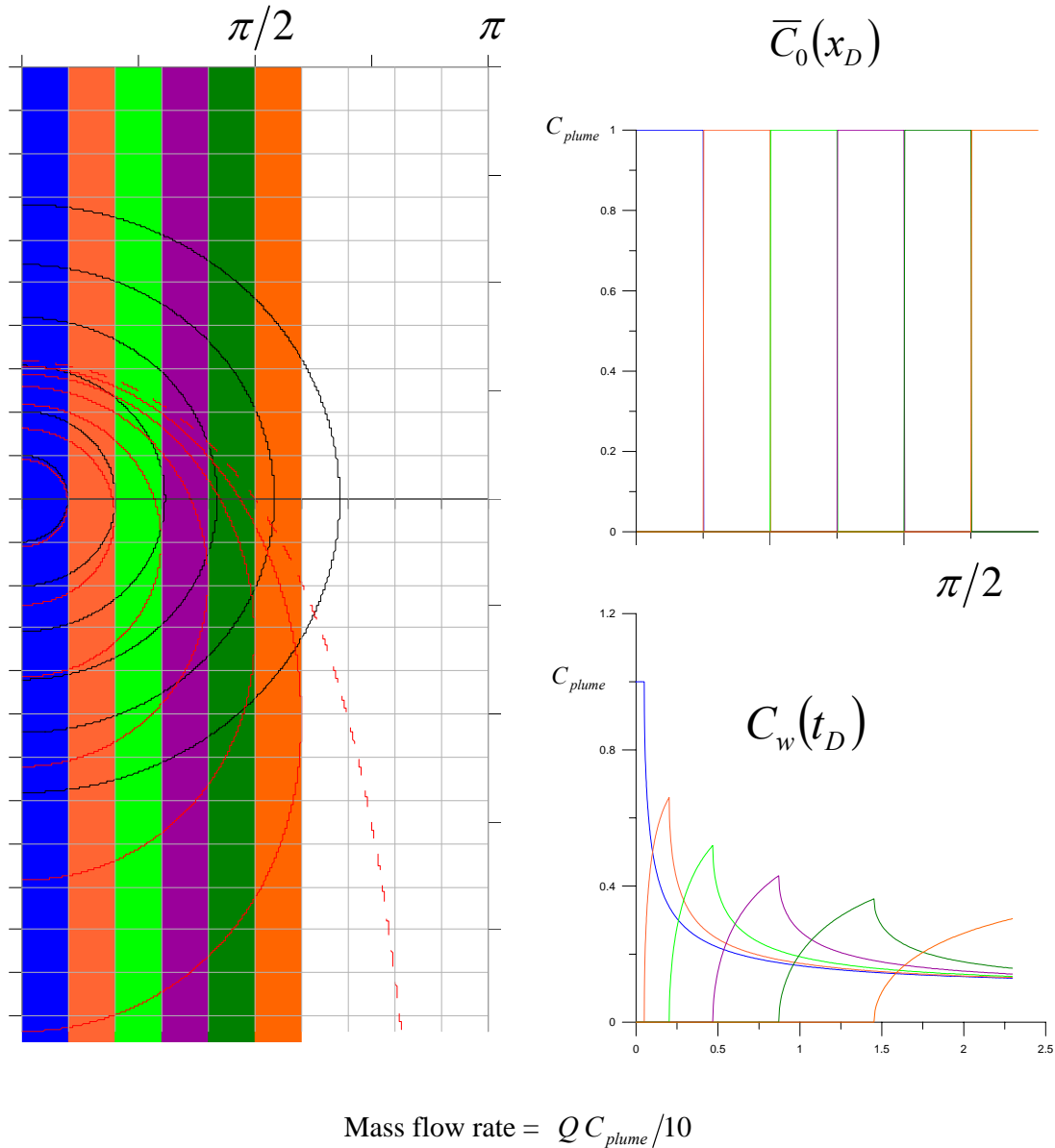


Figure 3.11: Left: plume(s) position Upper right: Concentration profiles along x . Lower right: Concentrations obtained at the pumping well.

The previous figure summarizes the functions that will be used to test the simplified approach based on the cylinder formula. The bottom-right $C_w(t)$ -curves are used as input for both formulae: eq. (3.28) for the simplified approach and eq. (3.16) for the general approach.

A constant increment of the capture width $R_i - R_{i-1} = \Delta R$ was selected using dimensionless increments of $\Delta R = \pi/1000$ and a total of 600 isochrones shown in Figure 3.12.

The output of both approaches is compared to the plume concentrations $\overline{C}_0(x)$ shown in the top-left figure 3.11, and to the total mass flow rate, which equals to $Q C_{plume}/10$.

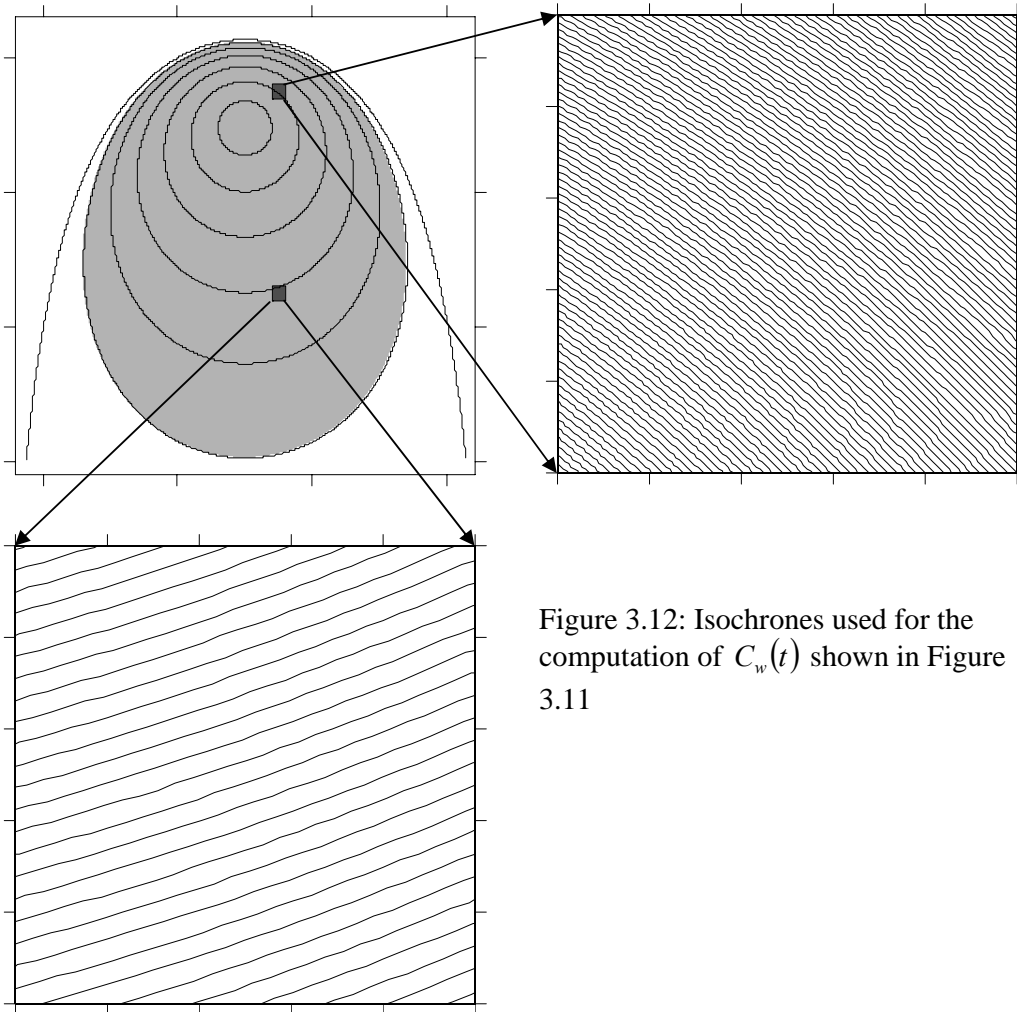


Figure 3.12: Isochrones used for the computation of $C_w(t)$ shown in Figure 3.11

The mass flow rate is computed by integrating the (inverted) concentrations $\overline{C}_0(x)$. Therefore, the errors in the estimated $\overline{C}_0(x)$ will lead to errors in the estimated mass flow rate.

Figure 3.13 shows the result of the inversion in terms of $\overline{C}_0(x)$, namely that the simplified approach leads to an underestimation of the concentration and an overestimation of the capture width. The error, in general, depends on the observed $C_w(t)$.

simplified approach is shown in Figure 3.15.

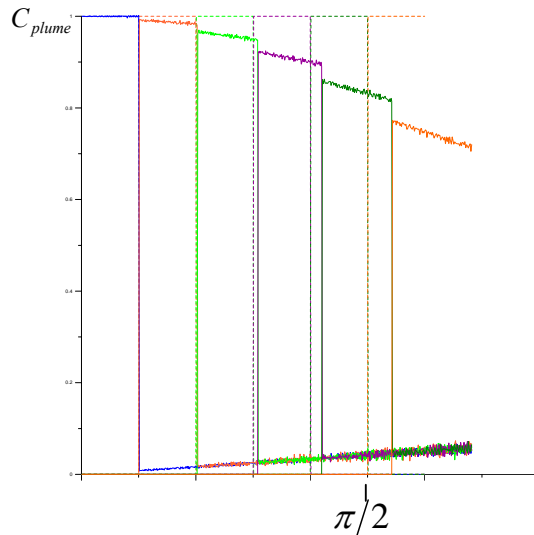


Figure 3.13: $\overline{C}_0(x)$ inversion. Solid line: general approach (equation 3.16). Dotted line: simplified approach (equation 3.28)

Figure 3.13 shows how the general approach leads to the original concentrations $\overline{C}_0(x)$ (compare to Figure 3.11 top-right) while the simplified approach provides an approximation. The differences observed in Figure 3.13 lead to differences in the mass flow rate estimates (obtained from formula (3.28) in the simplified approach; and formula (3.16) in the general approach). The different mass flow rate estimates are compared as a function of the (dimensionless) time in Figure 3.14, the relative error of the

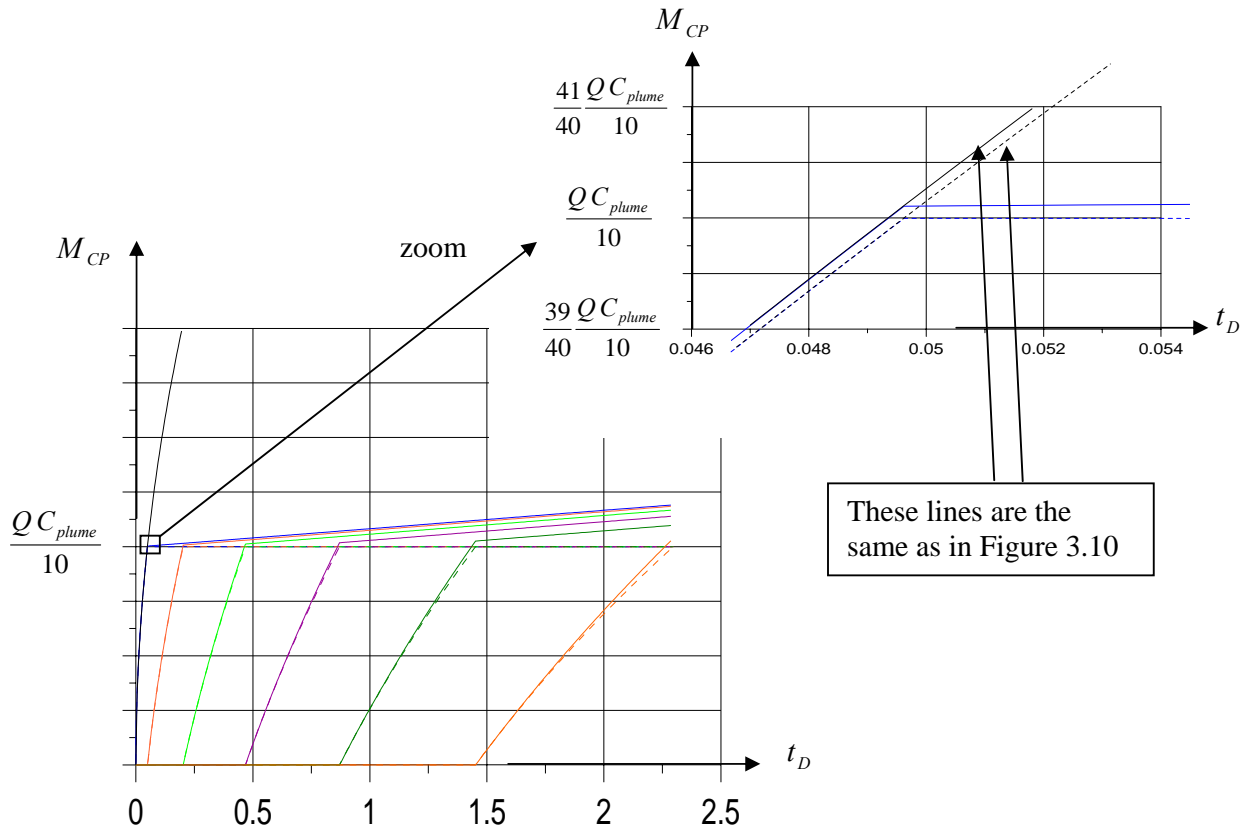


Figure 3.14: M_{CP} inversion as a function of t_D . Solid line: general approach (equation 3.16). Dotted line: simplified approach (equation 3.28).

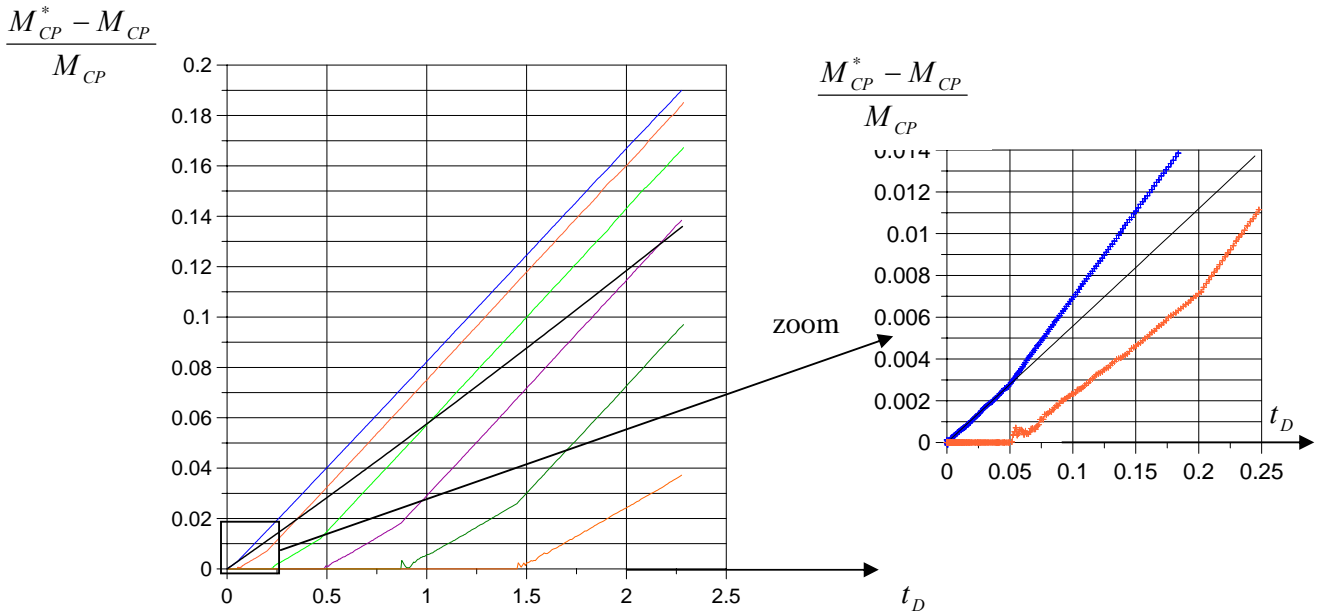


Figure 3.15: M_{CP} relative error for the simplified approach: thick line: trivial case $\bar{C}_0(x) = C_{plume}$ $C_w(t) = C_{plume}$ Thin lines: plumes described in figure 3.11. Max error: 19% at $t_D = 2.3$

3.5.3 Applicability of the simplified approach

The simplified approach based on the cylinder formula lead to relative errors of up to 14% for the trivial case $\overline{C}_0(x) = C_{plume}$ and $C_w(t) = C_{plume}$. For the plumes described in figure 3.11 and dimensionless pumping test durations $t_D < 2.25$ and errors range between 3% and 19% (and $t_D < 2.25$). Generally, the relative errors increase with increasing t_D .

These results suggest that pumping tests of (dimensionless) duration smaller than 1 may be inverted using the simplified approach (equation 3.28), however longer pumping tests should be inverted through the general approach (equation 3.16). Most field scale applications (e.g. Holder et al., 1998; Bockelmann et al., 2001; 2003 and Jarsjö et al., 2003 in the Neckar Valey in Stuttgart, Germany; Bayer-Raich et al., 2002 in Bitterfeld, Germany; Béland-Pelletier et al. (2003) in Borden, Canada) were performed through pumping tests of duration $t_D < 1$. However, some of the pumping tests did not fulfill this condition.

Table 3.1 shows the duration of the pumping tests performed in Bockelmann et al. (2001 ; 2003): in 4 of the wells the dimensionless pumping test duration was longer than 1. It should be noted also than the condition $t_D < 1$ is necessary but not sufficient to perform adequate inversions when $C_w(t) \neq 0$ (the trivial case $C_w(t) = 0$ leads to $\overline{C}_0(x) = 0$ and $M_{CP} = 0$): other processes (e.g. heterogeneity or influence of previous pumping tests) may be sources of error when using the analytical approach. The condition $t_D < 1$ only guarantees that the isochrone geometry is not strongly influenced by the natural parallel flow. However when multiple wells are used (simultaneously or sequentially) the isochrone geometry of each well is influenced by previous pumping tests. The effect of heterogeneity will be a main source of error (quantified in the next section). When the isochrone geometry may not be assumed to be circular the best method to perform the inversion is the numerical algorithm CSTREAM (based on particle tracking and described in the next chapter).

Table 3.1. Dimensionless duration of the integral pumping tests performed in Bockelmann et al. 2001;2002.

Well	Porosity n_e [-]	Thickness b [m]	Hydr.Cond. K [m/s]	Gradient $ \nabla h $ [-]	q_0 [m/s]	Pumping rate Q [m ³ /s]	$r(t_{max})$ [m]	t_{max} [h]	$R(t_{max})$ [m]	t_D
B42	0.15	4	1.95E-03	2.00E-03	3.90E-06	4.08E-03	33.5	144	262	0.324
P2	0.15	3.8	8.42E-04	1.20E-03	1.01E-06	1.44E-03	16.7	96	375	0.039
B41	0.15	2.96	1.05E-02	1.50E-03	1.57E-05	4.16E-03	32.1	96	89.5	2.541
P1	0.15	3.35	8.36E-03	1.30E-03	1.09E-05	4.85E-03	32.6	96	133	1.182
NT01	0.15	0.9	5.78E-03	1.30E-03	7.51E-06	2.95E-03	39.4	62	436	0.161
NT01*	0.15	0.9	5.78E-03	1.30E-03	7.51E-06	3.46E-03	59.4	120	512	0.266
B73	0.15	0.8	5.00E-03	1.60E-03	8.00E-06	2.33E-03	40.3	73	364	0.241
B72	0.15	0.3	2.00E-02	6.50E-04	1.30E-05	1.03E-04	11.3	49	26.4	3.614
2069	0.15	1.5	1.40E-02	3.60E-03	5.04E-05	2.52E-03	39.2	120	33.3	27.299

3.6 Applicability in heterogeneous aquifers: effective parameters of the equivalent homogeneous aquifer

The approaches described in the previous sections of this chapter require homogeneous aquifers for their applicability. However, they can still be used in heterogeneous aquifers by assigning effective parameters (porosity, thickness, hydraulic conductivity and natural gradient) to an equivalent homogeneous aquifer in the surroundings of each pumping well. For verification purposes, a numerically simulated example was developed in Bayer-Raich et al. (2003) using the groundwater model of the Neckar Valley (Holder et al., 1998).

3.6.1. Plume development under heterogeneous conditions and integral pumping tests

A 200-day forward simulation was performed with a source zone of constant concentration c_0 using the Method of Characteristics (MOC) within the code MT3D (Zheng, 1990). Independent pumping tests (i. e. with sufficiently long time lag between the pumping events) were performed in each well. Figure 3.16 shows the concentration time series obtained at each well and the plume position before pumping.

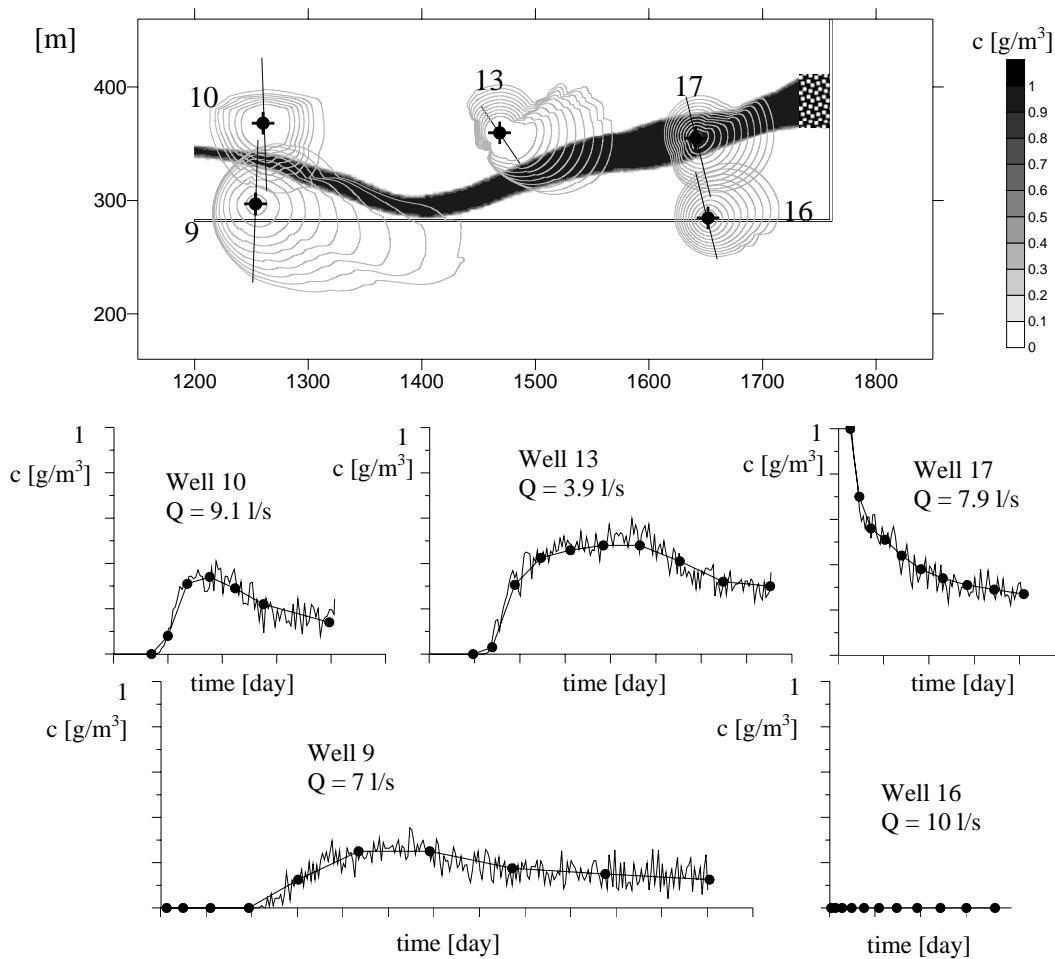


Figure 3.16: Heterogeneous model domain indicating the capture zone of each well (top). Plume developed under steady-state flow and advective conditions (bottom). After Bayer-Raich et al. (2003). Noisy line: Method of characteristics. Dots: "samples" used for inversion.

3.6.2. Effective parameters of the equivalent homogeneous aquifer

As mentioned earlier, the application of the analytical approach in heterogeneous aquifers requires effective values of the following parameters: direction (azimuth) of the mean flow direction, mean gradient of the piezometric head, mean hydraulic conductivity, porosity and aquifer thickness.

For the estimation of the mean flow direction and the gradient of the water table, several measures of the hydraulic head at different locations may be used to fit the effective gradient and azimuth through the following formulae (obtained from the best fit of a plane by the least squares method)

$$\begin{pmatrix} \sum x_i^2 & \sum x_i y_i & \sum x_i \\ \sum x_i y_i & \sum y_i^2 & \sum y_i \\ \sum x_i & \sum y_i & n \end{pmatrix} \begin{pmatrix} a \\ b \\ c \end{pmatrix} = \begin{pmatrix} \sum x_i h_i \\ \sum y_i h_i \\ \sum h_i \end{pmatrix}$$

$$\text{azimuth} = \arctan\left(\frac{a}{b}\right)$$

$$\text{gradient} = \sqrt{a^2 + b^2}$$
(3.37)

where (x_i, y_i, h_i) are the coordinates of the i -th well location and its piezometric head, and n is the number of observation wells (minimum 3, not all contained on the same straight line).

The mean hydraulic conductivity may be obtained through the drawdown observed during the pumping test (e.g. Jacob's method). Alternatively, when a numerical flow model is available, the effective hydraulic conductivity may be obtained from the groundwater flow rate across the control plane. Porosity and aquifer thickness may be measured at the wells (or taken from the numerical model).

The isochrone geometry is compared in Figure 3.17. It can be observed that the "circularity" of the isochrones decreases with increasing t_D , however the influence of heterogeneity is the more important factor that leads to "non circular" isochrones.

Table 3.2. Effective parameters used for the analytical evaluation.

Well	Porosity n_e [-]	Thickness b [m]	Hydr.Cond. K [m/s]	Gradient $ \nabla h $ [-]	q_0 [m/s]	Pumping rate Q [m ³ /s]	$r(t_{\max})$ [m]	t_{\max} [h]	$R(t_{\max})$ [m]	t_D
9	0.1	3.6	0.00834	1.17E-03	9.76E-06	7.01E-03	80.3	289	67.3	3.19
10	0.1	4.27	0.00685911	8.60E-04	5.90E-06	9.07E-03	48.1	95	47	0.35
13	0.1	2.6	0.00760918	7.66E-04	5.83E-06	3.95E-03	56.0	180	53.3	0.91
16	0.1	5.14	0.02308126	3.40E-04	7.85E-06	1.0 E-02	44.0	87	42.5	0.62
17	0.1	3.85	0.01797874	3.17E-04	5.71E-06	7.9E-03	48.0	98	47.1	0.35

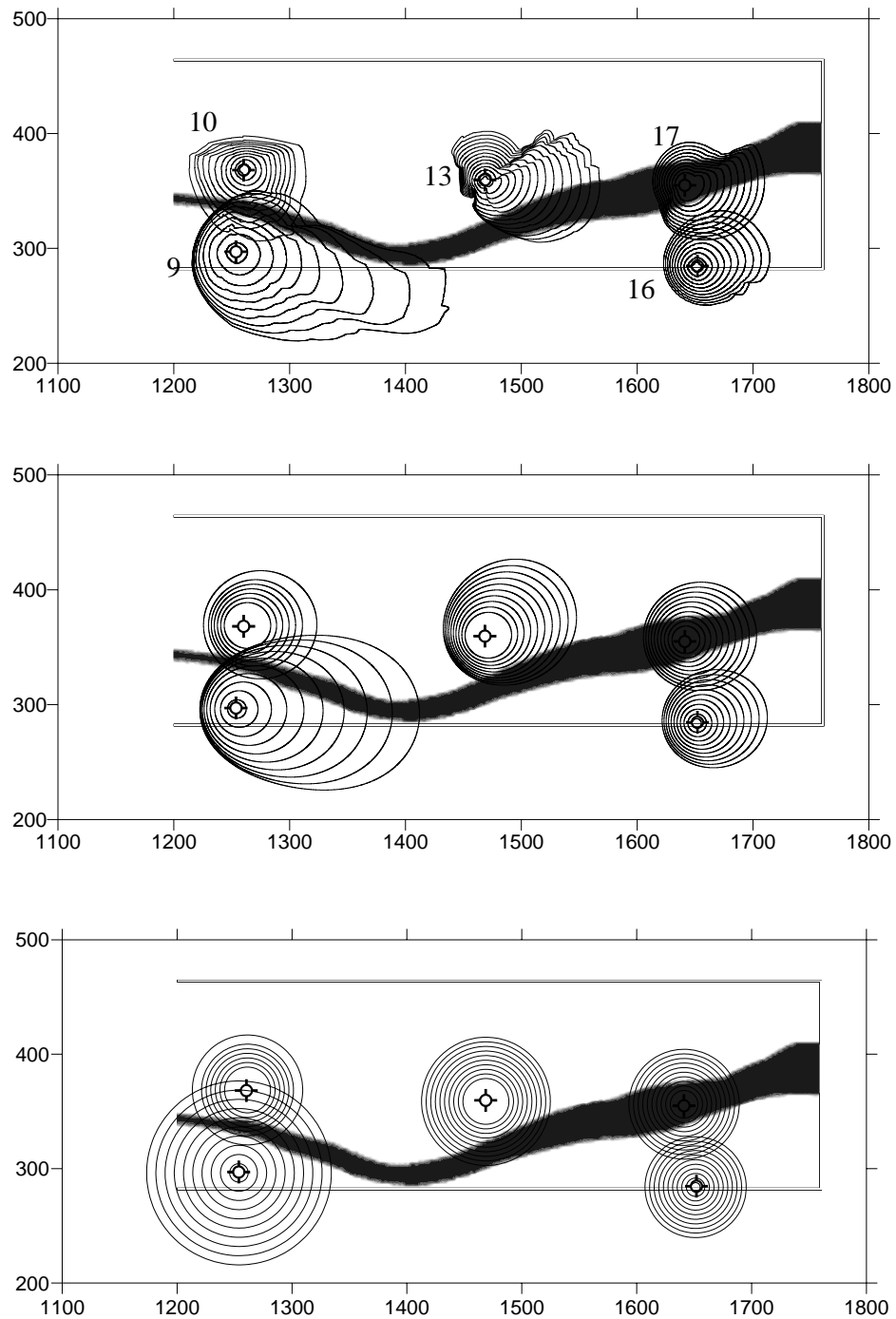


Figure 3.17: Comparison of isochrone geometry:
top: particle tracking (MODPATH, accounting for heterogeneous flow field and natural gradient)
middle: Bear & Jacobs equation. (neglecting heterogeneity, accounting for the natural gradient)
Bottom: Cylinder formula (neglecting heterogeneity and natural gradient)

3.6.3. Mass flow rate estimates

Using the parameters given in Table 3.2 and the $C_w(t)$ -curves of figure 3.16, I obtain the mass flow rate estimate for both the general and the simplified approach (evaluating equation (3.16) and (3.28) respectively). The estimated mass flow rates obtained in each well may be compared to the actual mass flow rate ($M_{CP}=1$) simulated in the numerical model (Figure 3.18).

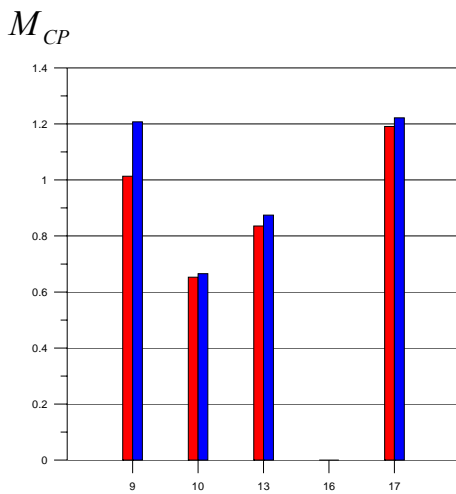


Figure 3.18: M_{CP} estimates for both analytical approaches, to be compared with the actual value $M_{CP}=1$. (left bars: general approach eq. 3.16; right bars: simplified approach eq. 3.18)

The overall relative errors in the mass flow rate estimates for wells 9, 10, 13 and 17 are 1%, -35%, -16% and 20% (general approach) and 21%, -33%, -13% and 22% (simplified approach). In wells 10, 13 and 17 the duration of the integral test fulfilled the condition $t_D < 1$, and the estimates provided by both approaches are almost the same: the errors of 20 – 30 % are due to the heterogeneity (neglecting the natural gradient does not lead to additional errors). However, in well 9, the duration of the pumping test is considerably longer ($t_D = 3.2$) and the isochrone geometry is influenced by the natural gradient (rather

developing towards the upstream direction, top figure 3.17). The relative homogeneity of the transmissivity field around well 9 (isochrones appear to be rather symmetric) is the explanation for the good performance of the general approach (error 1%), the overestimation observed for the simplified approach (error 21%) can be explained from the overestimation of the length of the control plane (circular isochrones result in a larger control plane, leading to a larger mass flow rate, see further section 3.5.1.).

The heterogeneous aquifer (mean transmissivity $T = 6.85 \times 10^{-3} \text{ m}^2 \text{ s}^{-1}$, standard deviation (of $\ln T$) = 1.6, mean saturated thickness = 3.5m) consists of poorly sorted sand and gravel deposits. The wells analysed in this section were also used to quantify mass flow rates of benzene and chlorinated hydrocarbons in Jarsjoe et al. (2003) in the Neckar Valley

In summary, this section gives a quantitative study of M_{CP} errors in a heterogeneous example (variance of $\ln T$ 2.6). Two conclusions may be extracted:

- Neglecting the heterogeneity (variance of $\ln T$ $\sigma_{\ln T} = 2.56$) leads to errors of $\pm 30\%$.

- For long pumping tests ($t_D > 1$) the simplified approach leads to overestimations of the actual mass flow rate (in the case $t_D = 3.2$ lead to a error of +20%, witch is consistent with the predictions summarized in Figure 3.10)

3.7 Depth differentiated vs. depth integrated approaches

In this section, we use the integral investigation approach to analyze a numerical realization of a contaminant plume in a heterogeneous, multi-layered aquifer, relevant for field-scale conditions. The objective is to expand the analytical approach to enable the interpretation of multi-level integral measurements, and to test the applicability of both the depth integrated and depth differentiated approaches. This verification example was developed in Bayer-Raich et al. (2002).

3.7.1. Numerical model and forward simulations

In the framework of the SAFIRA project a regional groundwater flow and transport model was developed by Borkert (1999) for transient flow conditions. The application of the integral investigation approach was carried out employing an adapted version of this transient groundwater flow and transport model.

The model was created using the graphical interface Visual MODFLOW for the numerical program code MODFLOW (McDonald & Harbaugh, 1988).

The model area is located between the Gauss-Krüger coordinates 4519000 and 4525000 (West-East direction) and 5724000 and 5717500 (North-South direction) and covers 39 km² (Figure 3.19 left). The model grid is discretized by cell widths between 25 and 200 m. At the pumping well locations, a grid refinement down to 0.5 m was introduced. The aquifer thickness of about 45 m is represented by 8 layers. Layer 1 corresponds to an artificial fill, layers 2 to 4 represent the Quaternary so-called “aquifer 110”, and layers 5 to 8 the Tertiary so-called “aquifer 500” in the vicinity of the test site. The mean groundwater recharge amounts to about 3.1 l/(s km²). The detailed distribution of the hydraulic parameters and the boundary conditions are documented in Borkert (1999). Figure 3.19 shows the geological units and a cross section of the numerical model where these units are represented.

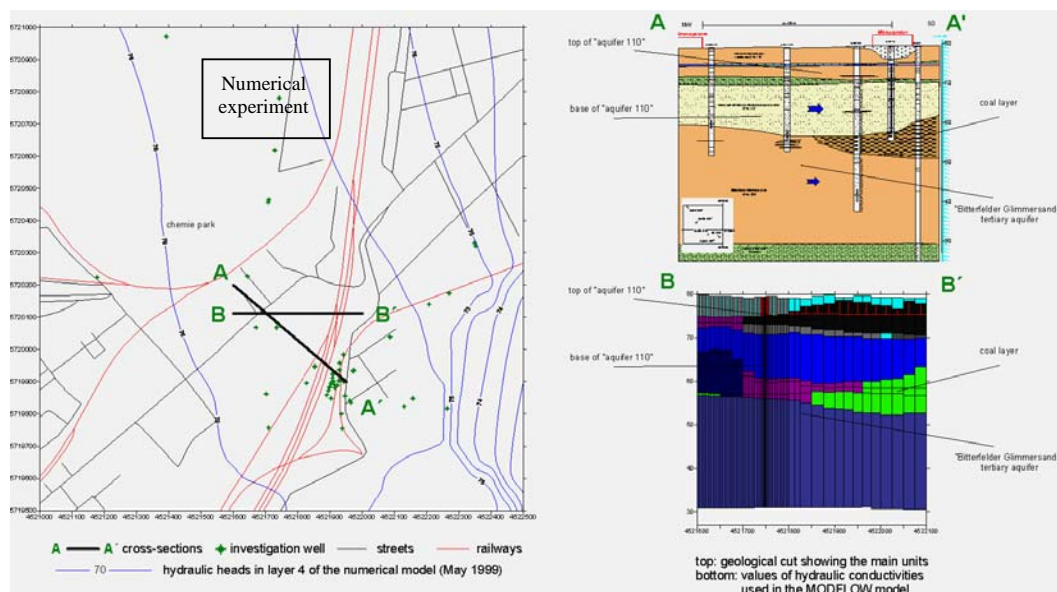


Figure 3.19: SAFIRA test site, geological units and Finite Differences flow model. The rectangle within the model domain was used to perform the numerical experiment (after Bayer-Raich et al., 2001)

The first step in the numerical experiments was the generation of a plume. Therefore I introduced a contaminant source with a length (North-South direction) of 30 m and a width (East-West direction) of 5 m into the model domain. The source was placed in layers 2, 3 and 4, with different fixed contaminant concentrations (Figure 3.20). Concentrations of 0.5 mg/l in layer 2, 0.1 mg/l in layer 3 and 1 mg/l in layer 4 were used. The distance from the source to the pumping well was about 160 m. For the generation of the plume a transient simulation over a time period of 10 years was performed. During this simulation the contaminant source acted as a constant concentration boundary condition.

The second step dealt with simulating the pumping test employed in the integral investigation approach. For this pumping test a well location outside the generated plume was selected (see Figure 3.20). The well was represented by a column of model cells with high hydraulic conductivity. A constant pumping rate of 10 l/s and a pumping time of 14 days were chosen.

Two different numerical experiments were carried out. In the depth-integrated experiment I 10 ‘samples’ (c(t)-values) of the groundwater pumped at the well were collected at the ‘pump inlet’ (model cell where discharge is applied), i.e. only one depth-integrated c(t)-curve was generated. In the multi-layered numerical experiment II, 8 ‘samples’ were taken from layer 2, another 8 ‘samples’ from layer 3, and 10 from layer 4. In the field, a new multi-level sampling technique allowing to obtain multi-level groundwater samples out of pumped wells was applied within measurements at the SAFIRA site (see further in chapter 4).

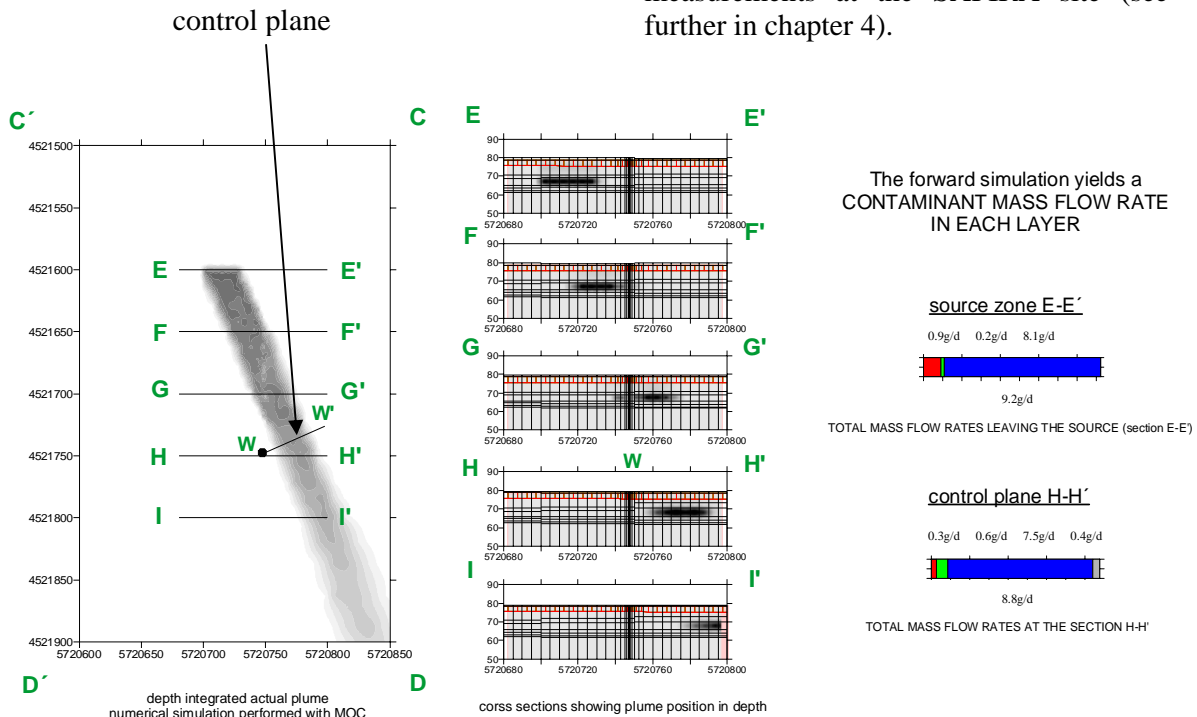


Figure 3.20: Numerically simulated plume (after Bayer-Raich et al., 2001)

3.7.2. Depth integrated approach

When there is no information about the multi-layered nature of an aquifer, it is common to assume homogeneous conditions. In this section we apply the depth-integrated approach using the $c(t)$ -curve arising from numerical experiment I in an equivalent homogeneous aquifer. The aquifer is characterized by a constant estimate of the effective value for porosity, transmissivity, natural gradient and saturated thickness.

Figure 3.21a summarizes the upscaled values used for the characterization of the aquifer (considering a constant aquifer thickness of 11 m). The position of the plume when the pumping test started is shown in Figure 3.21b, where a steady-state mass flow rate of $M=8.8$ g/d is crossing the control plane.

As a result of the (numerical) pumping test described in the previous section the depth-integrated $c(t)$ -curve shown in Figure 3.21c is obtained. Both the Method of Characteristics (MOC) and Finite Differences (FD) were used in the numerical experiment. The 10 $c(t)$ -values used for the inversion are shown in Figure 3.21c as dots (estimates between the numerically generated $c(t)$ -curves). The result of the inversion, i.e. the concentration distribution along the control plane, is shown in Figure 3.21d in comparison with the concentration along the cross section of the depth-integrated actual plume. The total (dimensionless) duration of the pumping test is $t_D = 0.02$, therefore both the general and the simplified approaches (equations (3.16) and (3.28)) lead to the same mass flow rate estimate of $M^*=12.1$ g/d.

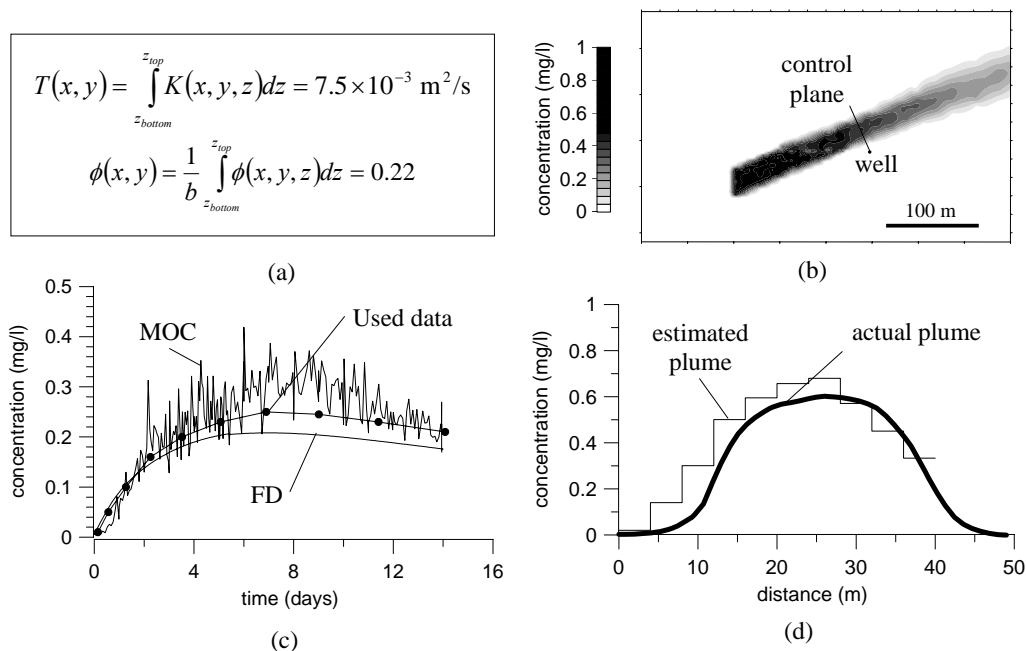


Figure 3.21 Application of the depth-integrated integral investigation approach.
 (a) Characteristic aquifer parameters. (b) 2D plume and position of the control plane.
 (c) Depth-integrated $c(t)$ -curve arising from the pumping test.
 (d) Estimated and actual values of concentration along the control plane.
 after Bayer-Raich et al. (2001)

3.7.3. Depth differentiated approach

The main limitation of the depth-integrated approach, when considering stratified aquifers, is that it cannot indicate at which aquifer level the contamination is situated. In this section, I present a new multi-layered approach that overcomes this limitation. To account for the multi-layered nature of the aquifer, the total thickness of 11 m was divided into three homogeneous layers. Different capture zones and pumping rates are considered to perform independent inversions in each layer. Since the dimensionless duration of the integral tests is very small ($t_D < 0.05$ in all cases) both approaches (simplified eq. 3.28 and general eq. 3.16) lead to the same mass flow rate estimate (differences smaller than 1 %)

Figure 3.22(a) shows the position of the plume in each layer (before the pumping starts in each layer), with steady-state mass flow rates of $M_{L2}=0.3 \text{ g day}^{-1}$; $M_{L3}=0.6 \text{ g day}^{-1}$ and $M_{L4}=7.5 \text{ g day}^{-1}$, observed at the control plane. The $c(t)$ -curves, Fig. 3.22 (b), obtained from numerical experiment II (independent sampling in each layer employing both the MOC and FD methods) are inverted with equation (3.28), yielding the estimated concentrations (Fig. 3.22 (c)) and the mass flow rates in the individual layers: $M^*_{L2}=0.9 \text{ g day}^{-1}$; $M^*_{L3}=1.6 \text{ g day}^{-1}$ and $M^*_{L4}=10.3 \text{ g day}^{-1}$.

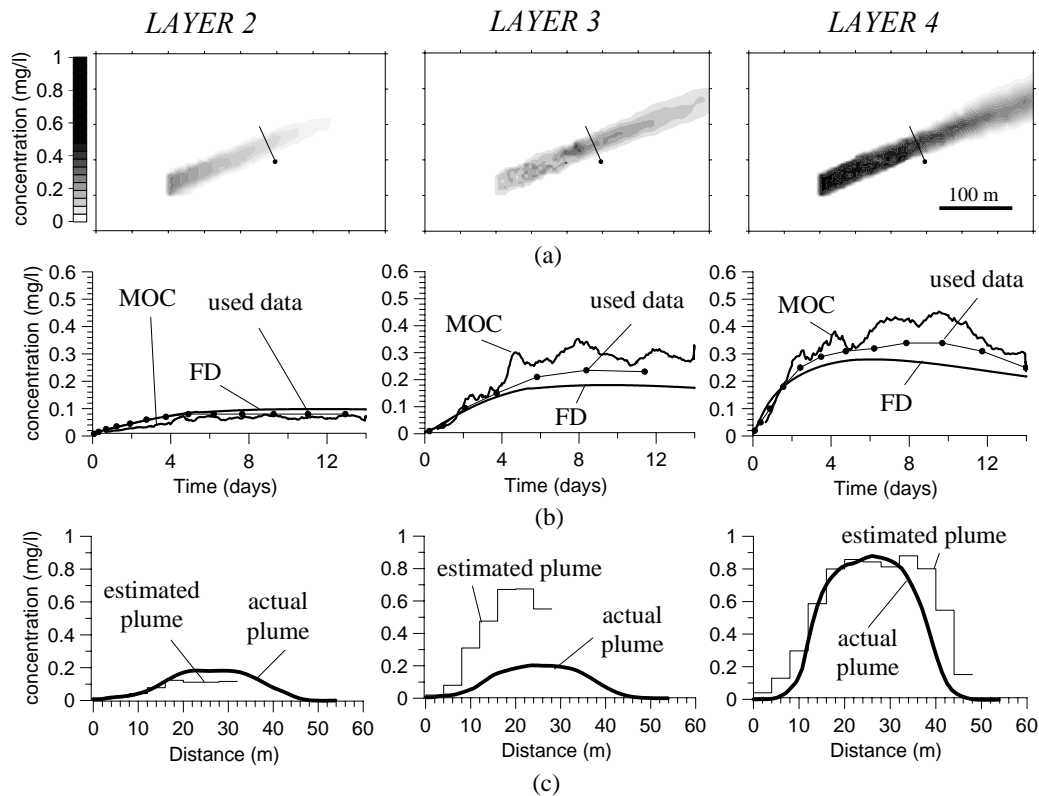


Figure 3.22. (a) plume position at the beginning of the pumping (b) $C_w(t)$ used for the inversion. (c) $C_0(x)$ Concentration along the control plane

The parameters used for the inversion are given in table 3.3

Table 3.3 Parameters used for the analytical inversion in each layer (last row gives the parameters used for the depth integrated approach)

Layer	Porosity n_e [-]	Thickness b [m]	Hydr.Cond. K [m/s]	Gradient $ \nabla h $ [-]	q_0 [m/s]	Pumping rate Q [m ³ /s]	$r(t_{\max})$ [m]	t_{\max} [h]	t_D
2	0.2	4	0.000235	1.1E-03	2.58E-07	4.56E-03	52.0	310	0.0015
3	0.2	3	0.000464	1.1E-03	5.10E-07	1.22E-03	25.2	273	0.020
4	0.25	4	0.001	1.1E-03	1.10E-06	6.0E-03	48.0	335	0.025
all	0.22	11	0.00068	1.1E-03	7.48E-07	1.0 E-02	40.0	338	0.021

3.7.4. Comparison of depth differentiated and integrated approaches

In this section I tested both the depth-integrated and the multi-layered versions of the integral investigation approach employing a contaminant plume generated in a 3D advective transport model. The simulation time was 10 years with a constant emission of the contaminant. The mass flow rate was estimated at a control plane (located 160 m downstream of the source) through a (numerical) pumping test with both the depth-integrated (method I) and the new multi-layered (method II) integral investigation approaches. Figure 3.23 summarizes the mass flux estimates arising from both methods.

Both the depth-integrated and multi-layered approaches lead to acceptable results.

The numerical experiment shows that it is possible to estimate the contaminant mass flow rate in each layer. The multi-layered approach is applicable in real aquifers when the (geological) layers are practically continuous within a zone around the pumping well, being large enough to avoid significant vertical gradients in the vicinity of the pumping well. The depth integrated approach has already been applied in practice at several sites (e.g. Holder et al. (1998), Ptak et al (2000), Bockelmann et al. (2001)).

The new multi-layered version of the integral investigation approach was applied for the first time under field conditions in Bitterfeld, using a new multi-level sampling technique allowing to obtain multilevel $c(t)$ -curves during pumping. The detailed description of the multi-level integral tests and the inversion is given in chapter 4.

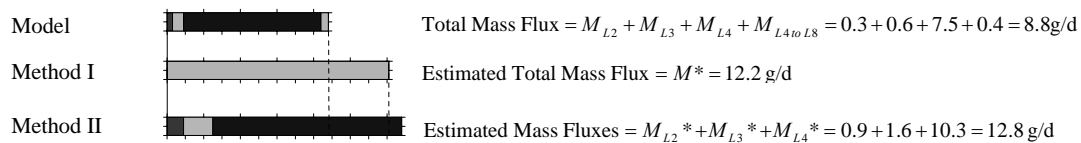


Fig. 3.23. Mass fluxes (M) in each layer and estimations of the mass fluxes (M^*) for both methods I and II

3.8. Dimensioning of Integral Pumping Tests

In this section, we investigate the dimensioning of integral pumping tests by analysing real data of already conducted pumping tests through the solutions derived in this chapter. We use the derived solution given in section 3.3 (valid for any dimensionless duration t_D of the IPT) as well as two limiting analytical solutions for both short pumping duration $t_D \rightarrow 0$ (given in section 3.4) and long pumping duration $t_D \rightarrow \infty$.

3.8.1. Analytical solution for indefinitely long pumping tests

If (dimensionless) pumping is indefinitely long ($t_D \rightarrow \infty$) the pumping well captures all contaminant located within a capture zone extension $\ell_{CP} = Q/(q_0 b)$, (Bear & Jacobs, 1965) and the concentration measured at the well becomes time-independent $C_w(t) \rightarrow C_w$. The mass flow rate is (Teutsch et. al., 2000)

$$M_{CP} = Q C_w \quad (3.38)$$

To compare this limiting solution with the solution derived in section 3.3 we express (3.38) in the form

$$C_w(t) = \int_0^{R(t)} \bar{C}_0(x) g(x, t) dx \text{ yielding,}$$

$$C_w(t_D \rightarrow \infty) = \int_0^R \bar{C}_0(x) g(x, t) dx = \frac{1}{R} \int_0^R \bar{C}_0(x) dx \quad (3.39)$$

where $R = Q/(2 q_0 b)$ is half the extent of the capture zone leading to

$$g(x, t \rightarrow \infty) = \frac{1}{R}.$$

3.8.2. Simple analytical solutions versus exact solution

To compare the limiting analytical solutions for $t_D \rightarrow 0$ and $t_D \rightarrow \infty$ to the general solution for any t_D we express them as

$$M_{CP} = q_0 b 2 R C_{av} \quad (3.40)$$

where R is half of the width of the capture zone and C_{av} is the average concentration.

3.8.2.1. Average concentration

To compare average concentrations given by the analytical and numerical approaches in a general way (i. e. valid for all $C_w(t)$), we compare the approaches in terms of the kernel of the integral equation $g(x, t)$ as written in eq. (3.26) (3.39) and (3.19). Physically, $g(x, t)$ is the contribution of the streamtube located at a distance x to the concentration sampled at the pumping well $C_w(t)$. $g(x, t)$ is defined only for $0 < x < R(t)$ since only the streamtubes located in $0 < x < R(t)$ contribute to the sample taken at time t . Figure 3.24 shows $g(x, t)$ solved numerically for $t_D = 0.1, 1, 5, 15, 30$ together with the limiting analytical solutions $g(x, t) = 2 \pi^{-1} (R(t)^2 - x^2)^{-1/2}$ (equation 3.26) and $g(x, t) = 1/R(t)$ (equation 3.39) for $t_D \rightarrow 0$ and $t_D \rightarrow \infty$, respectively. The general solution $g(x, t)$ is obtained through numerical integration with 100 isochrones, constant $\Delta x = R(t)10^{-2}$ and 1 million base points with constant $\Delta \theta = \pi 10^{-6}$ for each isochrone.

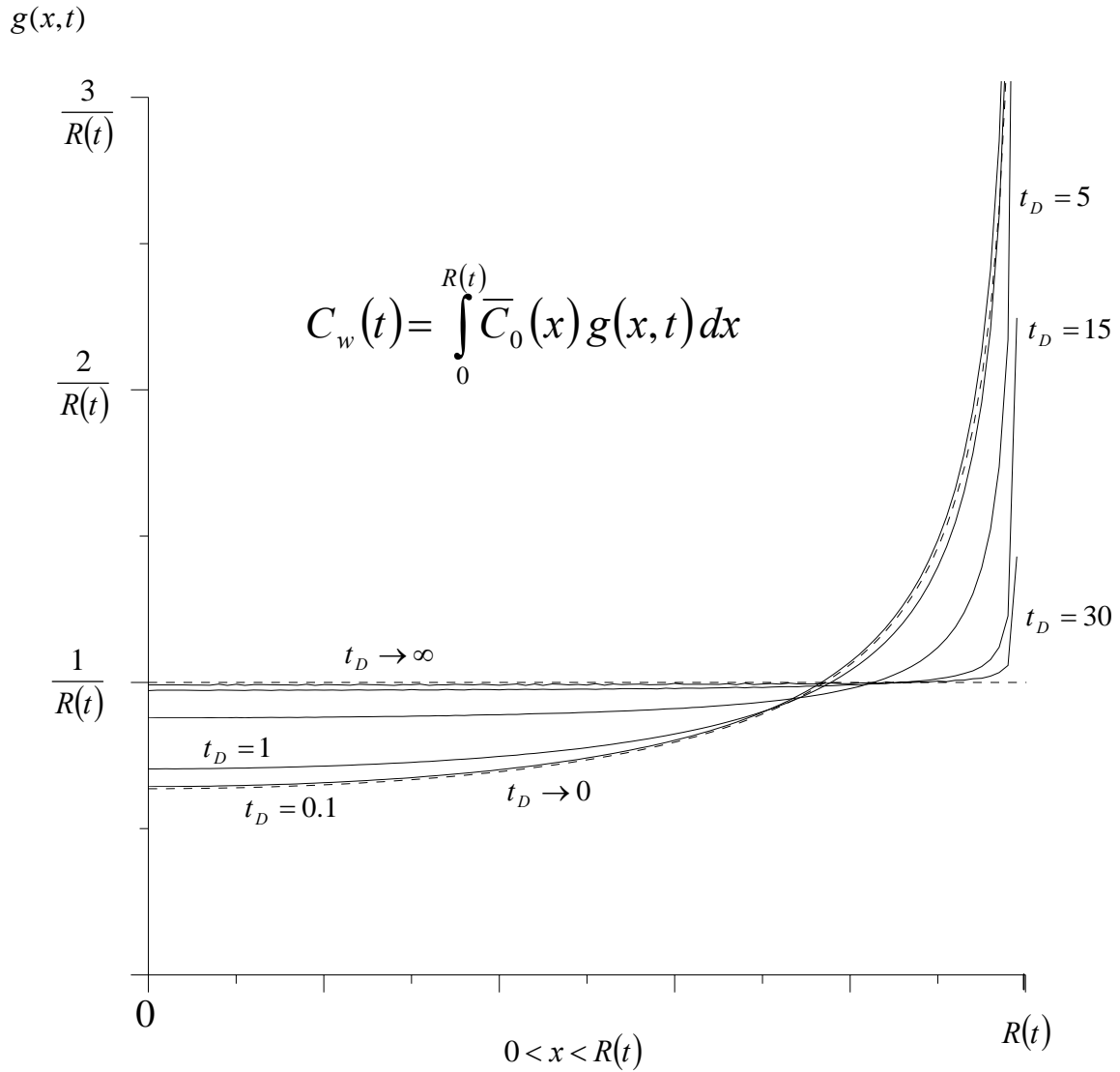


Figure 3.24: Comparison of approaches for $t_D = 0.1, 1, 5, 15, 30$.
Dotted lines: limiting analytical solutions $t_D \rightarrow 0$ and $t_D \rightarrow \infty$.

In all cases the kernel has the property $\int_0^{R(t)} g(x,t) dx = 1$, therefore the area under all curves is equal to one. It is clear from Fig. 3.24 that the differences between the limiting case $t_D \rightarrow 0$ and the general solution for $t_D = 0.1$ are relatively small (both curves overlap), and even for $t_D = 1$ the averaging function is relatively close to the analytical solution $t_D \rightarrow 0$. In the other extreme, the general solution for the case $t_D = 30$ is very close to the analytical solution $t_D \rightarrow \infty$, except at locations close to $R(t)$, where the general approach displays a steep increase. This increase is confined to a very small portion of the domain, since the total area under both curves is one, and $g(x,t)$ for $t_D = 30$ remains above $0.98/R(t)$ within the whole domain $0 < x < R(t)$. In the case of $t_D = 15$, the same reasoning holds for $g(x,t)$ being above $0.97/R(t)$ within $0 < x < R(t)$.

The above comparison is general in the sense that it does not depend on $C_w(t)$ but solely quantifies the differences in the kernel functions $g(x,t)$. One should note that these quantified core differences may, or may not, contribute to overall differences in the $C_{av}(t)$ predictions of the different methods, depending on the actual $C_w(t)$ observations. For instance, for the trivial case $C_w(t) = \text{constant} = C$, the two limiting assumptions $t_D \rightarrow 0$ and $t_D \rightarrow \infty$ both yield the correct average concentration $C_{av}(t) = C$, despite the large difference between the respective kernels (Fig. 3.24).

3.8.2.2. Mass Flow Rate

Generally, the mass flow rate in our 2D-case can be expressed as:

$$M_{CP}(t_D) = q_0 b \ell_{CP}(t_D) C_{av}(t_D) \quad (3.41)$$

The proportionality between $M_{CP}(t)$ and $C_{av}(t)$ implies that the limiting assumption effects on the predicted $C_{av}(t)$, shown in section 3.8.2.1., also influence analytical $M_{CP}(t)$ -estimations. The linearity in eq. (3.41) furthermore implies that the relative magnitude of this influence is the same for both concentrations and mass flow rates. However, the limiting assumptions also affect estimates of the capture zone extension $\ell_{CP}(t) = 2R(t)$, which in turn influences mass flow predictions through equation (3.41); this is in contrast to the $C_{av}(t)$ -estimates which are independent of the estimated $\ell_{CP}(t)$. For the limiting cases $t_D \rightarrow 0$ and $t_D \rightarrow \infty$, $\ell_{CP}(t)$ is explicitly given by $\ell_{CP}(t) = 2r(t)$ with $r(t)$ from the cylinder formula, and $R = Q/(2q_0 b)$, respectively. For the general case, we have $\ell_{CP}(t) = 2R(t)$, where $R(t)$ is given implicitly through equation (3.9). Predictions of $\ell_{CP}(t)$ by analytical expressions for the two limiting cases are shown as a function of t_D in Figure 3.25(a) (dotted lines), and are also compared to the exact, numerical, expression (solid line). Furthermore, the error introduced by these two limiting assumptions is shown as a function of t_D in Figure 3.25(b). The figure shows that the $t_D \rightarrow 0$ solution yields errors smaller than 10% for t_D smaller than 1.7, and the $t_D \rightarrow \infty$ solution yields errors smaller than 10% for t_D larger than 13. Even though the errors hence are relatively small for early and late times, they are larger than 10% for all t_D -values between 1.7 and 13, and I can conclude that analytical solutions for ℓ_{CP} resulting from these two assumptions are often not as useful as the corresponding solutions for $C_{av}(t)$ were shown to be in

the previous section. However, whereas numerical solutions for $C_{av}(t)$ are relatively cumbersome, corresponding solutions for l_{CP} (equation (3.9)) are easily obtained, and can hence be used for estimating mass flows through Equation (3.41), in combination with a relevant analytical solution for $C_{av}(t)$. In addition, more accurate and explicit polynomial expressions for $l_{CP}(t_D)$ can be obtained through series expansion of equation (3.9).

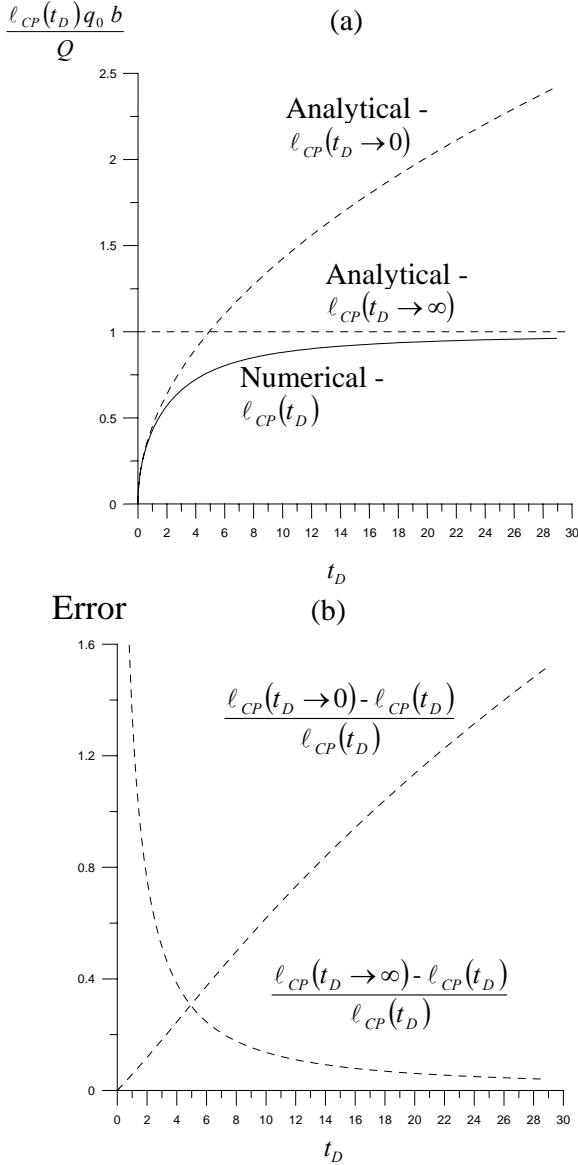


Figure 3.25: Comparison of capture zone width for the three approaches.

3.8.3. Analytical expressions versus field test conditions

In the definition of dimensionless time (equation 3.6), we recognise that there is one component that is fully determined by the aquifer properties, hereafter denoted the aquifer property term A :

$$A = bq_0^2/n_e \quad (3.42)$$

Furthermore, there is one component that is determined by the pumping rate and the pumping time:

$$E_w = t/Q \quad (3.43)$$

The dimensionless pumping time t_D can now be expressed as a function of Equations (3.42) and (3.43):

$$t_D = 2\pi A E_w \quad (3.44)$$

In contrast to A , the extraction well term E_w , can to a large extent be controlled through the way the pumping test is designed. In the following, we will investigate the relevance and accuracy of the two analytical solutions more generally, considering the range of field conditions that were reported for 55 already conducted integral pumping tests at Stuttgart, Germany (Holder et al. 1998; Bockelmann et al. 2001, 2003; Jarsjö et al. 2003), Milano, Italy (Alberti et al., 2003), Strasbourg, France (Schäfer et al. 2003), Linz, Austria (Kolesar et al. 2003; Bauer et al. 2003), Bitterfeld, Germany (Bayer-Raich et al., 2003) and Osterhofen, Germany (Rügner et al., 2003).

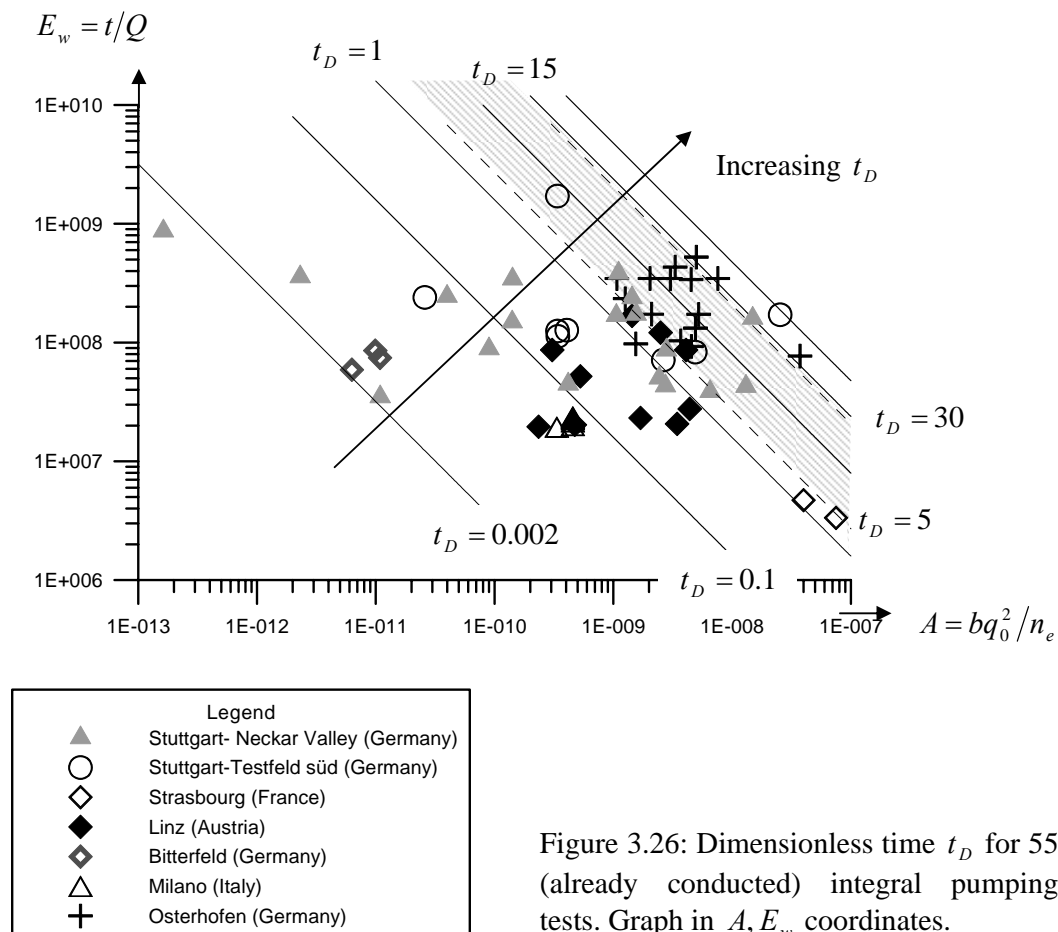


Figure 3.26: Dimensionless time t_D for 55 (already conducted) integral pumping tests. Graph in A, E_w coordinates.

The dimensionless duration t_D varies within $0.00089 < t_D < 27.36$ in these 55 tests, as shown in Fig. 3.26. Both A and E_w vary by approximately two orders of magnitude. In 42% of the tests $t_D < 1$, while $t_D < 5$ in 84%. However, these ranges are site dependent, for example, for the site in Osterhofen (Rügner et al., 2003; Maier et al., 2003) only 1 out of 15 tests had duration $t_D < 1$ (crosses in figure 3.26). In Osterhofen, nitrate mass flow downstream a land fill is strongly influenced by a steep slope of the aquifer bottom (up to 2%) leading to a high discharge q_0 (and t_D is proportional to q_0^2)

From the analysed data, both the Neckar Valley data (Holder & Teutsch, 1999) and the Testfeld Süd data (obtained further downstream in the same valley, see Bockelmann et al. 2001, 2003) display the highest variability of the aquifer property term A . Data from 185 wells with withdrawal, recovery and slug tests indicate a variance (of $\ln T$) as high as $\sigma_{\ln T}^2 = 2.6$.

The minimum value of A is found in the Neckar Valley data set where the aquifer parameters are as follow: thickness $b = 1.2$ m, specific discharge $q_0 = 8.33 \cdot 10^{-9}$ m/s and porosity $n_e = 0.1$ leading to $A = 1.63 \cdot 10^{-13}$ m³ s⁻². The very low hydraulic conductivity ($K = 8.33 \cdot 10^{-5}$ m/s)

limits the extraction Q to 0.6 l/s (at this site, the mean value is 4.6 l/s) and therefore a relatively long pumping period of $t=6$ days was required (mean value at the site: 5 days). This resulted in a dimensionless pumping duration as low as $t_D = 0.0009$.

The maximum values of A are found in wells 2069 in (Bockelmann et al. 2001, 2003) with parameters ($A=2.5 \cdot 10^{-8}$) B60 in Rügner et al. 2003 with ($A=3.7 \cdot 10^{-8}$) and well IPT2 in Schäfer et al. 2003 ($A = 7.5 \cdot 10^{-8}$). Although the values of A are similar, the aquifer parameters are significantly different, as shown in Table 3.4.

Table 3.4: Parameters of the IPTs with high values of $A = bq_0^2/n_e$ [s^2m^{-1}]

Well	b [m]	q_0 [m/s]	n_e [-]	Q [l/s]	t [h]	t_D [-]
2069	1.5	$5 \cdot 10^{-5}$	0.15	2.52	120	27.4
B60	11.2	$2 \cdot 10^{-5}$	0.12	4.49	96	18.06
IPT2	49.7	$1.4 \cdot 10^{-5}$	0.13	77.5	72	1.6

Both wells B60 and 2069 were characterized by a very high Darcy flux q_0 and a relatively small thickness, which limited the possible extraction rates. For these wells the dimensionless time is the highest of the study. In the case of IPT1 and IPT2 in Strasbourg, high pumping rates were possible in the thick aquifer, thereby reducing $E_w = t/Q$ by two orders of magnitude, compared to the pumping rates in Bockelmann et al. (2001) and Rügner et al. (2003), yielding t_D -values of 1.2 and 1.6 (one order of magnitude smaller).

3.8.4. Dimensioning the duration of integral pumping tests

I here express the conclusions in terms of a dimensionless pumping time $t_D = 2\pi b q_0^2 t / Q n_e$. The reason for the focus on t_D is that each t_D yields unique problem characteristics, for instance in terms of the shape of the well capture-zone border, in contrast to other influential parameters such as Q , t or q_0 , for which one can find a very large number of relevant parameter combinations that still yield the same overall characteristics. Two different limiting analytical solutions were obtained considering the 2D problem, corresponding to short and long t_D . In addition I obtained a general, numerical, solution relevant for any t_D .

A comparison between the general numerical solution for C_{av} and the limiting analytical solution for short t_D showed that the approximate, analytical solution was accurate, at least, for $t_D \leq 1$. A corresponding comparison showed that the analytical solution for long t_D is accurate, at least, for $t_D \geq 30$. This conclusion is general in the sense that it holds for any physically feasible variability of the concentration observations (samples) in the well. Moreover, mathematical analysis of the derived expressions also shows that, and in which way, their accuracy generally increases with decreasing variability. Specifically, deviations caused by the limiting assumption will be averaged out through integration, which takes place to a larger degree if the concentration variability is smaller. For instance, this implies that the limiting assumption for short t_D can be accurate for t_D -values up to 5 or more (for the trivial case of constant concentration, both the limiting solution for short t_D and the one for long t_D yield

the same and correct result, regardless of the actual t_D -value).

Furthermore, we formulate expressions for mass flow rates across control planes (perpendicular to the flow direction with their extent being defined through the capture-zone extent). The limiting analytical solutions for C_{av} are also directly relevant for the M_{CP} -expressions, however the latter expressions require, in addition, quantification of the control plane length, which can be determined exactly through relatively limited numerical effort, or even analytically using a power series expansion. Note that this is in contrast to the numerical solution of the equations for C_{av} (also developed here), which is generally non-trivial, providing motivation for our further development of accurate limiting analytical expressions.

An assessment of t_D -values using field data from throughout Europe, for 55 conducted Integral Pumping Tests (IPTs, in which the contaminant concentration was measured as a function of time in pumping wells) showed $t_D \leq 1$ in 42% of the cases, $t_D \leq 5$ in 84% of the cases, and $5 < t_D < 30$ for the last 16% of the cases, indicating that the limiting analytical solution for short t_D is relevant for a vast majority of the cases. Furthermore, even though aquifer properties influence t_D , we show through relatively simple analyses that the t_D -values can be considerably adjusted (by an order of magnitude or more) in the design of the pumping test, enabling relevant application of the solution for short t_D in many aquifers. The solution for long t_D on the other hand, is primarily relevant if the pumping is of more permanent nature (e.g., for establishing hydraulic barriers).

Chapter 4

NUMERICAL APPROACH FOR HETEROGENEOUS AQUIFERS

This chapter describes the numerical approach for the interpretation of integral pumping tests in heterogeneous aquifers. To solve the governing equations in heterogeneous media, the flow field and the aquifer geometry have to be represented in a numerical groundwater model. The numerical approach for the interpretation of integral pumping tests was first proposed in Ptak et. al. (2000) and implemented in the C++ code C1 (Schwarz, 2002). The code C1 has been rewritten and extended in a newly implemented algorithm called CSTREAM. The code CSTREAM has been tested using numerical simulations and applied to a total of 5 different real sites during the framework of this thesis: Bitterfeld (Germany) for the project SAFIRA and Stuttgart (Germany), Strasbourg (France), Linz (Austria) and Milano (Italy) for the project INCORE.

4.1 Groundwater modeling with MODFLOW and MODPATH

To enable numerical interpretation of concentration time data in heterogeneous flow fields I use the finite-difference code MODFLOW96 (McDonald & Harbaugh, 1988) for solving the groundwater flow and the particle-tracking code MODPATH 3.0 (Pollock, 1994) for describing streamlines and isochrones through particle tracking. For the development of the MODFLOW-MODPATH model, graphical pre-processors may be used (the programs VISUAL MODFLOW 3.0.0 (Waterloo Hydrogeologic Inc., 2002) and Processing

MODFLOW 5.1.7 (Chiang & Kinzelbach, 1999) have been tested explicitly). Future versions of MODFLOW and MODPATH will require to updating CSTREAM to correctly write/read the MODPATH input/output files to perform the particle tracking.

4.2 Code CSTREAM

Within the code CSTREAM, both the analytical approach (described in chapter 2) and the numerical approach have been implemented. In addition, a module for producing SURFER files out of MODPATH simulations has been included. The structure of the program is diagrammed in Figure 4.1:

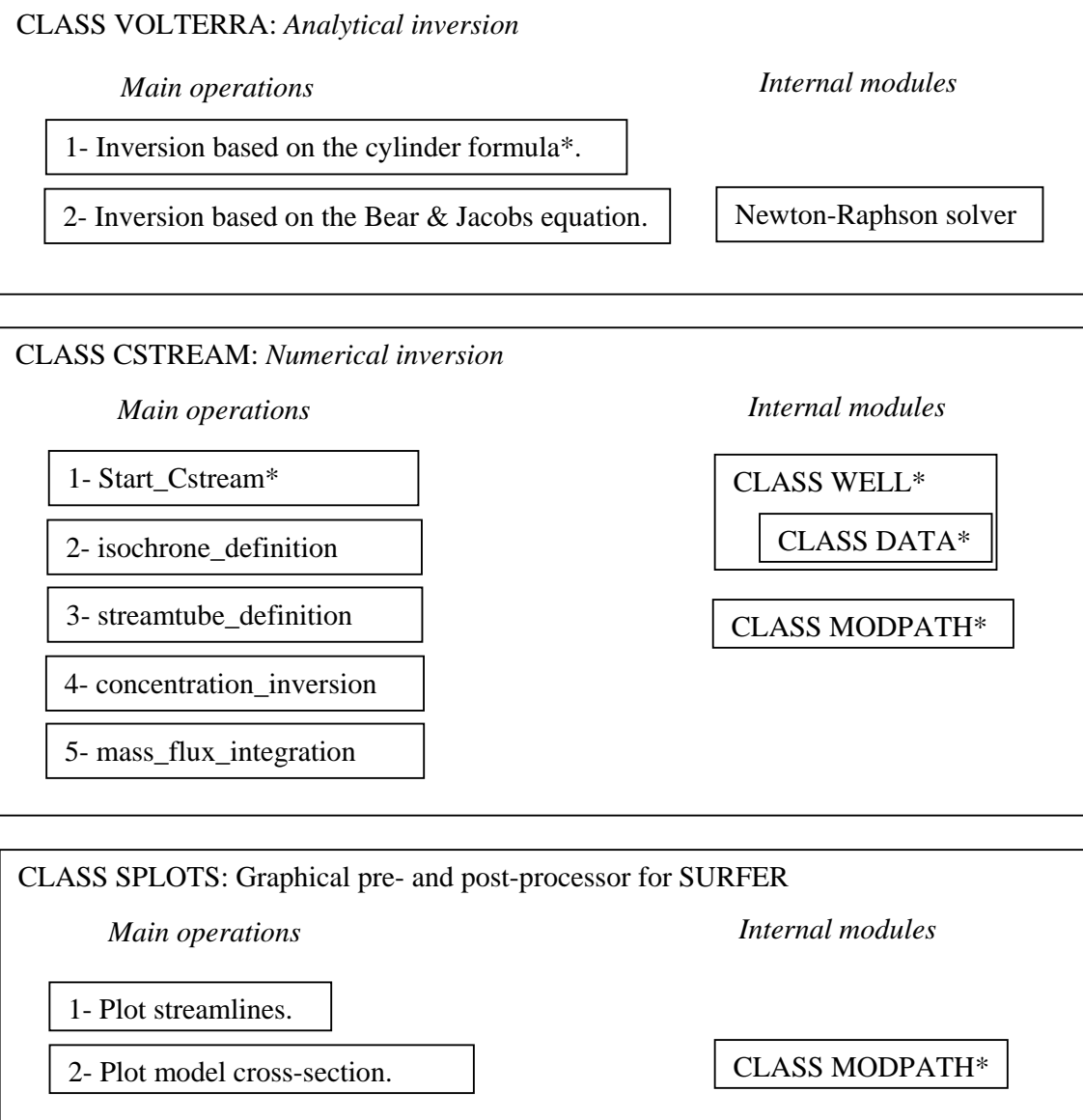


Figure 4.1: Main modules of the code CSTREAM. The modules marked with * were originally developed for the code C1 (Schwartz, 2002). All other modules have been developed and tested in the framework of this thesis.

4.2.1. History of CSTREAM: the code C1

The original code C1 (Schwarz, 2002) was used, modified and finally rewritten in the framework of this Thesis. The object oriented structure of the code C1 was very useful for implementing both new and old algorithms in C++. The newly developed code CSTREAM is divided in 5 steps to perform the numerical inversion:

- Initialization
- Isochrone definition
- Streamtube definition
- Concentration inversion
- Mass flow rate integration

Only the first step (initialization) is based on the previous work developed by Schwarz (2002) in the code C1. The object oriented structure of the code C1 made possible to analyze each internal module independently. After testing, the classes “modpath” and “well”, originally implemented in C1, were modified and implemented in the new code CSTREAM. The following four steps (Isochrone definition, streamtube definition, concentration inversion & mass flow rate integration) are newly written: a description of each is given in the following sections.

4.2.2. Initialization

During the initialization of Cstream, the codes MODFLOW and MODPATH are executed, the geometry of the MODFLOW grid as well as the flow velocities in all grid cells are read from the ASCII and binary input/output files using the module “class modpath”, originally developed within the code C1 (Schwarz, 2002). A first MODPATH run is used to find the limits of the capture zone for each well. Based on the geometry and extent of the capture zone, a uniform grid is created, the

so-called “CSTREAM grid”, which defines the sub-domain of the MODFLOW model. The CSTREAM grid is uniform (constant $DX=DY$) and is defined by the coordinates of the bottom left (OX,OY) and the number of cells in x and y directions (NX,NY). Given the top, bottom, left and right limits ($max_y, min_y, max_x, min_x$) of the capture zone defined through particle tracking, the Cstream grid is automatically defined using the formulas:

$$\begin{aligned} OX &= \min_x - \frac{(\max_x - \min_x)}{2} \\ OY &= \min_y - \frac{(\max_y - \min_y)}{2} \\ NX &= (\text{int}) 2 \frac{(\max_x - \min_x)}{DX} \\ NY &= (\text{int}) 2 \frac{(\max_y - \min_y)}{DY} \end{aligned} \quad (4.1)$$

where $max_y, min_y, max_x, min_x$ are obtained from the coordinates of the particles (read from the MODPATH output files) and DX must be input by the user (int) indicates integer part (i. e. closest natural number). The CSTREAM Grid may be defined by the user by setting (OX, OY, NX, NY and DX). The CSTREAM grid is placed “on the top” of the MODFLOW grid, as indicated in Figure 4.2.

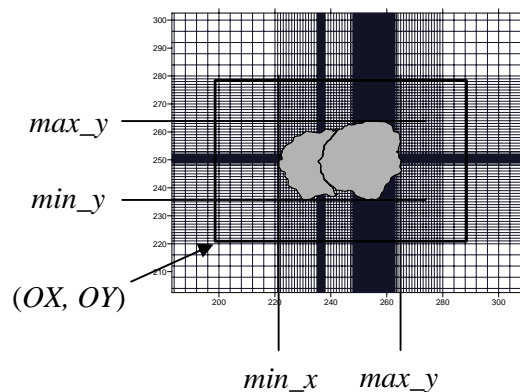


Figure 4.2: Definition of the limits of the CSTREAM grid.

In order to define the control plane perpendicular to the *mean flow direction*

CSTREAM uses the hydraulic heads obtained at the end of the first stress period, which represent the steady-state flow field before the integral pumping test started. In order to obtain a representative *mean flow direction* for the area surrounding the integral pumping tests, 9 “observation points” are used to fit the hydraulic heads $h_0(x, y)$ to a linear equation $h_0^*(x, y) = ax + by + c$. The location of these 9 observation points is defined as a function of max_y , min_y , max_x , min_x as indicated in Figure 4.3.

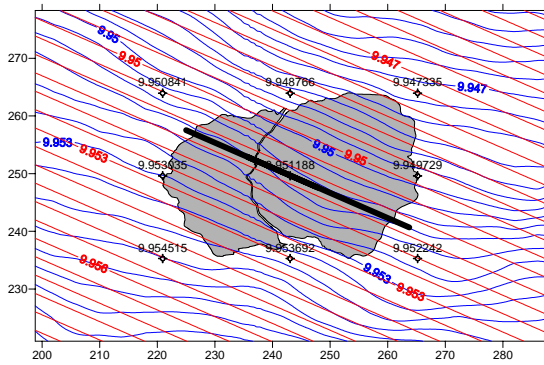


Figure 4.3. Location of the 9 points used to fit a linear equation. Curved lines: Steady-state hydraulic heads (extracted from the MODFLOW model), Straight lines: best fit of the linear equation. Thick line: Control plane.

Fitting a linear equation $h_0^*(x, y) = ax + by + c$ to the 9 sets of values (x_i, y_i, h_i) for $i=1$ to 9 using the least squares method, reduces to solving the following system of linear equations:

$$\begin{pmatrix} \sum x_i^2 & \sum x_i y_i & \sum x_i \\ \sum x_i y_i & \sum y_i^2 & \sum y_i \\ \sum x_i & \sum y_i & 9 \end{pmatrix} \begin{pmatrix} a \\ b \\ c \end{pmatrix} = \begin{pmatrix} \sum x_i h_i \\ \sum y_i h_i \\ \sum h_i \end{pmatrix} \quad (4.2)$$

From the solution (a, b, c) , both the average hydraulic gradient and the mean flow direction are obtained through:

$$\begin{aligned} azimuth &= \arctan\left(\frac{a}{b}\right) \\ gradient &= \sqrt{a^2 + b^2} \end{aligned} \quad (4.3)$$

Azimuth and gradient will be used in the last step of the computation “mass flow rate integration”: the azimuth provides the direction of the control plane, and the mean gradient is used to estimate an effective value of the mean hydraulic conductivity.

During the initialization, the hydraulic head, Darcy velocities, and aquifer thicknesses are read at all cells of the MODFLOW grid. The concentration-time data are read from the well information ASCII file and all relevant variables that will be used in the program are allocated in the memory and initialized.

4.2.3. Isochrone definition

The objective of this phase is the definition of the isochrones for each sample taken during the integral pumping test. The isochrone at the sampling time t is defined here as the initial location (i. e. $t=0$) of the volume of water sampled at the pumping well between the times $t_i - \Delta t_i$ and t_i (taking the limit at $\Delta t_i \rightarrow 0$), therefore we get

$$\begin{aligned} Q\Delta t_i &= \\ &= \int_{V_i(t_i)} n_e(x, y, z) dV - \int_{V_i(t_i - \Delta t_i)} n_e(x, y, z) dV = \\ &= \sum_{k=1}^{NPART} \Delta V_{ik} \end{aligned} \quad (4.4)$$

where $V_i(t)$ is the aquifer volume captured up to time t . The numerical implementation of equation (4.4) requires the discretization of the isochrone length by $NPART$ backtracked particles. Two MODPATH runs with $NPART = 3600$ particles each ($NPART = 3600$ is the default value, but may be changed by the user) are performed, both ending at the time when the well starts pumping (i. e. $t = 0$) but starting at times t and $t - \Delta t_i$. The $NPART$ particles are located along a circle inscribed in the well cell. The isochrone volume is then defined through $NPART$ cells ΔV_{ik} (for each isochrone i), each cell defined with a 4-vertex polygon of area $Area(\mathbf{x}_{ik})$ (defined by 2 particles of the “inner” isochrone and two particles of the “outer” isochrone as shown in Figure 4.4. Then the final volume is computed as the sum of ΔV_{ik} for all k , defined as

$$\Delta V_{ik} = n_e(\mathbf{x}_{ik}) b(\mathbf{x}_{ik}) Area(\mathbf{x}_{ik}) \quad (4.5)$$

where $n_e(\mathbf{x}_{ik})$ is the porosity and $b(\mathbf{x}_{ik})$ is the aquifer thickness (the thickness of the

considered layer as set in the MODFLOW GRID geometry) at the location \mathbf{x}_{ik} .

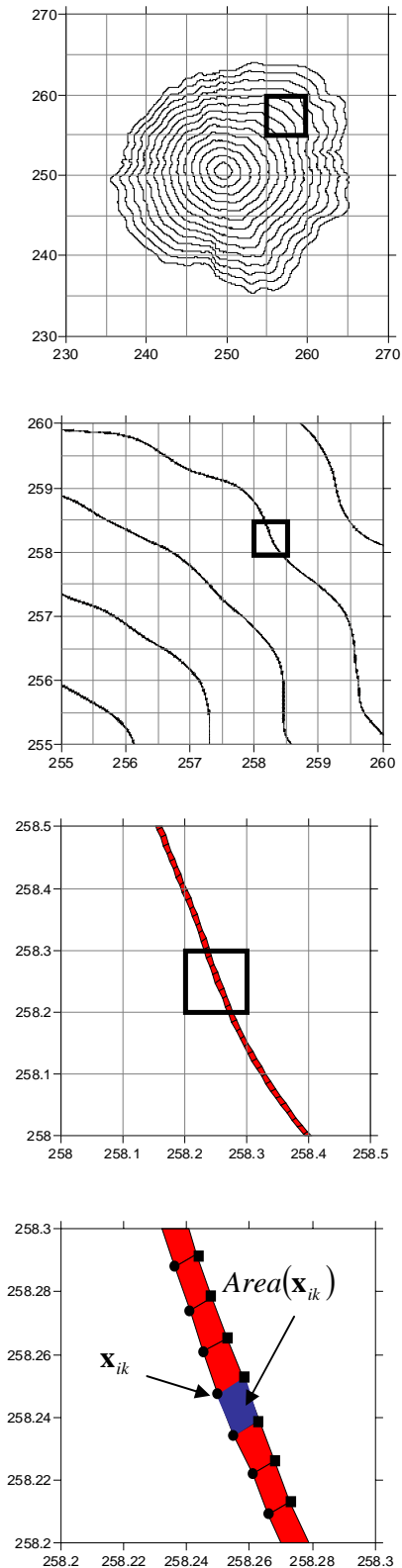


Figure 4.4. Detail of the volume defined by the isochrone.

Δt_i is computed for each isochrone as a function of both t_i and $NPART$, with the formula:

$$\Delta t_i = \frac{8 \pi t_i}{NPART} \quad (4.6)$$

which was derived by imposing a condition on the shape of ΔV_{ik} : the distance between particles in the “inner” and “outer” isochrones is twice the distance between both isochrones for perfectly radial flow. This algorithm was also tested under heterogeneous conditions, as will be shown later in this chapter.

The numerical computation of the isochrones opens the possibility to define irregular capture zones in homogeneous and heterogeneous media. Even if the heterogeneity is not known in detail (and therefore an equivalent homogeneous aquifer is assumed) it is clear that when using multiple well interpretations, the integral tests may influence each other. The mass flow rate estimates may be affected by the way we perform the integral tests: sequential and/or simultaneous pumping and the order the wells are pumped. Figure 4.5 shows different possibilities for the computation of the isochrones and compares the geometry to the analytical isochrones. A homogeneous aquifer with a natural Darcy’s flow field $q_0 = 0.2169$ m/day, porosity $n_e = 0.25$ and thickness $b = 4$ m was used to perform 5 integral pumping tests of 1 day duration each, at a constant pumping rate of $Q = 10$ l/s. The first possibility for the computation of the isochrones is called here *independent isochrones*, and consists in neglecting the influence of previous integral tests in other wells. Under this assumption, the isochrones may be computed analytically, which is easier and cheaper since no numerical modeling is involved. The numerical approach is capable of considering the actual position of the

capture zone of each well (accounting for the order the wells were pumped in). A numerical experiment with 3 different sequences of pumping show how the overlapping in this case is virtually zero.

The second sub-figure in 4.5 shows the shape of the isochrones when all 5 wells were pumped simultaneously: what is called here *simultaneous isochrones*. In practice, this approach is limited by the total number of pumps available.

The last two sub-figures in 4.5 show the isochrones obtained by sequential pumping tests: *sequential isochrones*. Many possibilities could be designed here, including a combination of sequential pumping of groups of wells pumped simultaneously.

It is interesting to observe that simultaneous or sequential pumping of wells located along the same control plane does not produce significant overlapping of the well capture zones (therefore is not capable to resolve the left-right uncertainty for each well), however the total length of the control plane is captured and any potential plume located between the wells would be detected in such a test. Here, the analytically derived isochrones show a fictitious overlapping, since the size of the capture zone is overestimated. If the position of the plume relative to the wells needs to be resolved, the control plane could be divided in two rows of wells better than locating all wells along the same line. The reason why the isochrones computed numerically do not overlap is that $t = 0$ is the start of pumping of the first well. The location of the capture zones are obtained for all wells at $t = 0$ since this is the latest time where the flow field and the plume position corresponded to natural undisturbed conditions $\vec{q}_0 \cdot \vec{\nabla} C_0 = 0$. The interpretation time has to be $t = 0$ since after this time, pumping leads to a displacement of the plume leading to $\vec{q}_0 \cdot \vec{\nabla} C_0 \neq 0$.

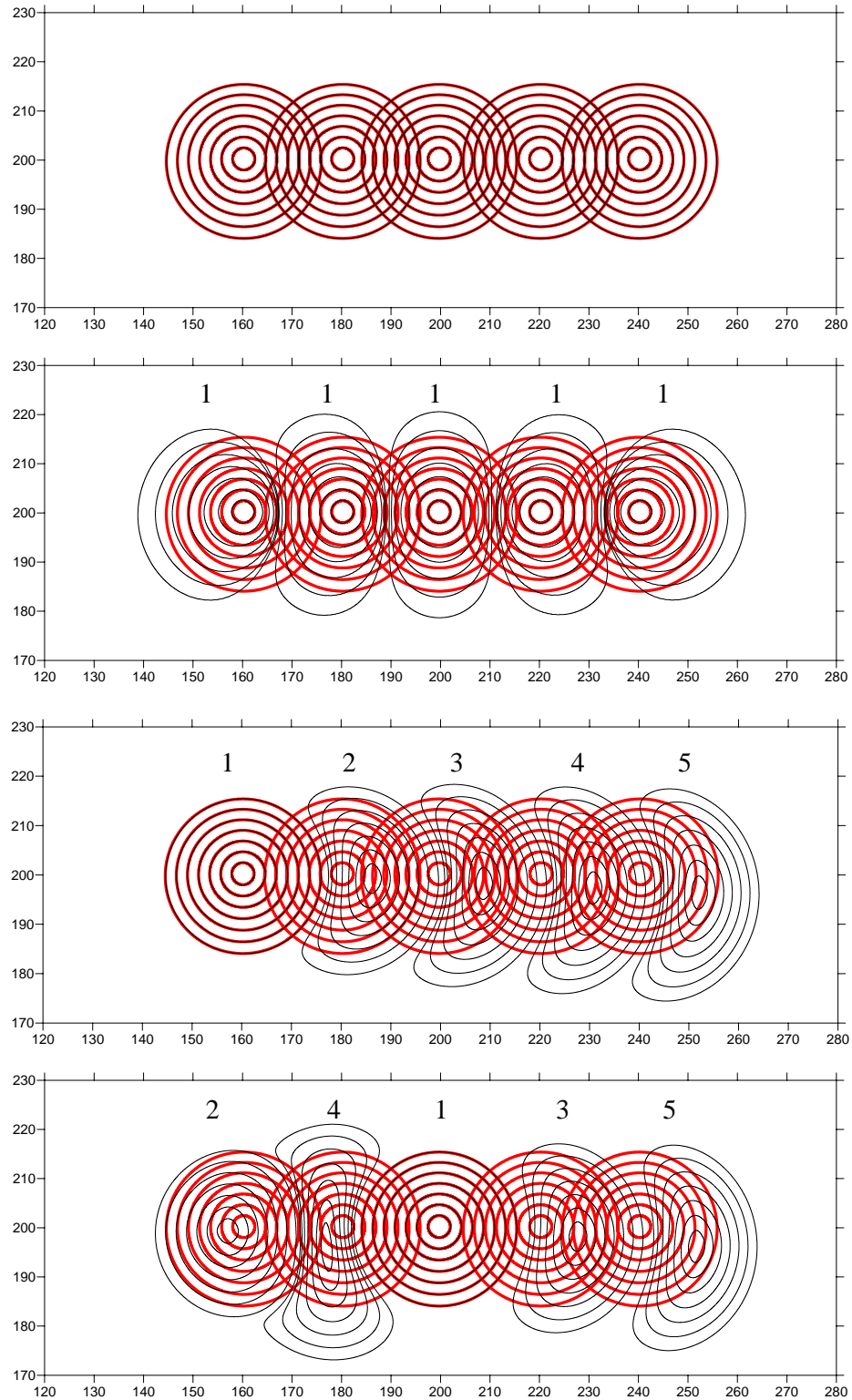


Figure 4.5: Comparison of numerical and analytical isochrones: *independent isochrones* (top), *simultaneous isochrones* (below) and two different possibilities for *sequential isochrones* (bottom). The numbers indicate the order of pumping, all pumping tests were 1 day long. Analytical geometry of the isochrones (Bear & Jacobs, 1965) shown in thick lines.

4.2.4. Streamline definition

The inversion of the concentrations requires partitioning of the domain into a finite number of streamtubes. The steady-state flow field (before the integral tests start) is used to track particles in the direction of the flow. The pathlines correspond exactly to the streamlines (since the flow field is steady-state). The natural flow field \bar{q}_0 is read from the MODPATH CBF binary file at the center of each cell of the CSTREAM GRID. The methodology used to perform the particle tracking is shown in Figure 4.6.

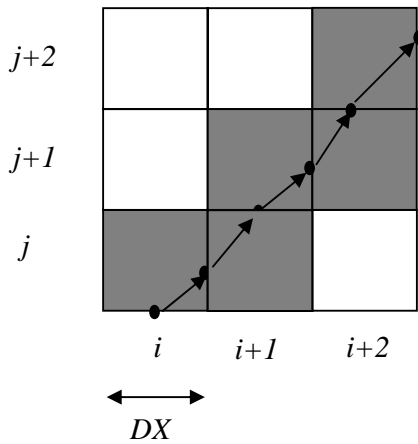


Figure 4.6: Definition of the streamlines along the CSTREAM GRID

The (x,y) position of the particle is calculated and the corresponding cell (i,j) is marked with an integer index. This particle tracking algorithm is started from all cells which belong to the boundaries of the CSTREAM GRID, i. e. cells of the bottom boundary $(i,1)$ for $i=1,NX$; cells of the left hand side boundary $(1,j)$ for $j=1,NY$; cells of the right hand side boundary (NX,j) for $j=1,NY$; cells of the top boundary (i,NY) for $i=1,NY$.

The necessary conditions for a streamline to be considered well defined are:

1- The streamline quits the domain without intersecting previously defined streamlines

2- The streamline contains a minimum of MIN_NUM_CELLS cells.

The variable MIN_NUM_CELLS is set by default to the smaller of $NX/2$ and $NY/2$, but can be modified by the user. The field of streamlines must be such that one streamline (and only one) is at the left extreme, and one streamline (and only one) is at the right extreme (were left and right are considered with respect to the flow direction, Figure 4.7). The reason is that in the next step, all streamlines will be re-numbered from left to right (and therefore, only one streamline must be at the left extreme and also one streamline must be to the right). The algorithm for defining the streamtubes is described in figure 4.8

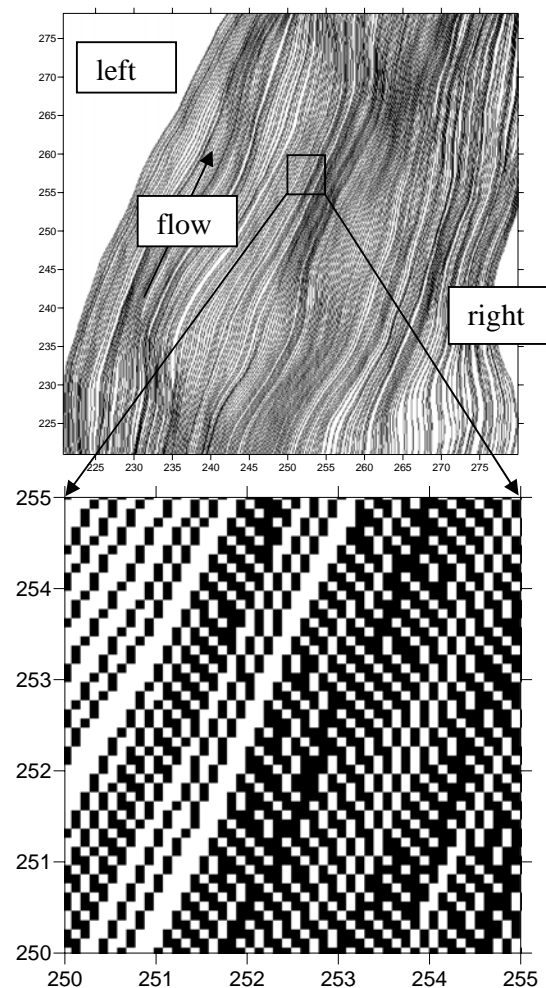


Figure 4.7: Field of streamlines generated with $DX=0.1$ m

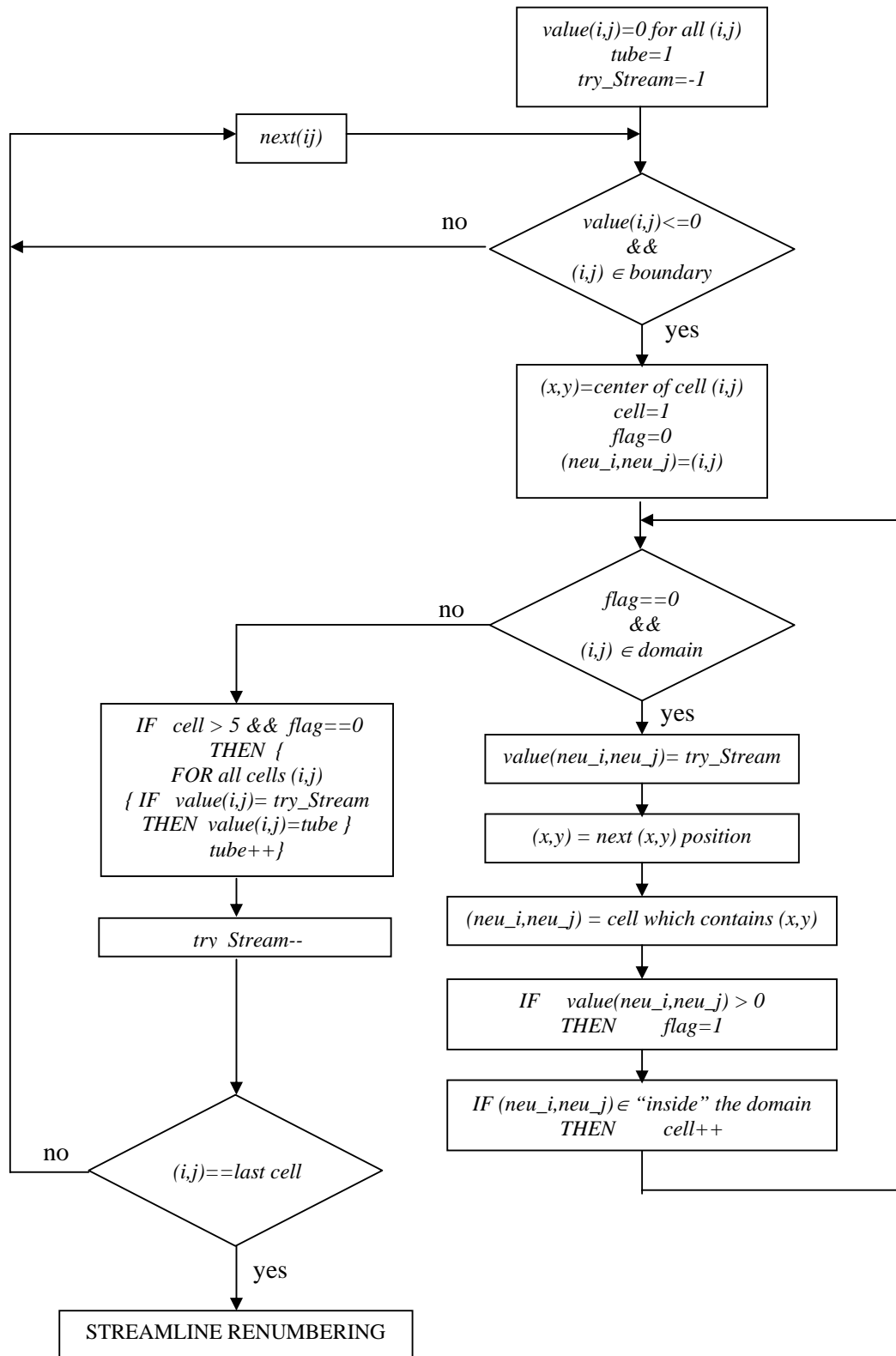


Figure 4.8: Flow diagram of the algorithm implemented in CSTREAM for the definition of the streamlines.

As a result of the previous phase, a matrix of size $NX \times NY$ was partially filled with numbers identifying the streamlines. However, many cells of the domain do not belong to any streamline (i. e. white cells in figure 4.9). To renumber the streamlines from left to right, four different possibilities are considered depending on the mean flow direction: North-East, South-East, South-West and North-West.

In the example shown in Figure 4.9, the mean flow direction is to the North-East, therefore the renumbering of the streamlines starts at the top-left cell moving in the direction of the rows and ending at the bottom-right cell.

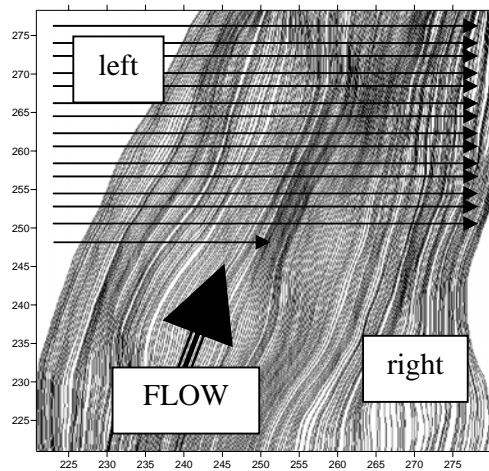


Figure 4.9. Direction of the renumbering when the mean flow is to the North-East.

When the mean flow direction is to the South-East, South-West or North-East, the algorithm is the same but only the direction of the re-numbering changes. If the flow is to the South-East the renumbering starts at the top-right cell and moves along columns until the bottom-left corner. If the flow is to the South-West the renumbering starts at the bottom-right cell and moves along rows until the top-left corner. If the flow is to the North-West the renumbering starts at the bottom-left cell and moves along columns until the top-right corner.

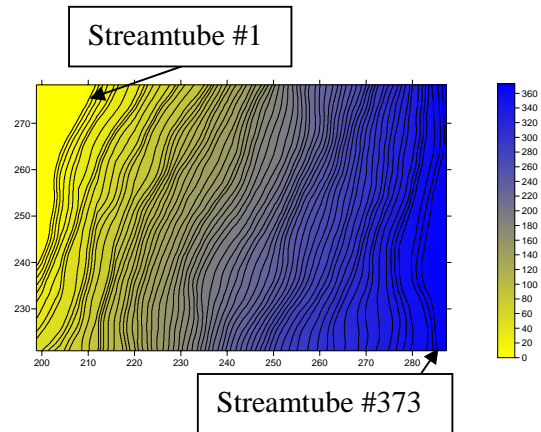


Figure 4.10. Streamlines after renumbering.

Figure 4.11 gives an example of the renumbering algorithm for the case of North-East flow. The first cell (top-left) is set with the value 0 and all successive cells (moving from left to right) are also set to 0 until the first streamline is encountered (in this case, streamline number 56). At this point the cell is set to 1, from this point all successive cells are marked with a 1 until the next streamline is encountered (streamline number 54). The cell containing the streamline 54 is set to 2. Figure 4.11 shows the values at the matrix both before and after the renumbering. At the end of this process all cells belong to one (and only one) streamline, and the streamtube number increases from left to right in the flow direction.

At the end of this phase, a single matrix is printed in a SURFER grid file, which allows to plot the streamtubes as a contour lines. As shown in Figure 4.12 the flow lines are perpendicular to the piezometric lines.

	1	2	3	4	5	6	7	8	9	10	<i>i</i>		1	2	3	4	5	6	7	8	9	10	<i>i</i>	
<i>100</i>	0	0	0	0	0	56	0	54	0	0	<i>100</i>	0	0	0	0	0	1	1	2	2	2			
<i>99</i>	0	0	0	0	0	56	0	54	0	53	<i>99</i>	0	0	0	0	0	1	1	2	2	3			
<i>98</i>	0	0	0	0	56	0	0	54	53	0	<i>98</i>	0	0	0	0	1	1	1	2	3	3			
<i>97</i>	0	0	0	0	56	0	54	0	53	0	<i>97</i>	0	0	0	0	1	1	2	2	3	3			
<i>96</i>	0	0	0	56	0	54	0	53	0	1	<i>96</i>	0	0	0	1	1	2	2	3	3	4			
<i>95</i>	0	0	0	56	0	54	53	0	1	2	<i>95</i>	0	0	0	1	1	2	3	3	4	5			
<i>94</i>	0	0	56	0	54	53	0	1	2	0	<i>94</i>	0	0	1	1	2	3	3	4	5	5			
<i>93</i>	0	56	0	54	0	53	1	2	0	3	<i>93</i>	0	1	1	2	2	3	4	5	5	6			
<i>92</i>	0	56	0	54	53	0	1	2	3	4	<i>92</i>	0	1	1	2	3	3	4	5	6	7			
<i>91</i>	0	56	0	54	53	1	2	0	3	4	<i>91</i>	0	1	1	2	3	4	5	5	6	7			
<i>j</i>											<i>j</i>													

Figure 4.11 A portion of the TOP-LEFT corner of a matrix ($N_x=100$ $N_y=100$) before (left) and after (right) renumbering.

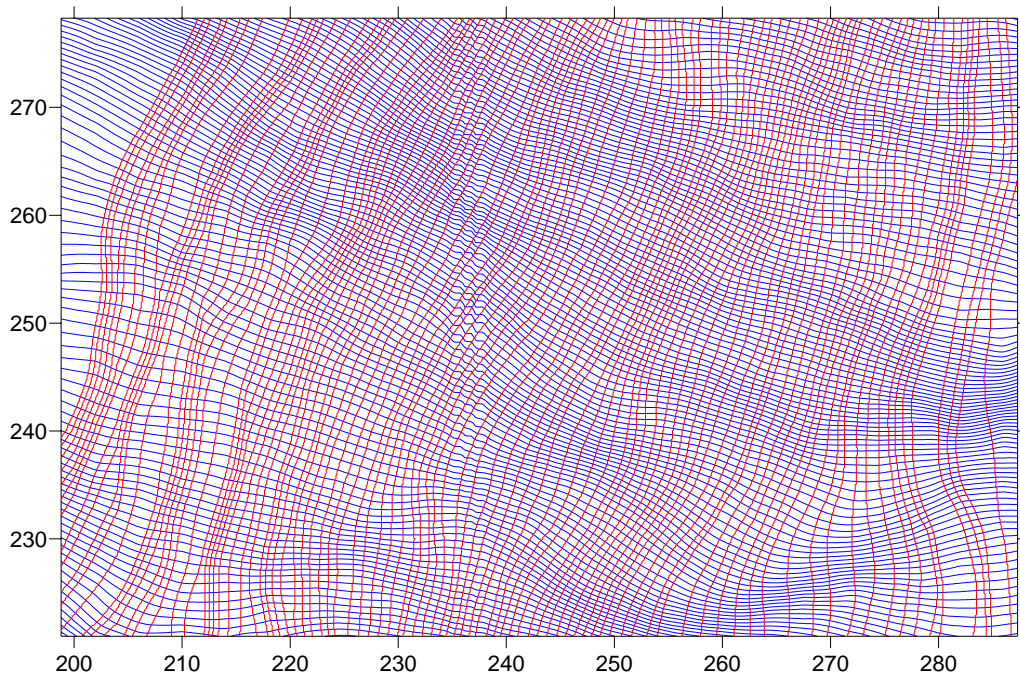


Figure 4.12 Streamlines and head contours.

4.2.5. Concentration inversion

The inversion of concentrations requires the discretization of the flow domain by streamtubes, accounting for the geometry of the isochrones. A streamtube is the region limited by two streamlines. Each isochrone captures a certain width of the flow field, defining a streamtube. Given the number of isochrones n the flow domain is discretized into $2n-1$ streamtubes as indicated in figure 4.13.

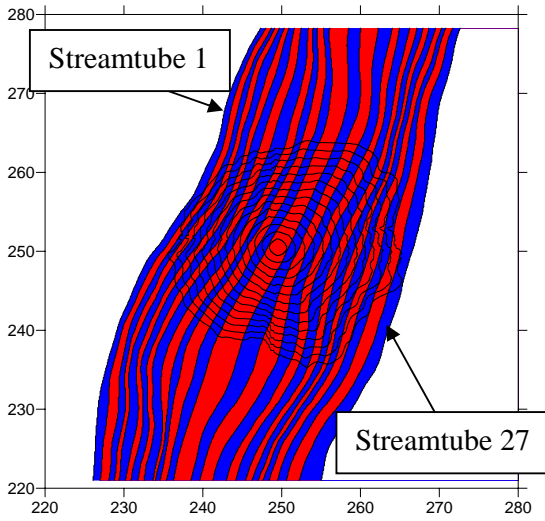


Figure 4.13. Discretization of the flow domain by streamtubes, given the geometry of the isochrones. Example with $n=14$ isochrones and $2n-1=27$ streamtubes.

Discretizing the problem assuming that the concentration is constant within a streamtube consists in simplifying the initial concentration distribution $C_0(\mathbf{x})$ as

$$C_0(\mathbf{x}) = \sum_{j=1}^{NSTUBE} C_0(x_j) \xi_j(\mathbf{x}) \quad (4.7)$$

where $C_0(x_j)$ is the concentration in streamtube j , $NSTUBE$ is the number of streamtubes and $\xi_j(\mathbf{x})$ is defined as

$$\xi_j(\mathbf{x}) = \begin{cases} 1 & \text{for } \mathbf{x} \in \text{streamtube } j \\ 0 & \text{for } \mathbf{x} \notin \text{streamtube } j \end{cases} \quad (4.8)$$

Inserting equation (4.7) in the integral equation (2.4) using the discretization of the isochrones defined in (4.4) leads to

$$\begin{aligned} C_w(t_i) &= \\ &= \frac{1}{Q\Delta t_i} \sum_{k=1}^{NPART} C_0(\mathbf{x}_{ik}) \Delta V_{ik} = \\ &= \frac{1}{Q\Delta t_i} \sum_{k=1}^{NPART} \sum_{j=1}^{NSTUBE} C_0(x_j) \xi_j(\mathbf{x}_{ik}) \Delta V_{ik} = \\ &= \sum_{j=1}^{NSTUBE} C_0(x_j) \frac{1}{Q\Delta t_i} \sum_{k=1}^{NPART} \xi_j(\mathbf{x}_{ik}) \Delta V_{ik} = \\ &= \sum_{j=1}^{NSTUBE} C_0(x_j) g_{ij} \end{aligned} \quad (4.9)$$

The definition of the matrix g_{ij} is completely analogous to the definitions given for the analytical approach in homogeneous media (equations (3.16) and (3.27)). The physical interpretation may be written as

$$g_{ij} = \frac{\text{Water volume of the sample } i, \text{ located at the streamtube } j}{\text{Total water volume of the sample } i} \quad (4.10)$$

However, a fundamental difference between the analytical and numerical approaches here is that equation (4.9) considers the concentration at each streamtube (that is $2n-1$ values of $C_0(x_j)$) instead of considering n values of $\bar{C}_0(x) = (C_0(x) + C_0(-x))/2$ as in the analytical approach). Writing equation (4.9) in matrix notation for a case with $n=7$ samples leads to

$$\begin{bmatrix}
0 & 0 & 0 & 0 & 0 & 0 & g_{17} & 0 & 0 & 0 & 0 & 0 & 0 & 0 \\
0 & 0 & 0 & 0 & 0 & g_{26} & g_{27} & g_{28} & 0 & 0 & 0 & 0 & 0 & 0 \\
0 & 0 & 0 & 0 & g_{35} & g_{36} & g_{37} & g_{38} & g_{39} & 0 & 0 & 0 & 0 & 0 \\
0 & 0 & 0 & g_{44} & g_{45} & g_{46} & g_{47} & g_{48} & g_{49} & g_{410} & 0 & 0 & 0 & 0 \\
0 & 0 & g_{53} & g_{54} & g_{55} & g_{46} & g_{57} & g_{58} & g_{59} & g_{510} & g_{511} & 0 & 0 & 0 \\
0 & g_{62} & g_{63} & g_{64} & g_{65} & g_{46} & g_{67} & g_{68} & g_{69} & g_{610} & g_{611} & g_{612} & 0 & 0 \\
g_{71} & g_{72} & g_{73} & g_{74} & g_{75} & g_{46} & g_{77} & g_{78} & g_{79} & g_{710} & g_{711} & g_{712} & g_{713} & 0
\end{bmatrix}
\begin{bmatrix}
C_0(x_1) \\
C_0(x_2) \\
C_0(x_3) \\
C_0(x_4) \\
C_0(x_5) \\
C_0(x_6) \\
C_0(x_7) \\
C_0(x_8) \\
C_0(x_9) \\
C_0(x_{10}) \\
C_0(x_{11}) \\
C_0(x_{12}) \\
C_0(x_{13})
\end{bmatrix}
=
\begin{bmatrix}
C_w(t_1) \\
C_w(t_2) \\
C_w(t_3) \\
C_w(t_4) \\
C_w(t_5) \\
C_w(t_6) \\
C_w(t_7)
\end{bmatrix}
\quad (4.11)$$

In equation (4.11) we can clearly identify the non-uniqueness of the solution: we have only 7 equations (given by each sample $C_w(t_i)$) but 13 unknowns (given by the concentration at each streamtube $C_0(x_j)$). However, our ultimate intention is to estimate the mass flow rate M_{CP} and therefore we may introduce additional assumptions, obtain the mass flow rates for each case and finally compare the mass flow rates: in this manner we are quantifying the uncertainty introduced by these (necessary) additional assumptions.

Three different possibilities are considered:

- 1- All contaminant was initially located at the right hand side of the well: $C_0(x_j) = 0$ for all $j < n$
- 2- The initial contaminant distribution was symmetrical about the well: $C_0(x_{n-j}) = C_0(x_{n+j})$ for all $j > 0$
- 3- All contaminant was initially located at the left hand side of the well: $C_0(x_j) = 0$ for all $j > n$

Being non-realistic, these assumptions provide extreme cases and therefore are useful to quantify the final uncertainty in the mass flow rate estimate.

Introducing these additional equations in (4.11) we obtain three linear systems of equations with a lower triangular matrix and get the three solutions $C_0^{left}(x_j)$, $C_0^{sym}(x_j)$ and $C_0^{right}(x_j)$ by forward substitution. The three solutions for the initial concentration distribution are printed into SURFER GRID files for graphical output. (Figure 4.14.)

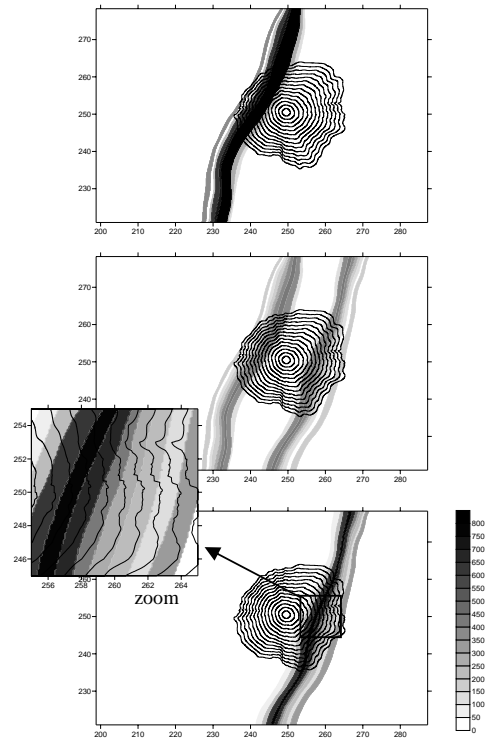


Figure 4.14: Left, symmetrical and right solutions.

4.2.6. Mass Flow Rate integration

When the concentration has been estimated at all cells of the CSTREAM grid, the total mass flow rate crossing the control plane is computed by integrating the contaminant mass flux along the control plane. The concentration is obtained as finite sum, where the Darcy flow and thickness are read from the MODFLOW grid, while the concentration is read from the CSTREAM grid. The integration is performed for each solution $C_0^{left}(x_j)$, $C_0^{sym}(x_j)$ and $C_0^{right}(x_j)$, and therefore, three mass flow rates are obtained: M_{CP}^{left} , M_{CP}^{sym} and M_{CP}^{right} .

Each mass flow rate is computed as

$$M_{CP} = \int_{\ell_{CP}} C_0(x, y) \mathbf{q}_0(x, y) \cdot \mathbf{n}_{CP} b(x, y) d\ell \quad (4.12)$$

by replacing $C_0(x, y)$ with the (discrete) solutions $C_0^{left}(x_j)$, $C_0^{sym}(x_j)$ and $C_0^{right}(x_j)$.

Additionally, the total groundwater flow rate across the control plane is also obtained as:

$$F_{CP} = \int_{\ell_{CP}} \mathbf{q}_0(x, y) \cdot \mathbf{n}_{CP} b(x, y) d\ell \quad (4.13)$$

F_{CP} is used to compute the effective hydraulic conductivity by applying Darcy's law with the mean gradient of the hydraulic heads (as computed in phase 1):

$$K_{eff} = \frac{F_{CP}}{\text{gradient} \times \text{area}} \quad (4.14)$$

where $\text{area} = \int_{\ell_{CP}} b(x, y) d\ell$ is the cross sectional area of the control plane.

The effective average concentration is also computed as M_{CP}/F_{CP} , for each solution M_{CP}^{left} , M_{CP}^{sym} and M_{CP}^{right} . The computations take place within the considered layer of the MODFLOW model.

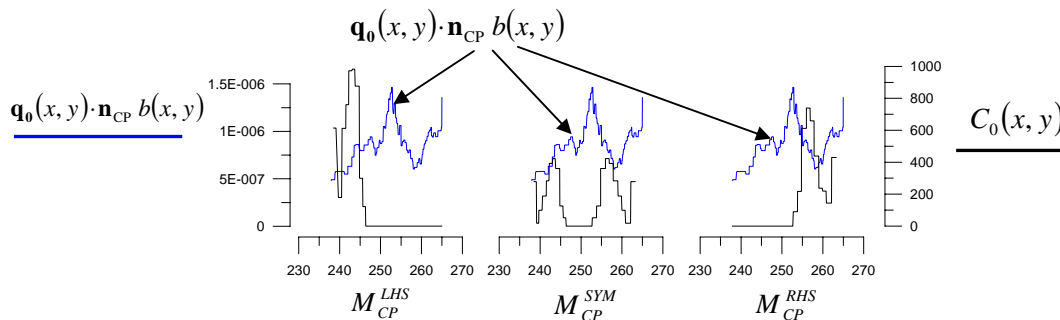


Figure 4.15: Mass flow rate integration for Left, Symmetrical and Right solutions.

4.3. 2D verification in homogeneous media

In this section, we compare the results of CSTREAM with the analytical solutions derived in chapter 3 for homogeneous and confined aquifers. The homogeneous case is simple, and therefore is very useful for verification purposes. At first we study the simplest case, that is the isochrones are considered to be circular ($t_D < 1$). In this case, a continuous analytical solution (i. e. mass flow rate as a function of a continuous $C_w(t)$ function) can be used for comparison. The second homogeneous problem is more general, and considers unlimited pumping test duration. In this case, the discrete analytical solution (instead of the continuous one) is used for comparison.

4.3.1. Verification for short pumping tests

A simple homogeneous aquifer with thickness $b = 4 \text{ m}$, porosity $n_e = 0.14$ and natural Darcy flux $q_0 = 0.0086 \text{ m/day}$ was used to simulate an integral pumping test of 3 days duration at rate $Q = 3 \text{ l/s}$. Under these conditions, the dimensionless duration of the pumping test is $t_D = 0.0002$ and therefore, the isochrones can be considered to be circular. For the case of radial flow, the integral equation governing the problem is (Schwarz, 2002)

$$C_w(t) = \frac{2}{\pi} \int_0^r \frac{\overline{C_0}(x)}{\sqrt{r(t)^2 - x^2}} dx \quad (4.15)$$

which gives the relationship between $C_w(t)$ and $\overline{C_0}(x)$. To verify CSTREAM, we need a pair of functions $\overline{C_0}(x)$, $C_w(t)$ being a solution of equation (4.15).

The plume with concentration $\overline{C_0}(x)$ indicated in Figure 4.16 was used. It is continuous and with continuous derivative, and therefore yields a smooth $C_w(t)$ (i. e. continuous with continuous derivative). The function $\overline{C_0}(x)$ is defined by 3 parabolical splines with continuous derivative:

$$\overline{C_0}(x) = \begin{cases} 0 & x < a \\ m(x-a)^2 & a < x < b \\ m_2(x-p)^2 + s & b < x < b' \\ m(x-a')^2 & b' < x < a' \\ 0 & a' < x \end{cases} \quad (4.16)$$

where

$$m = \frac{s}{(b-a)(p-a)} \quad ; \quad b' = 2p - b$$

$$m_2 = \frac{m^2(b-a)^2}{m(b-a)^2 - s} \quad ; \quad a' = 2p - a$$

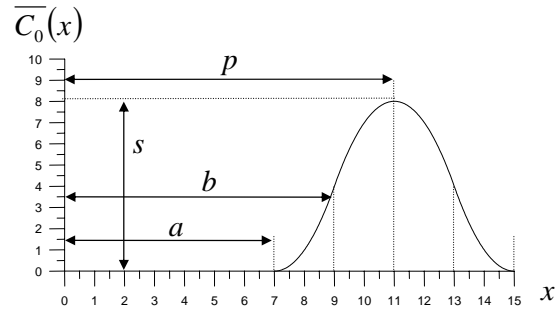


Figure 4.16: Plume cross section.

Introducing equation (4.16) in equation (4.15) we obtain an explicit equation for $C_w(t)$, in which the integration can be performed analytically. The integration of (4.15) for the particular case of (4.16) is obtained by parts, leading to a rather long solution (but explicit, continuous and with continuous derivative!):

$$C_w(t) = \begin{cases} f_1(t) & t < \frac{a^2 \pi h n}{Q} \\ f_2(t) & \frac{a^2 \pi h n}{Q} < t < \frac{b^2 \pi h n}{Q} \\ f_3(t) & \frac{b^2 \pi h n}{Q} < t < \frac{b'^2 \pi h n}{Q} \\ f_4(t) & \frac{b'^2 \pi h n}{Q} < t < \frac{a'^2 \pi h n}{Q} \\ f_5(t) & \frac{a'^2 \pi h n}{Q} < t \end{cases}$$

with

$$f_1(t) = 0$$

$$f_2(t) = \left(\frac{m}{2} \frac{Qt}{\pi h n} + ma^2 \right) \frac{1}{\pi} \arccos \left(\sqrt{\frac{a^2 \pi h n}{Qt}} \right) + \left(\frac{ma}{2} - 2ma \right) \frac{1}{\pi} \sqrt{\frac{Qt}{\pi h n} - a^2}$$

$$f_3(t) = \left(\frac{m_2}{2} \frac{Qt}{\pi h n} + m_2 p^2 + s - \frac{m}{2} \frac{Qt}{\pi h n} - ma^2 \right) \frac{1}{\pi} \arccos \left(\sqrt{\frac{b^2 \pi h n}{Qt}} \right) + \left(\frac{m_2 b}{2} - 2m_2 p - \frac{mb}{2} + 2ma \right) \frac{1}{\pi} \sqrt{\frac{Qt}{\pi h n} - b^2} + \left(\frac{m}{2} \frac{Qt}{\pi h n} + ma^2 \right) \frac{1}{\pi} \arccos \left(\sqrt{\frac{a^2 \pi h n}{Qt}} \right) + \left(\frac{ma}{2} - 2ma \right) \frac{1}{\pi} \sqrt{\frac{Qt}{\pi h n} - a^2}$$

$$f_4(t) = \left(\frac{m}{2} \frac{Qt}{\pi h n} + ma'^2 - \frac{m_2}{2} \frac{Qt}{\pi h n} - m_2 p^2 - s \right) \frac{1}{\pi} \arccos \left(\sqrt{\frac{b'^2 \pi h n}{Qt}} \right) + \left(\frac{mb'}{2} - 2ma' - \frac{m_2 b'}{2} + 2m_2 p \right) \frac{1}{\pi} \sqrt{\frac{Qt}{\pi h n} - b'^2} + \left(\frac{m}{2} \frac{Qt}{\pi h n} + ma^2 \right) \frac{1}{\pi} \arccos \left(\sqrt{\frac{a^2 \pi h n}{Qt}} \right) + \left(\frac{ma}{2} - 2ma \right) \frac{1}{\pi} \sqrt{\frac{Qt}{\pi h n} - a^2}$$

$$f_5(t) = - \left(\frac{m}{2} \frac{Qt}{\pi h n} + ma'^2 \right) \frac{1}{\pi} \arccos \left(\sqrt{\frac{a'^2 \pi h n}{Qt}} \right) - \left(\frac{ma'}{2} - 2ma' \right) \frac{1}{\pi} \sqrt{\frac{Qt}{\pi h n} - a'^2} + \left(\frac{m}{2} \frac{Qt}{\pi h n} + ma'^2 - \frac{m_2}{2} \frac{Qt}{\pi h n} - m_2 p^2 - s \right) \frac{1}{\pi} \arccos \left(\sqrt{\frac{b'^2 \pi h n}{Qt}} \right) + \left(\frac{mb'}{2} - 2ma' - \frac{m_2 b'}{2} + 2m_2 p \right) \frac{1}{\pi} \sqrt{\frac{Qt}{\pi h n} - b'^2} + \left(\frac{m}{2} \frac{Qt}{\pi h n} + ma^2 \right) \frac{1}{\pi} \arccos \left(\sqrt{\frac{a^2 \pi h n}{Qt}} \right) + \left(\frac{ma}{2} - 2ma \right) \frac{1}{\pi} \sqrt{\frac{Qt}{\pi h n} - a^2}$$

where, in equation (4.17), h is the saturated thickness and n is the porosity.

Figure 4.17 shows $C_w(t)$ and $\bar{C}_0(x)$ for plumes characterized by $a = 2\text{ m}, 4\text{ m}, 6\text{ m}, 8\text{ m}, 10\text{ m}, 12\text{ m}, 14\text{ m}, 16\text{ m}, 18\text{ m}, 20\text{ m}, 22\text{ m}$ $b = a + 3\text{ m}$, $p = a + 8\text{ m}$ and $s = 1000 \frac{\text{g}}{\text{m}^3}$

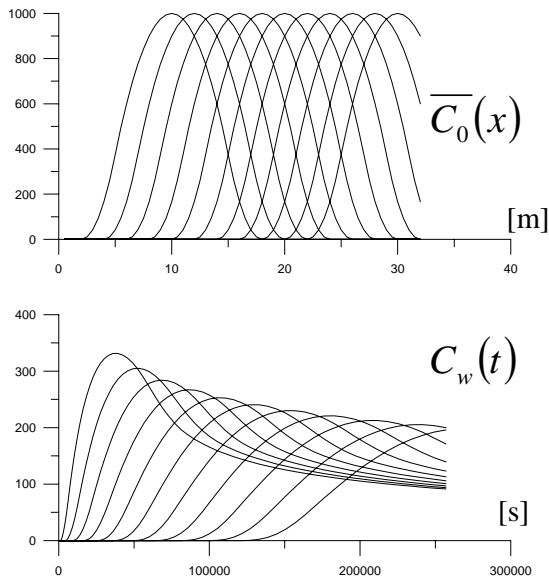


Figure 4.17: Plume cross section $\bar{C}_0(x)$ and $C_w(t)$ measured at the well.

Using the $C_w(t)$ for $a = 12\text{ m}$, 16 “samples” were extracted as $(t_i, C_w(t_i))$, for $i=1,2,\dots,16$. These samples, together with the aquifer parameters and the pumping rate, were used to perform the inversion by using: 1: Schwarz analytical solution, 2: New analytical solution accounting for q_0 and 3: CSTREAM.

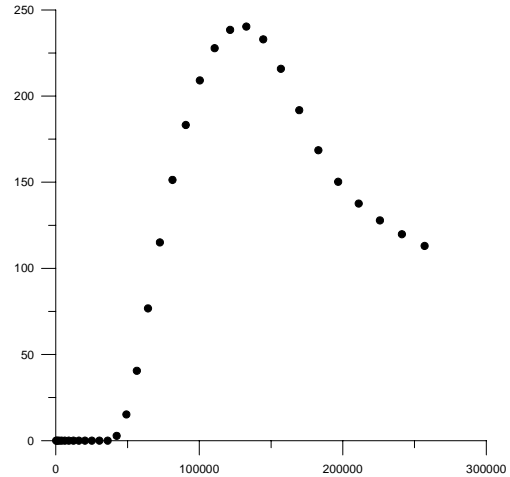


Figure 4.18: Example of $(t_i, C_w(t_i))$ data used for the inversion with 32 “samples”.

The actual mass flow rate is obtained by integrating (4.14), and equals 299.52 g/day. The inversion using Schwarz formula provides an estimate of 299.7 g/day (error +0.06%). The new analytical solution was integrated with 1000 points along the isochrone, with a constant increment of the angle, provides an estimate of 299.8 g/day (error +0.09%). CSTREAM, with a grid of $DX=0.1\text{m}$, gives an estimate of 295 g/day (error - 1.5%). All three approaches lead to a very reasonable estimate of the mass flow rate. In this case, Schwarz’ analytical solution is the fastest and most accurate choice since no numerics are involved and the dimensionless duration of the pumping test ($t_D = 0.0002$) can be neglected without introducing significant errors. The plume cross sections for all inversion methods are shown in Figure 4.19. The isochrone geometry obtained from CSTREAM is also compared to the analytically computed in Figure 4.20.

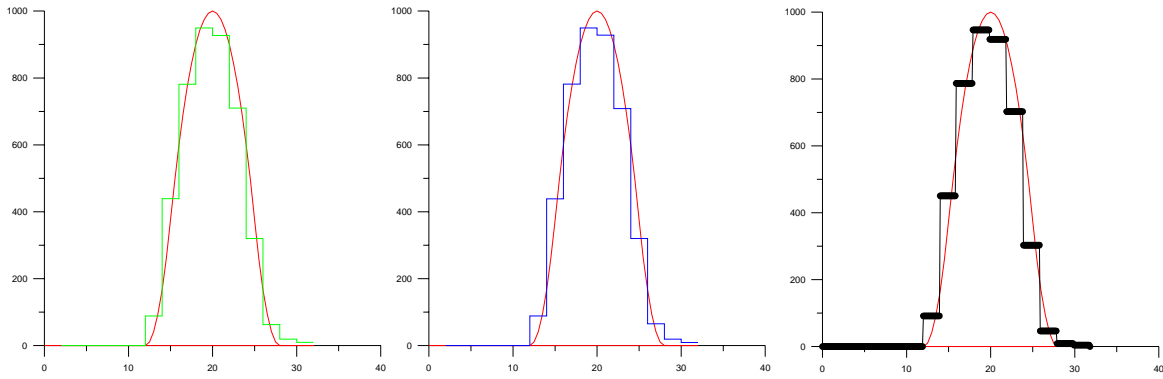


Figure 4.19. Verification in homogeneous medium. Left: Schwarz formula , Center New solution based on Bear & Jacobs equation, right: CSTREAM (with $DX=0.1$)

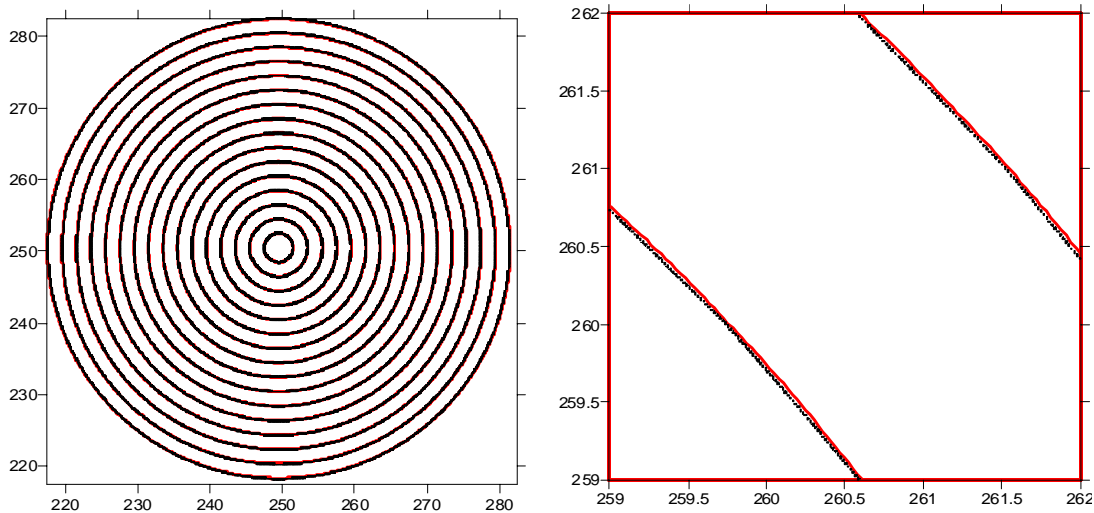


Figure 4.20. Verification in homogeneous medium for radial flow. Comparison of the isochrone geometry. Line: Bear & Jacobs equation, Dots: location of the backtracked particles with MODPATH.

4.3.2. Verification for long pumping tests

In this section, we also use a homogeneous confined aquifer, however in this case we want to emphasize the effect of the natural Darcy flux q_0 , which can only be neglected under the condition $t_D \ll 1$. Realistic aquifer parameters taken from a field scale application in the Neckar Valley, south Germany (Holder et al. 1998; Jarsjoe et al., 2002; Bayer-Raich et al., 2002) for thickness $b = 3.59 \text{ m}$, porosity

$n_e = 0.1$ and natural Darcy flux of $q_0 = 0.85 \text{ m/day}$ were used to simulate the integral pumping test performed in well 9, which had a duration of $t = 12$ days at rate $Q = 7.01 \text{ l/s}$. The dimensionless time in this case is $t_D = 3.24$. The objectives are to compare the numerical and analytical results in terms of isochrone geometry and mass flow rate estimates.

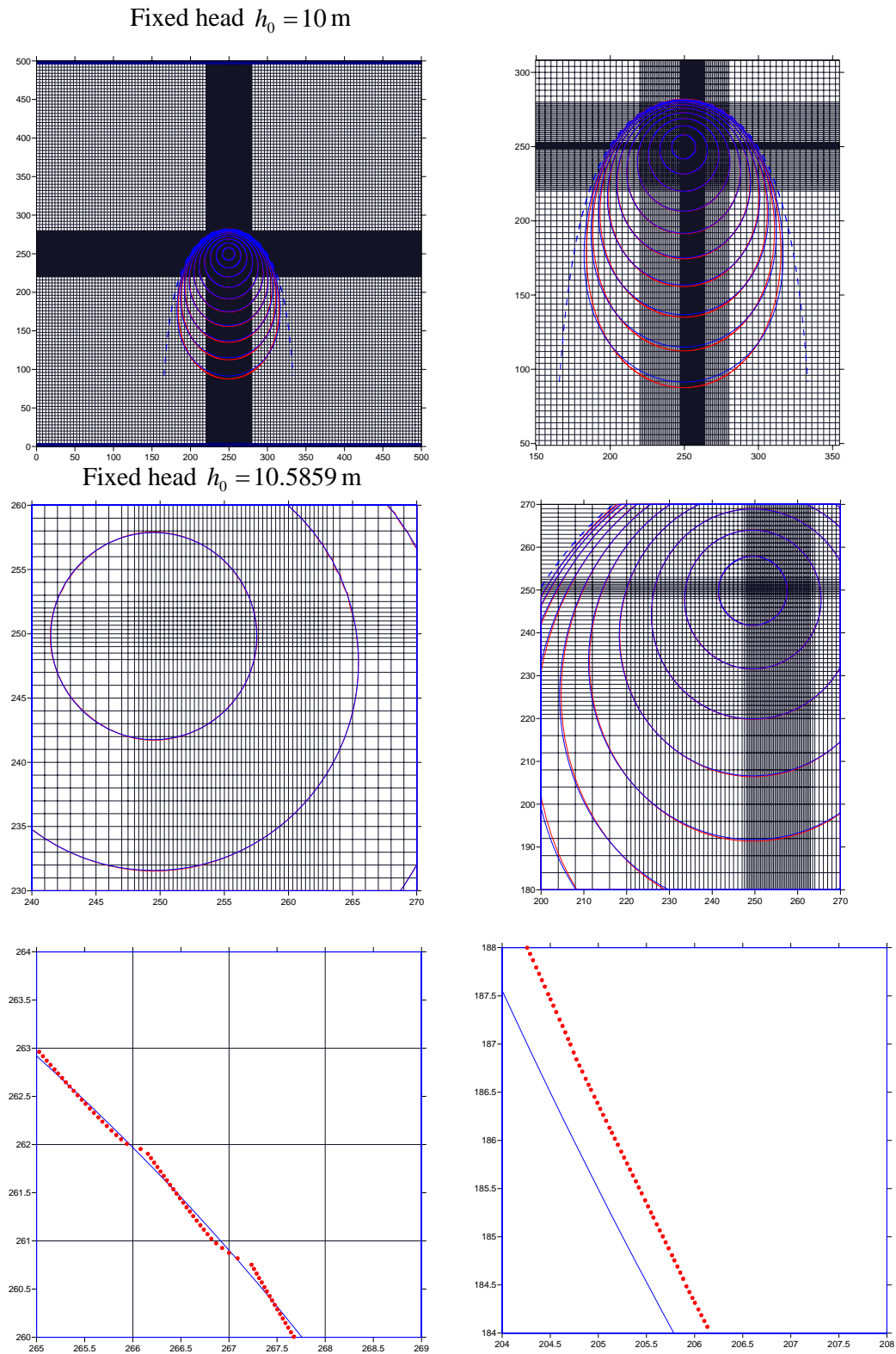


Figure 4.21. Comparison of numerical and analytical isochrones. Lines: Bear & Jacobs equation (1000 points in each isochrone with constant $\Delta\theta$), dotted line: water divide. Dots: Isochrones obtained by particle backtracking with MODPATH: 3600 particles. Grid: Finite differences grid used in the MODFLOW model.

In addition to the aquifer parameters given above, a specific storage of 10^{-4} m^{-1} , was (arbitrary) selected and the specific yield (or drainable porosity) was set equal to the porosity (0.1).

The geometry of the numerical isochrones shows an excellent agreement with Bear & Jacobs equation (Figure 4.21), despite the coarse discretization and the fact that the analytical solution is only strictly valid for steady state pumping (or specific storage=0)

To verify the mass flow rate estimates provided by CSTREAM, the (arbitrary) $C_w(t)$ shown in figure 4.22 was selected:

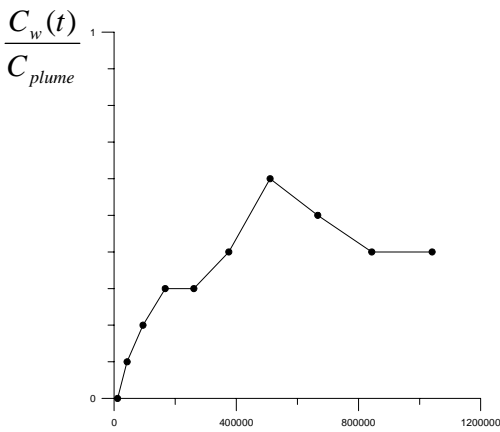


Figure 4.22: $C_w(t)$ used for the verification example

The inversion of the $C_w(t)$ given in figure 4.22 was performed with: 1: Schwarz analytical solution, 2: New analytical solution accounting for q_0 and 3: CSTREAM.

Figure 4.23 shows the plume cross section $C_0(x)$, obtained by assuming that the plume is located at the right hand side of the well (one-side solution).

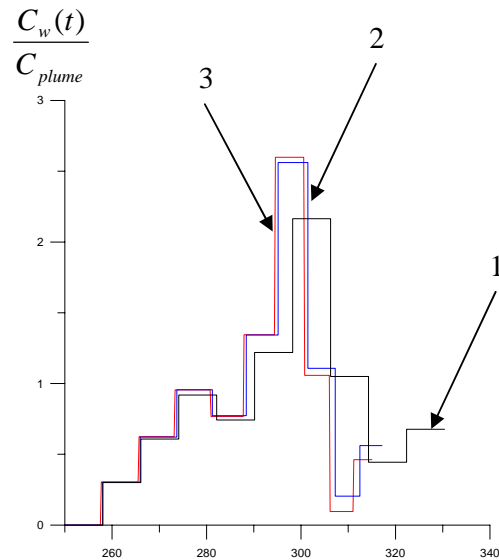


Figure 4.23: $C_0(x)$ obtained from the inversion. 1: Schwarz' solution; Blue: New analytical solution. Red: CSTREAM

In Figure 4.23, the solutions given by the new analytical solution and CSTREAM show a similar behavior, in terms of concentrations and distance to the well. In this case, Schwarz' solution displays an overestimation of the capture radius (line 1 in Figure 4.23 extends up to $x=330 \text{ m}$, while the new analytical solution and CSTREAM extend to $x=317 \text{ m}$ and $x=315.5 \text{ m}$, respectively). However the average concentration provided by the simplified analytical solution is still an excellent approximation of the effective Cav. The three inversion methods lead to $C_{av}=0.406$ $C_{av}=0.411$ and $C_{av}=0.403$ (Schwarz, new solution and CSTREAM respectively)

Finally the mass flow rate estimate for the three methods amount to $M=199 \text{ g/day}$ $M=168 \text{ g/day}$ and $M=162 \text{ g/day}$. The overestimation of the simplified approach may be predicted by the results shown in figure 3.10 in chapter 3: for $tD=3.24$ the expected error of Schwarz solution is +19.4%, and the error observed here is +18.4%.

4.4. 2D verification in heterogeneous media

The verification of the isochrone geometry and the mass flow rate estimates performed in the previous sections of this chapter for the case of homogeneous media could be performed by comparison with analytical solutions. However, in the heterogeneous case, no analytical solutions are available for comparison of the CSTREAM output. Therefore, we use the code MT3D (Zheng, 1990) to perform forward transport simulations for the plume development (under steady-state conditions) and the integral pumping tests. The output of the forward simulation (i. e. the $C_w(t)$ measured at the pumping well) is used as input for CSTREAM. The mass flow rate estimates obtained with CSTREAM are then compared to the actual mass flow rates of the forward MT3D simulation.

4.4.1. Verification through a Multigaussian K-field

The first verification example for heterogeneous media was developed in collaboration with Jerker Jarsjoe (see further details in Bayer-Raich et al., 2001). For simplicity, thickness and porosity are set constant within the aquifer, and the hydraulic conductivity field was generated using a Multigaussian distribution. This numerically simulated example is also described in section 2.3, where the differences between analytical and numerical approaches are pointed out. However, in this section we focus on the performance of CSTREAM by comparing in more detail the actual mass flow rate and concentration distribution to the inversion output obtained with CSTREAM.

The development of a contaminant plume in a heterogeneous $500 \times 500 \text{ m}^2$ domain is simulated using the code MT3D (Zheng,

1998). The heterogeneous conductivity field was generated using the Turning Bands Method with the code TUBA (Zimmerman & Wilson, 1990): geometric mean $K_G = 0.001 \text{ m/s}$, variance $\sigma_{\ln K}^2 = 0.25$, correlation length $\lambda = 20 \text{ m}$, porosity $\phi = 0.1$ and thickness $b = 5 \text{ m}$. Other details of the numerical experiment are given in chapter 2 and Bayer-Raich et al. (2001). The concentration values used for the inversion were obtained from the MT3D forward simulation of the integral pumping test. Both Finite Differences (FD) and the Method of Characteristics (MOC) were used, as shown in Figure 4.24

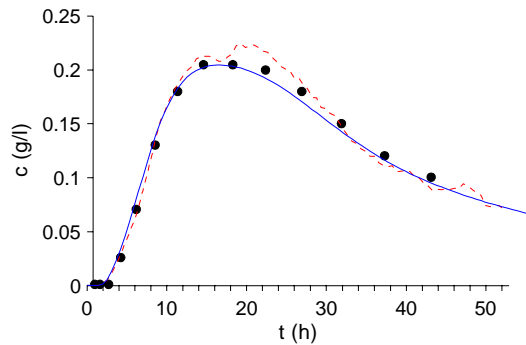


Figure 4.24. $C_w(t)$ from the MT3D simulation. Solid line: FD. Dotted line: MOC. Dots: values used for the inversion.

Here, I study the influence of the total duration of the pumping test by obtaining the mass flow rate estimate for increasing number of samples and increasing duration of the test. In general, both mass flow rate and average concentration depend on the total duration of the pumping test, however, the mass flow rate becomes constant when the plume is completely captured by the integral pumping test. The numerical inversion of the concentration was performed using a CSTREAM grid with $DX=0.05 \text{ m}$ for the definition of the streamtubes, and 3600 particles for the definition of the isochrones. The mass flow rate estimates are shown in Figure 4.25 as a function of the total duration of the integral pumping test.

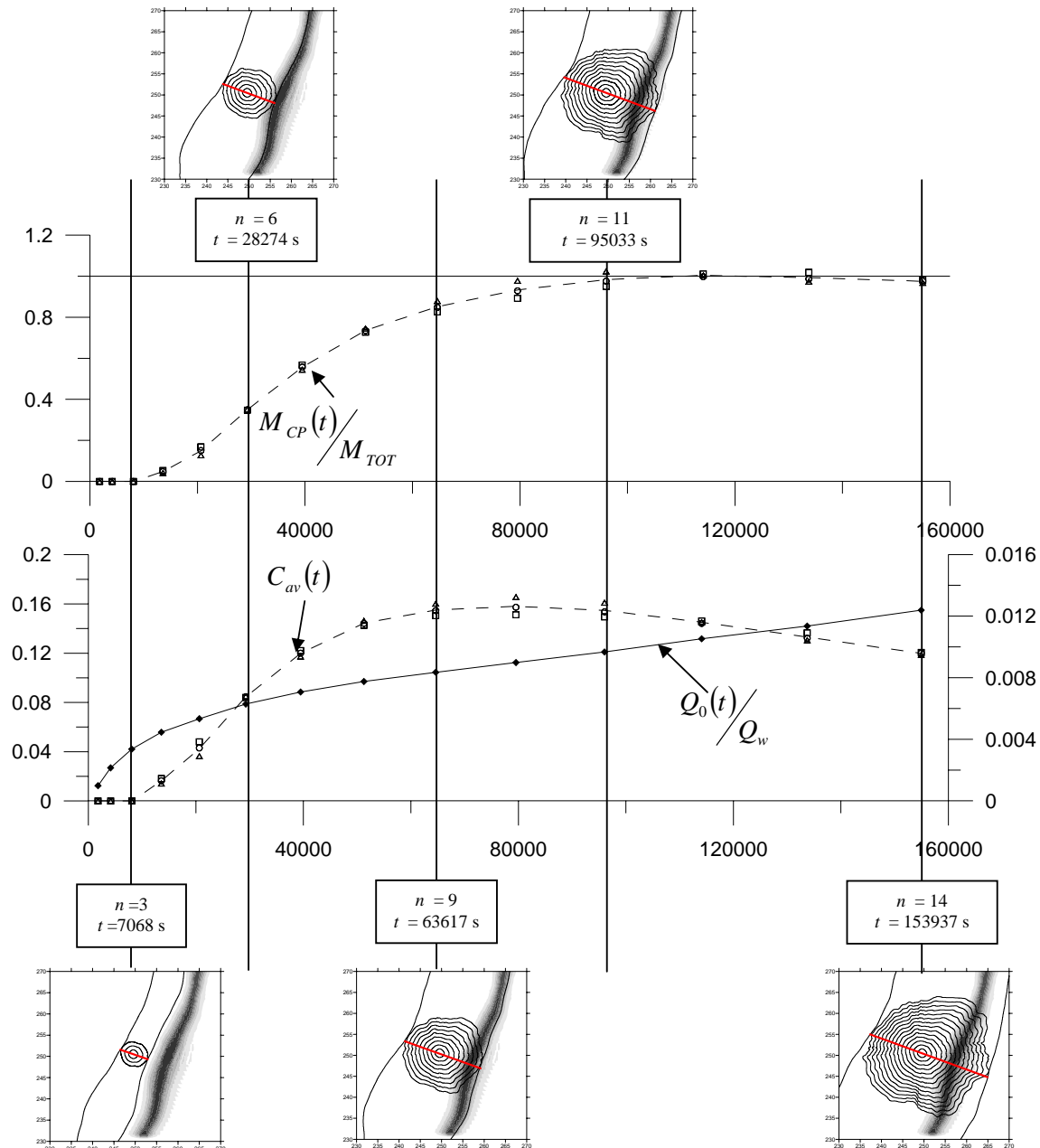


Figure 4.25. Estimates of average concentration $C_{av}(t)$ and mass flow rate across the control plane $M_{CP}(t)$ for increasing test duration t . $Q_0(t)$ is the groundwater flow rate (under natural steady-state conditions) across the control plane (i. e. within the streamtube indicated by the black lines). $M_{CP}(t) = C_{av}(t)Q_0(t)$

The triangles, circles and squares indicate the left, symmetrical and right solutions respectively the dotted line is the arithmetic average of these three (the expected value for average concentration and mass flow rate for unknown plume position).

The length of the control plane $\ell_{CP}(t)$ (line across the plume in Figure 4.25) is defined by the width of the streamtube (black open lines) included within the well capture zone (with increasing number of isochrones from $n=1$ to 14). The mass flow rate across the control plane under transient conditions is given by $M_{CP}(t) = C_{av}(t)Q_0(t)$, where $C_{av}(t)$ and $Q_0(t)$ are defined for the control plane $\ell_{CP}(t)$ defined along the x-coordinate as

$$C_{av}(t) = \frac{1}{Q_0(t)} \int_{\ell_{CP}(t)} C_0(x,0) q_{0,y}(x,0) b(x,0) dx \quad (4.18)$$

with

$$Q_0(t) = \int_{\ell_{CP}(t)} q_{0,y}(x,0) b(x,0) dx \quad (4.19)$$

A steady-state pumping situation (i. e. pumping duration $t \rightarrow +\infty$) leads to $\lim_{t \rightarrow +\infty} Q_0(t) = Q_w$. Under transient pumping $M_{CP}(t) = C_{av}(t)Q_0(t)$, the mass flow rate depends on the duration of the pumping, unless the plume is fully captured at $t = t^*$. For $t > t^*$ (fully captured plume) then $M_{CP}(t) = M_{TOT}$ (independent of t !). In figure 4.25, the plume is fully captured at $t^* = 90000$ s, where $M_{CP}(t) = M_{TOT}$ becomes time independent.

4.4.2. Neckar model, high variance: the new flow-weighted averaged approach

The next verification example for heterogeneous media was developed by performing a numerically simulated example within the Neckar Valley model (Holder et al., 1998), a preliminary verification was presented in Bayer-Raich et al. (2002) using a simplified version of CSTREAM that did not fully account for the flux averaged mixing to perform the

inversion. It was speculated then that further development of CSTREAM (implementation of the new equations) would lead to smaller errors: this speculation will be shown to be consistent with the results obtained here.

This numerical verification example was already described in section 3.6, where it was used to test the applicability of the analytical solutions in heterogeneous aquifers. Here, we compare the performance of the simplified approach used in Bayer-Raich et al. (2002) to the new approach accounting for flow mixing.

Figure 4.26 shows the set up of the numerical experiment: The source was located upstream of the wells 9, 10, 13, 16 and 17 as (see further description of the model and the pumping tests in Jarsjö et al. 2003). A 200-day forward simulation was performed with a source zone of constant concentration c_0 using the Method of Characteristics (MOC) within the code MT3D (Zheng, 1990). Independent pumping tests (i. e. with sufficiently long time lag between the pumping events) were performed in each well. Figure 4.26 shows also the concentration time series obtained at each well and the plume position before pumping.

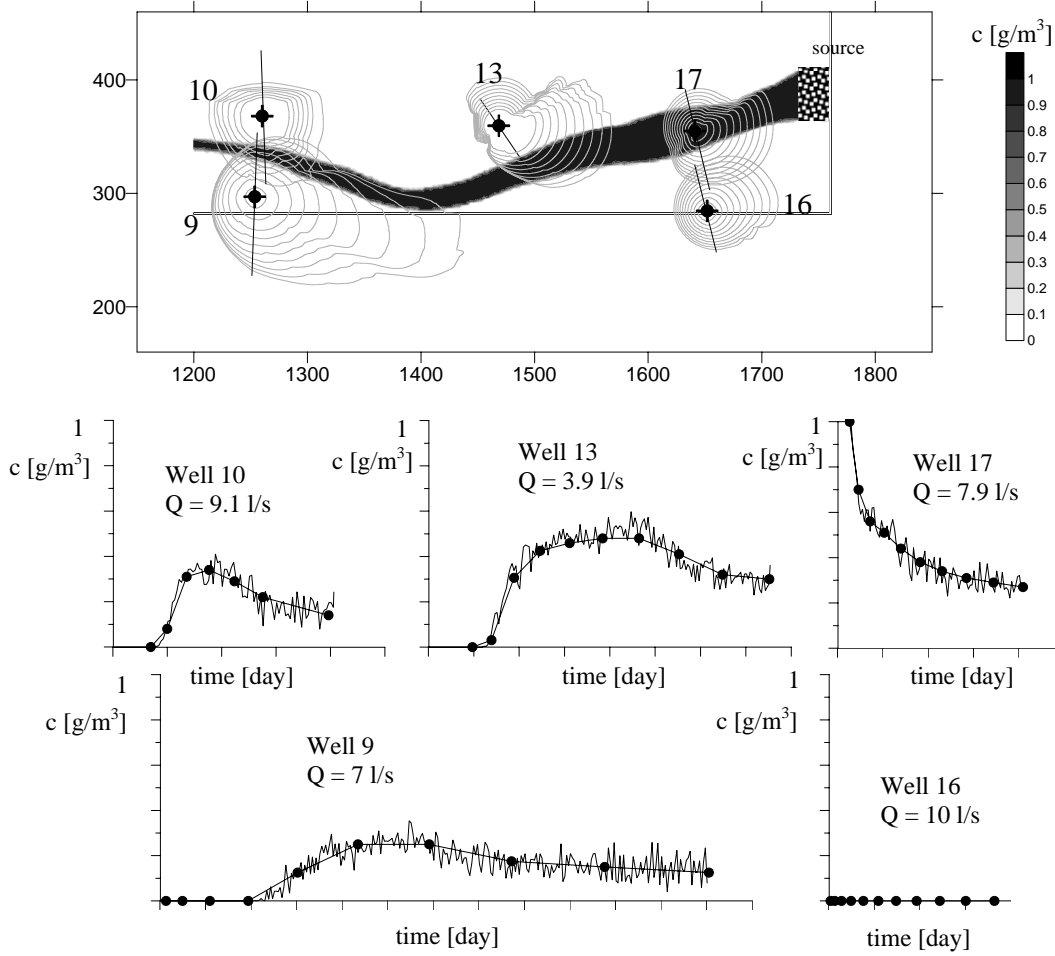


Figure 4.26: Heterogeneous model domain indicating the capture zone of each well (top). Plume developed under steady-state flow and advective conditions (bottom). After Bayer-Raich et al., 2003.

The necessary input for the inversion of average concentrations and mass flow rates was extracted from the numerical flow model (for q_0 , b , n_e , q_w), the pumping rate Q and the $C_w(t)$ measured at the pumping well. In this example, the estimates of the mass flow rate and average concentration depend on the considered solution (left, symmetrical, right) because the groundwater flow is highly non-uniform within the capture zone of the pumping wells. To quantify this uncertainty, the left-right ratio LRR was defined as

$$LRR = \max(M_{left}, M_{right}) / \min(M_{left}, M_{right}) \quad (4.20)$$

where M_{left} and M_{right} are the mass flow rate estimates for left and right positions.

Both the simplified and the new approach are compared in this section. The new approach considers flow averaged mixing when performing the integration along the isochrone, based on equation (4.21):

$$Q C_w(t) = - \oint_{\ell_r(t)} C_0(x, y) \bar{q}_w(x, y) \cdot \bar{n} b(x, y) d\ell \quad (4.21)$$

Figure 4.27 shows the estimates for both average concentration $C_{av}(t)$ and mass flow rates across the control plane $M_{CP}(t)$ for increasing test duration t . Since all wells captured the whole plume at the end of the tests, the mass flow rate becomes time independent and the average concentration decreases due to dilution. The triangles, circles and squares indicate the left, symmetrical and right solutions respectively. The heterogeneous conditions within the capture zone of each well lead to considerable differences between the different solutions (left, right, symmetrical).

The LRR (given in equation 4.20) amounts to 1.1, 2.8, 3.3 and 1.2 for the wells 9, 10, 13 and 17, respectively. These differences can be observed in Figure 4.27: the mass flow rate estimate for different plume positions (triangles for left and squares for right) becomes asymptotic at different values. For example in well 13, the mass flow rate amounts to 56.1 g/d if the plume is located to the left (triangles in figure 4.27) while the estimate corresponding to the right hand side is 17.2 g/d (this leads to $LRR=56.1/17.2=3.26$). The actual mass flow rate simulated with MT3D is 55 g/d and the plume is located to the left of well 13.

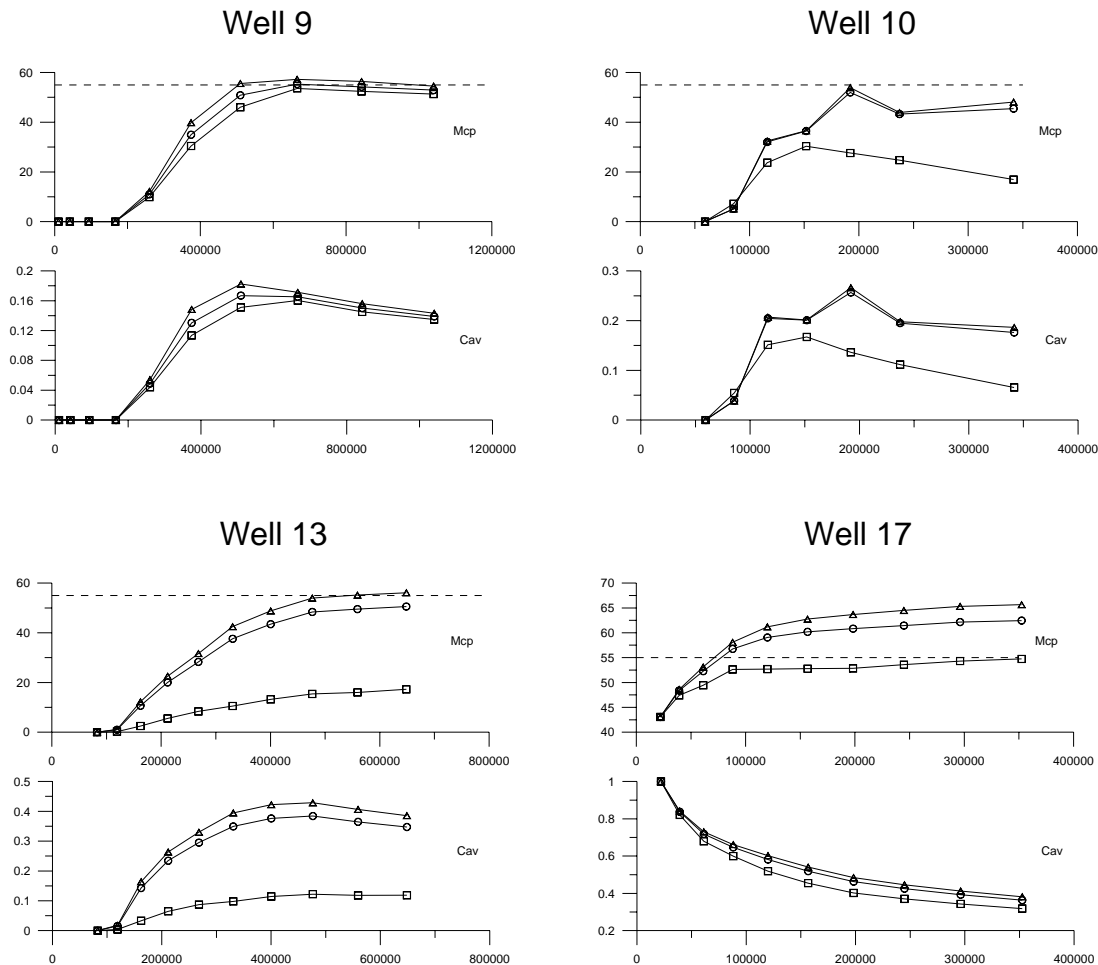


Figure 4.27: Estimates of average concentration $C_{av}(t)$ and mass flow rate across the control plane $M_{CP}(t)$ for increasing test duration t . The triangles, circles and squares indicate the left, symmetrical and right solutions, respectively. The location of the plume (as shown in Figure 4.26) is to the left for wells 13 and 10 and the right for wells 9 and 17.

The simplified approach used in Bayer-Raich et. al. (2002) and in all interpretations of integral tests performed before August 2002 neglect the influence of the term $\vec{q}_w(x, y) \cdot \vec{n} b(x, y)$, leading to the equation (4.22)

$$C_w(t) = \frac{1}{\tilde{\ell}_l(t)} \oint_{\ell_l(t)} C_0(x, y) dl \quad (4.22)$$

With $\tilde{\ell}_l(t) = \oint_{\ell_l(t)} dl$. Equation (4.22) is strictly valid only under homogeneous conditions and perfect radial flow. In the general (heterogeneous) case the flow mixing considered in equation (4.21) leads to more accurate results (maximum error is reduced from 64% to 13%, observed in well 10, see Figure 4.27)

Using the same numerical model of the Neckar Valley, the uncertainties related to the plume position for the case of real integral pumping tests were quantified in Jarsjö et. al. (2002) using the simplified approach (i. e. equation 4.22) and later with the more general approach (i.e. equation 4.21) in Jarsjö et. al. (in preparation). While the former version of CSTREAM based on equation 4.22 leads to $LRR > 10$ for some wells, this uncertainty has been reduced to $LRR < 4$ with the newly implemented formulation based on equation (4.21). For more details, compare Jarsjö et al. (2002) and Bayer-Raich et. al. (2002) with Jarsjö et. al. (in preparation).

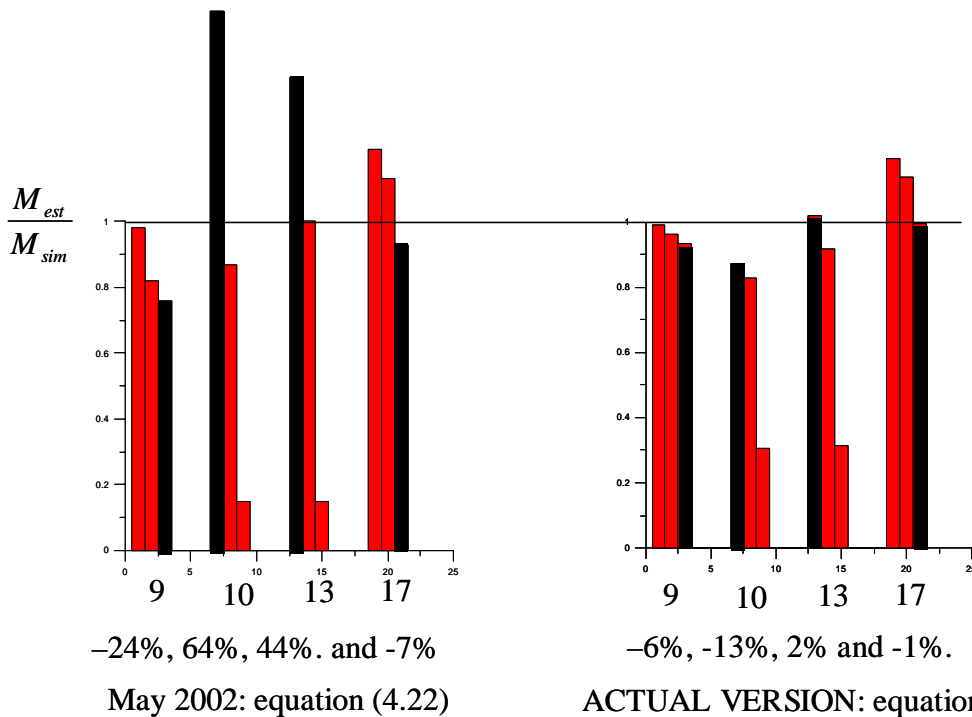


Figure 4.27: Comparison of the simplified approach and the new approach. The three bars indicate the left-symmetrical and right solutions, black bar indicates the true position of the plume.

4.4.3. Bitterfeld, multi-level

For the numerical inversion of the integral pumping tests performed in Bitterfeld, CSTREAM has been adapted to enable interpretation of depth-differentiated concentration-time series in multi-layered aquifers.

A regional 8-layer groundwater flow model was developed by Borkert (1999) to simulate the transient flow conditions of the SAFIRA-Bitterfeld site. As a verification example for the multi-layered analytical inversion, Bayer-Raich et al. (2001) developed a numerically simulated contaminant scenario through a forward simulation of advective transport, using the code MT3DMS (Zheng & Wang, 1999). In this section, we will apply CSTREAM to the same verification example in order to compare analytical and numerical inversions.

The first step in the numerical experiments was the generation of a plume. Therefore I introduced a contaminant source with a length (North-South direction) of 30 m and a width (East-West direction) of 5 m into the model domain. The source was placed in layers 2, 3 and 4, with different fixed contaminant concentrations. Concentrations of 0.5 mg/l in layer 2, 0.1 mg/l in layer 3 and 1 mg/l in layer 4 were used. The distance from the source to the pumping well was about 160 m. For the generation of the plume, a transient advective transport simulation over a time period of 10 years was performed with MT3DMS (Zheng & Wang, 1999). During this simulation the contaminant source acted as constant concentration boundary condition. The simulated plume is shown in Figure 4.28 (see further details in Bayer-Raich et al. 2001).

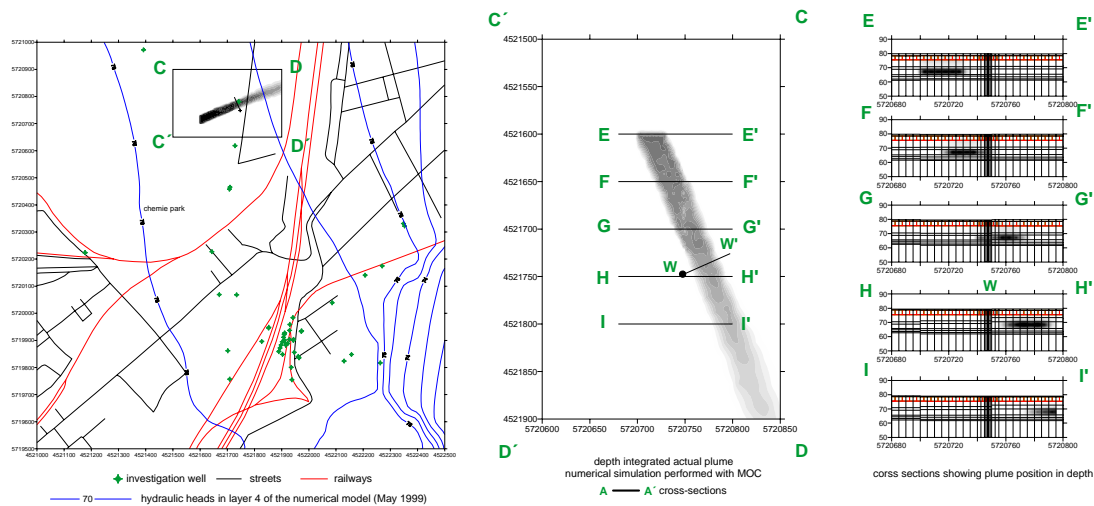


Figure 4.28: Numerically simulated plume within the SAFIRA-Bitterfeld MODFLOW model for verification of CSTREAM.

To obtain the input for the application of the integral investigation approach we simulated a pumping test through the numerical model. The well was represented by a column of model cells with high hydraulic conductivity. A constant pumping rate of 10 l/s and a pumping time of 14 days were chosen, and the concentration-time series of Figure 4.29 were obtained.

I use these $C_w(t)$ data to quantify the total relative error of the estimations, the mass flow obtained from the inversion is compared to the actual mass flow rate (forward MT3D simulation).

depth-differentiated analytical approach (Bayer-Raich et al. 2001). In this section, we perform the same comparison with the numerical estimations provided by CSTREAM.

Figure 4.30 shows the mass flow rate estimates provided by both the analytical approach and the numerical inversion. The numerical inversion could not be applied to layer 2, as this layer falls dry at the location of the well during the pumping test. Figure 4.31 gives the numerically computed isochrones as well as the plume obtained with CSTREAM in layer 4.

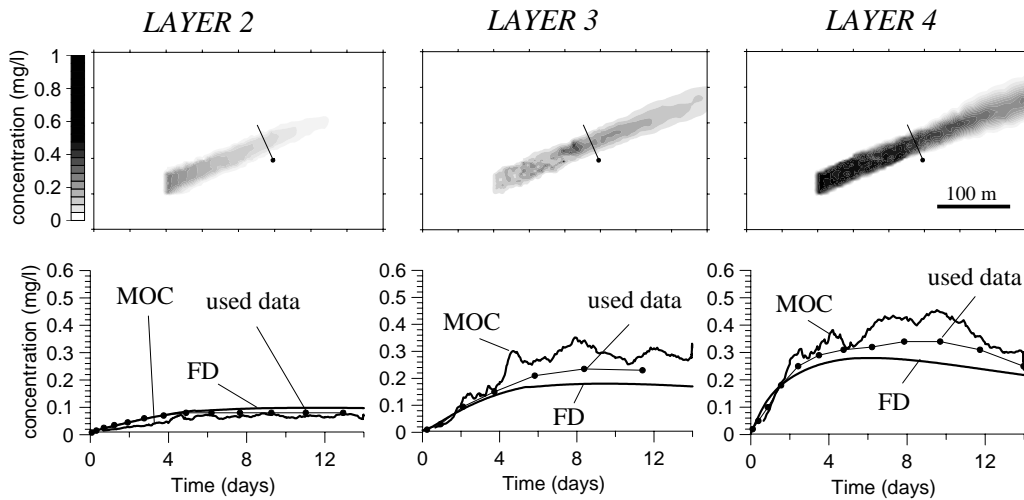


Figure 4.29: Numerical pump test with concentration-time series in layer 4 obtained through different numerical methods. FD: Finite differences; MOC: Method of Characteristics.

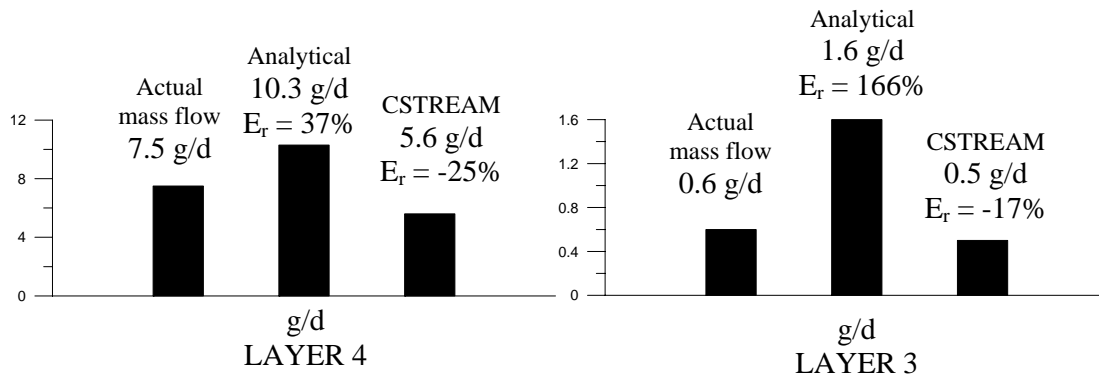


Figure 4.30: Numerical Comparison of results of numerical and analytical inversion in layers 4 and 3.

This numerically simulated example was used to demonstrate the applicability of the

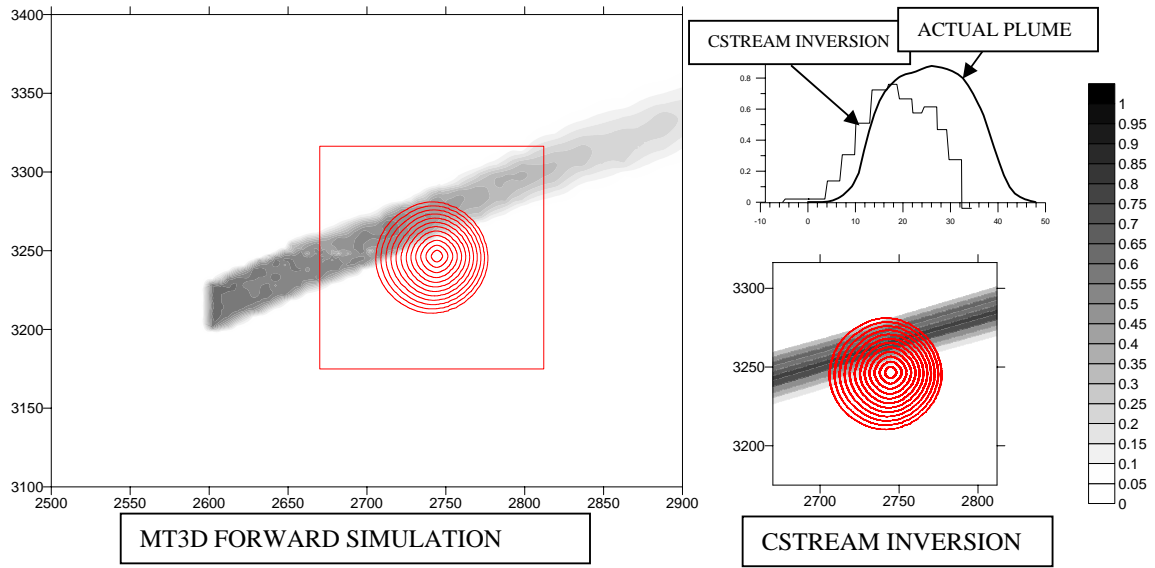


Figure 4.31: Geometry of isochrones and plume obtained with CSTREAM in layer 4

4.5. Application example: Depth integrated application in the Nekar Valley, Stuttgart (Germany): Quantifying model uncertainties

In this section I describe an application example performed in the context of the project INCORE described in more detail in Jarsjö et al. (2003; 2004). We used the same deterministic groundwater model as in the verification examples described in section 4.4.2. and in Bayer-Raich et al. (2003).

This section tackles the problem of quantifying model uncertainties in the estimations of average concentration, mass flow rate and possible source locations upstream the control plane. Since uncertainties related to point sample grid dimensions are avoided using integral measurements, the problem reduces mainly to a quantification of the effect of uncertainties related to the flow and transport properties of the aquifer. In particular, uncertainties in the estimation of the well capture zone border as a function of time (for the convergent flow field during pumping) and the streamlines (for the natural flow field before and after pumping) will affect integral estimations (Jarsjö et al. 2004).

We use the terminology introduced in Jarsjö et al (2004) where the term *direct integral measurement (IM) predictions* is used to refer to the range of possible values for mass flow rate and average concentration. In addition, *complex IM predictions* refer to delimiting possible source zones upstream of locations where contaminant was detected, where other measurements and/or model uncertainties (for instance, in biogeochemical models) need to be considered.

Also, Jarsjö et al. (2004) used the term *contamination model uncertainty* to refer to the uncertainty related to the position of the plume with respect to the pumping well

(i. e. the left-right uncertainty described in previous sections) as well as the *groundwater model uncertainty* to reflect that the numerical model used for simulating the flow may be inaccurate with regard to some aspects, for instance, transmissivity field and boundary conditions. The *groundwater model uncertainty* is quantified here by using different MODFLOW models with different boundary conditions, as shown in Figure 4.32.

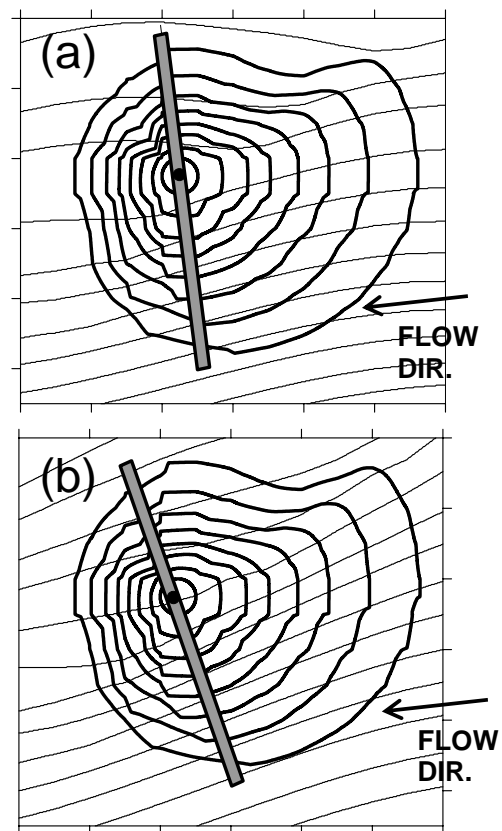


Figure 4.32: Control plane, streamlines at natural flow conditions (before pumping, thin lines) and isochrones (well capture zone borders, bold closed lines) defined at different pumping times, for two deterministic models (a) and (b) differing only by their boundary conditions.

4.5.1. Direct integral measurement predictions: left-right uncertainty

As introduced in the previous section, the *contamination model uncertainty* is related to the position of the plume with respect to the well. Figure 4.33 shows the differences in average concentrations and mass flow rates depending on the location of the plume. In the case of using a homogeneous model to perform the interpretation, then the average concentration is independent on the plume position.

However, if the heterogeneity is considered, the local conditions of the transmissivity field at left and right of the well lead to an uncertainty in terms of average concentration. In other words, if the contaminant is located at the place with highest groundwater velocities (choosing from left and right), then the mass flow rate will be higher than in the other case (contaminant located where the water flow rate is lower)

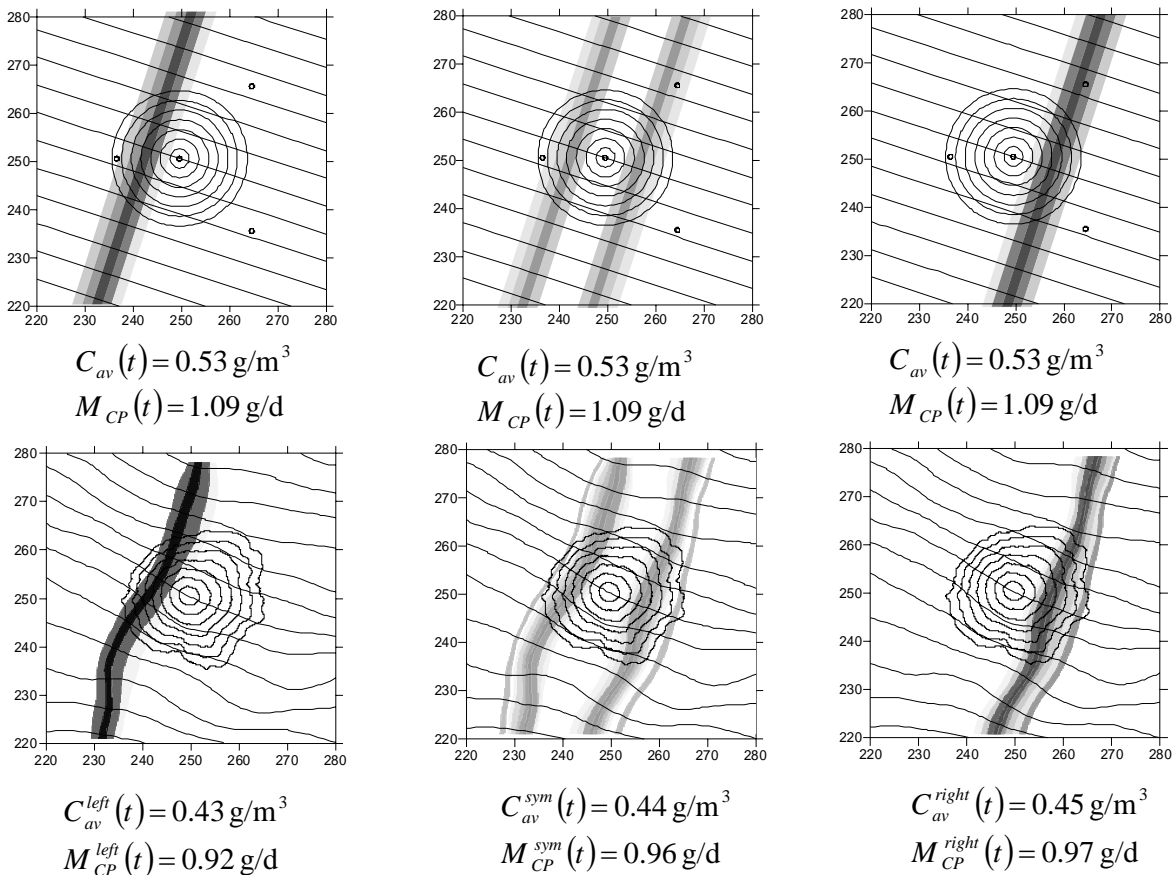


Figure 4.33: Influence of the plume position on the $M_{CP}(t)$ and $C_{av}(t)$ estimates for the analytical and numerical approaches (numerically simulated example with multigaussian T field with low degree of heterogeneity $\sigma_{\ln K}^2 = 0.25$, $\lambda = 20 \text{ m}$). Actual values from forward simulation: $M_{CP}(t) = 1 \text{ g/d}$, $C_{av}(t) = 0.46 \text{ g/m}^3$.

4.5.2. Complex integral measurement predictions: model uncertainty and possible source locations

Complex IM predictions are concerned with the delineation of source presence zones and source absence zones. The delineation of these areas is done here by defining the region upstream of CP by means of particle back-tracking with MODPATH. A specific deterministic *groundwater model* is used here for the delineation of the area upstream the CP.

The area to be investigated is then limited to the streamtube captured by integral pumping. In general, the source of the contaminant detected at the CP may be anywhere upstream the CP within the streamtube. In the case of reactive compounds, plume lengths are known to be limited (hundreds of meters). This could be considered in order to limit the possible source zone in the upstream direction by accounting for a *reaction model* that provides, for example, maximum possible plume lengths. We study this here by means of plume length statistics obtained from a large number of cases described in the literature.

Further, the investigated area defined by the captured streamtube (dotted lines in Figure 4.34) is defined through a deterministic *groundwater model*, and therefore is subject to the *quality and robustness* of the model: different *groundwater models* lead to different geometries of the captured streamtube. The general methodology here presented for quantifying uncertainty enables the estimation of the robustness of the model by introducing variability in the uncertain parameters of the model and then considering a number of deterministic models to repeat the processes for each considered *groundwater model*. This methodology was applied and described in more detail in Jarsjö et al., (2004).

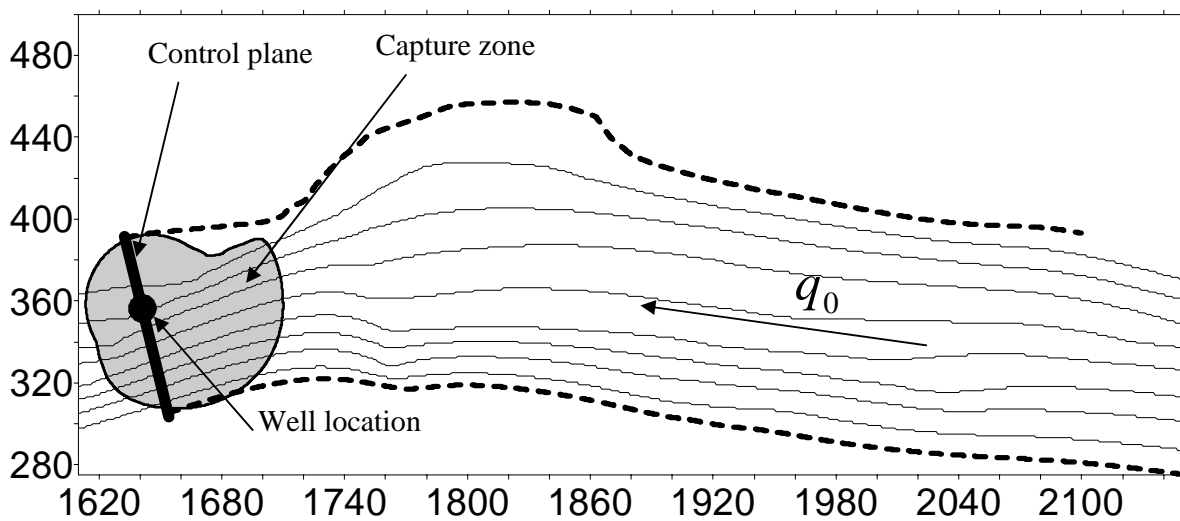


Figure 4.34: Principle of the complex IM predictions for investigating possible source zones (or source absent zone). Solid bold line: CP. Dotted bold line: limits of the streamtube captured by the IPT, limiting the source present zone (or source absent zone) 500 m upstream the CP. Thin lines: streamlines under natural conditions (no pumping)

4.5.3. Results of site application, analyses of real IPT

The measured $C_w(t)$ for all 19 wells are shown in Figure 4.35, together with the corresponding regulatory limits. These values of concentration-time, together with two groundwater numerical models (+30% and -30% hill slope inflow), were used to perform the numerical interpretation with CSTREAM and the uncertainty analyses (Jarsjö et al., 2004). In Table 4.1, we list the minimum value, the maximum value and the average value of the six mass flow estimates and the six concentration estimates obtained in the uncertainty analysis for each contaminant and well.

The interval between the minimum and maximum values reflects the combined effect of the considered *groundwater model uncertainty* and *contamination model uncertainty*. An omitted contaminant in Table 1 implies that its concentration was below the detection limit, and in the omitted well 359, the concentrations of acenaphthene, benzene and the CHCs were all below the corresponding detection limits.

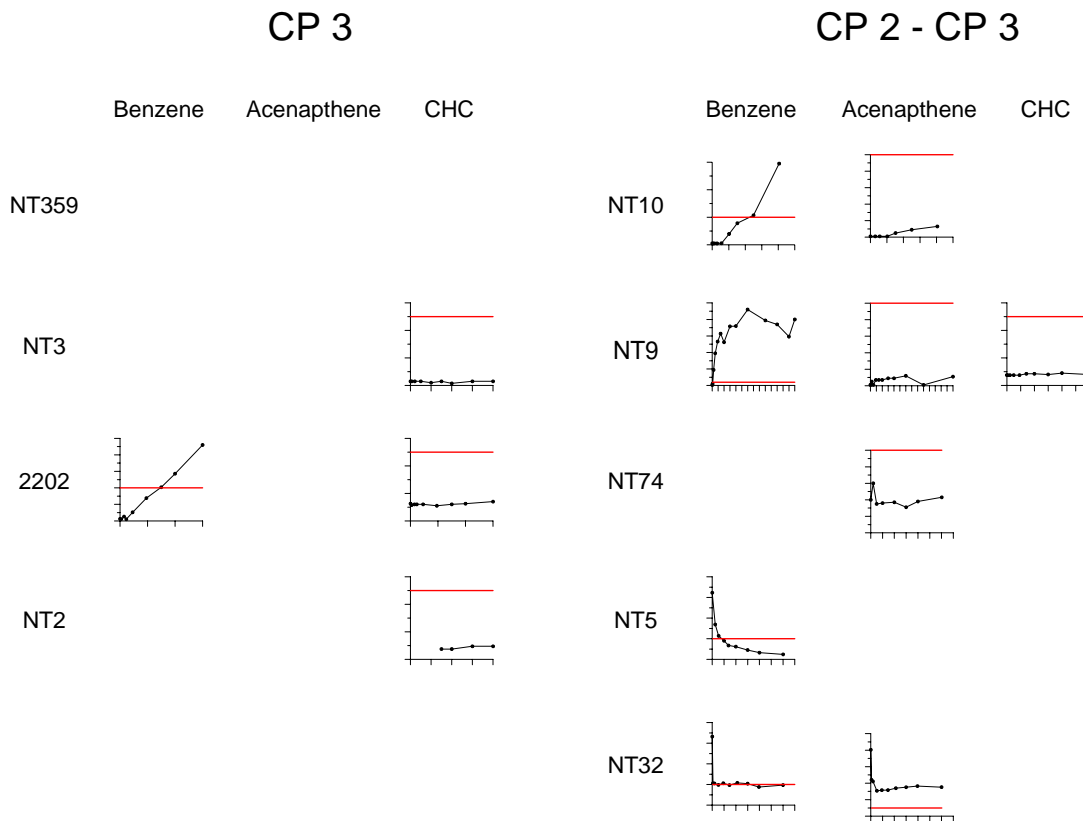


Figure 4.35a: Measured $C_w(t)$ curves in CP 2 and 3 for Benzene, Acenaphthene and sum CHC. Reference mark (horizontal line): Detection limit: Benzene=1 microg/L, Ace.=1 microg/L, sum CHC=10 microg/L. (omitted $C_w(t)$ means contaminant not detected)

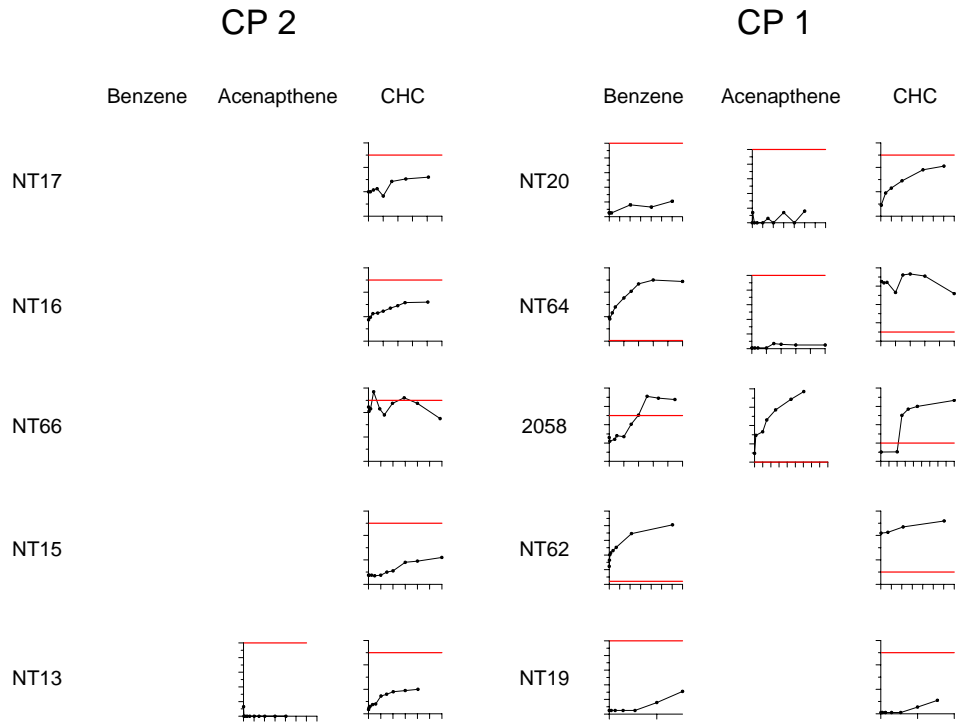


Figure 4.35a: Measured $C_w(t)$ curves in CP 1 and 2 for Benzene, Acenaphthene and sum CHC. Reference mark (horizontal line): Detection limit: Benzene=1microg/L, Ace.=1 microg/L, sum CHC=10 microg/L (omitted $C_w(t)$ means contaminant not detected)

Table 4.1. The direct IM results from the Stuttgart-Neckartalau field site.

Well	Contaminant	Mass Flow Rate (g/day)			Concentration (mg/l)		
		Min	Max	Average	Min	Max	Average
NT20	Acenaphthene	3.99E-03	6.73E-03	4.88E-03	6.47E-05	1.16E-04	8.19E-05
	Benzene	7.97E-03	1.25E-02	1.01E-02	1.23E-04	1.88E-04	1.56E-04
	ΣCHC	3.40E-01	5.05E-01	4.25E-01	5.16E-03	7.61E-03	6.60E-03
NT64	Acenaphthene	2.23E-03	4.77E-03	3.17E-03	3.85E-05	8.17E-05	5.49E-05
	Benzene	4.36E+00	9.99E+00	6.37E+00	7.51E-02	1.71E-01	1.11E-01
	ΣCHC	2.81E+00	5.94E+00	3.86E+00	4.94E-02	1.02E-01	6.70E-02
2058	Acenaphthene	1.16E-01	1.31E-01	1.23E-01	1.06E-03	1.27E-03	1.15E-03
	Benzene	5.76E+00	8.10E+00	6.83E+00	4.80E-02	6.79E-02	5.76E-02
	ΣCHC	2.17E+00	3.68E+00	2.83E+00	1.70E-02	2.86E-02	2.21E-02
NT62	Acenaphthene	2.54E-05	1.81E-02	1.40E-02	1.18E-07	8.20E-05	6.42E-05
	Benzene	4.03E+00	5.82E+00	4.61E+00	1.79E-02	2.27E-02	1.95E-02
	ΣCHC	1.07E+01	1.52E+01	1.22E+01	4.75E-02	5.90E-02	5.16E-02
NT19	Benzene	1.41E-02	2.75E-02	2.10E-02	1.32E-04	2.57E-04	1.94E-04
	ΣCHC	9.30E-02	1.91E-01	1.43E-01	8.70E-04	1.78E-03	1.33E-03
NT17	ΣCHC	4.11E-01	1.39E+00	8.86E-01	2.22E-03	8.50E-03	5.11E-03
NT16	ΣCHC	1.45E+00	1.82E+00	1.63E+00	5.32E-03	5.79E-03	5.56E-03
NT66	ΣCHC	7.51E-01	1.48E+00	1.09E+00	5.88E-03	1.03E-02	8.01E-03
NT15	ΣCHC	1.45E-01	2.35E-01	1.89E-01	3.28E-03	3.78E-03	3.52E-03
NT13	Acenaphthene	6.69E-06	1.78E-03	5.00E-04	5.87E-08	1.70E-05	4.69E-06
	ΣCHC	4.74E-02	5.98E-01	3.29E-01	4.52E-04	5.25E-03	3.00E-03
NT10	Acenaphthene	5.10E-03	3.11E-02	1.87E-02	1.85E-05	1.15E-04	6.87E-05
	Benzene	1.57E-01	6.49E-01	4.57E-01	5.71E-04	2.38E-03	1.67E-03
NT9	Acenaphthene	2.62E-02	2.97E-02	2.80E-02	8.78E-05	9.55E-05	9.17E-05
	Benzene	5.22E+00	5.71E+00	5.51E+00	1.74E-02	1.88E-02	1.81E-02
	ΣCHC	4.81E-01	5.24E-01	5.06E-01	1.61E-03	1.70E-03	1.66E-03
NT74	Acenaphthene	3.33E-03	4.01E-03	3.64E-03	3.67E-04	4.12E-04	3.94E-04
NT5	Benzene	1.19E-02	1.82E-01	8.13E-02	6.57E-05	9.89E-04	4.44E-04
NT32	Acenaphthene	6.25E-02	7.49E-02	6.85E-02	3.50E-03	3.56E-03	3.52E-03
	Benzene	1.69E-02	2.12E-02	1.92E-02	9.48E-04	1.01E-03	9.87E-04
NT3	Acenaphthene	2.04E-01	2.86E-01	2.49E-01	4.53E-04	6.35E-04	5.31E-04
	ΣCHC	2.09E-01	3.06E-01	2.59E-01	4.64E-04	6.60E-04	5.52E-04
2202	Benzene	1.18E-01	1.75E-01	1.45E-01	1.15E-03	1.64E-03	1.35E-03
	ΣCHC	2.43E-01	3.04E-01	2.79E-01	2.37E-03	2.87E-03	2.59E-03
NT2	ΣCHC	3.60E-01	5.00E-01	4.36E-01	1.44E-03	1.90E-03	1.70E-03

The average values of Table 4.1 show that benzene mass flow rates and concentrations are high in the CPs of the upgradient part of the model area (particularly in wells NT64, 2058 and NT62). However, following the flow direction approximately 300 metres to the next row of CPs (wells NT17, NT16, NT66 and NT15), there are no traces of benzene. Further downstream, there are CPs again with relatively high benzene concentration, e.g., well NT9, indicating multiple benzene sources. For CHCs, Table 4.1 shows that they are present throughout the aquifer, with exception of the upper-left corner (of Figure 4.36), containing wells NT3, 359, NT32, NT5, NT 74 and NT10. Generally, the CHC concentrations and mass flow rates decrease along the flow direction. The acenaphthene concentrations are relatively low in comparison with benzene and CHC.

Regarding prediction uncertainty, Table 4.1 indicates that the interval between the minimum and maximum predicted mass flow (and concentration) values may be relatively large for all contaminants found in a particular well (e.g., for NT10). There are also wells where these ranges are small for all contaminants (e.g., NT32). The origin of these ranges (i. e. groundwater model uncertainty and contamination uncertainty) is analyzed in Jarsjö et al. (2004). It was found that the range in both average concentration and mass flow rate depends on the standard deviation of the natural logarithm of transmissivity within the well capture zone, $\sigma_{\ln T}$. For this specific site and numerical model, wells located in heterogeneous regions of the aquifer ($\sigma_{\ln T} > 1.5$ within the well capture zone) may lead to ranges of maximum value being 3 times the minimum value (Jarsjö et al. 2004).

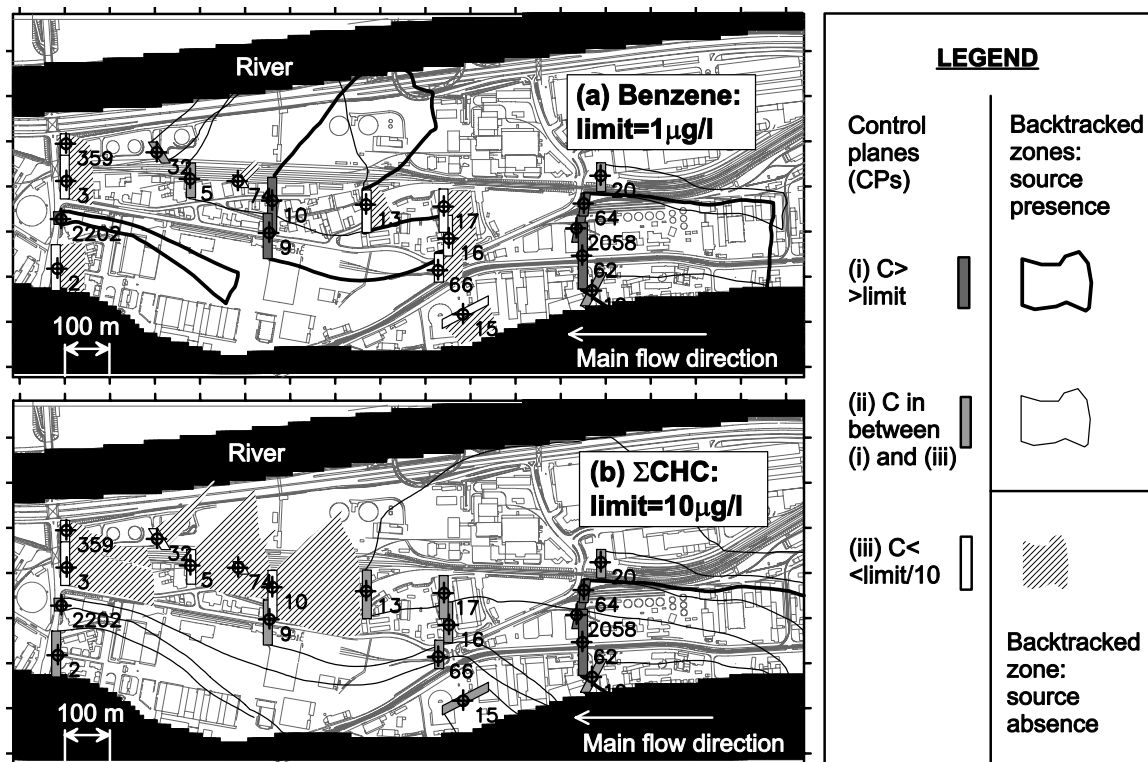


Figure 4.36. Predicted zones delimiting contaminant source, and zones absent of source, at the Stuttgart-Neckartalaue site, for (a) benzene and (b) ΣCHC . (Jarsjö et al, 2004)

4.6. Application example: Depth integrated application in Linz (Austria)

In this section we describe an application example performed in the context of the project INCORE also described in Bauer et al. (2004). Mass flow rates of PCE and TCE were quantified at an industrialized urban area in Linz, Austria. In this application, the numerical code CSTREAM was used to consider the influence of several wells pumping sequentially along a CP. If the influence of previous pumping is not considered, then each pumping well can be treated independently, resulting in so-called *independent isochrones* (see further description in section 4.2.3 and Figure 4.5). In contrast, if the influence of several wells needs to be accounted for (e.g. if there is not sufficient lag time between successive pumping events), then the interpretation needs to be done by considering *sequential isochrones* (see section 4.2.3. for detailed explanation on types of isochrones) as we did in this application example.

The investigated area is located within a bend of the Danube river. It is bounded by the Danube river in the south and the valley boundaries on the other sides, which are formed by smoothly rising crystalline rocks of the variszic mountains. It is part of a sedimentary basin of the Danube river, the “Linzer Bucht”.

The contaminated aquifer is composed of highly permeable fluvial Quaternary gravels and sands. Based on the pumping tests performed in this study, the mean hydraulic conductivity is 0.0063 m s^{-1} . The saturated thickness of the aquifer varies spatially between 5 and 10 m, and the aquifer is unconfined. Below these coarse clastic aquifer sediments, layered Tertiary marine sands and clays form the aquifer base. The flow regime is dominated by the Danube river, which provides most of the water flowing into the aquifer by bank

infiltration. Additional recharge stems from precipitation (average of 0.770 m a^{-1}) and flow from the hills. The main identified pollutant is PCE with maximum concentrations up to $60 \mu\text{g l}^{-1}$, and TCE in some wells with maximum concentrations of about $2 \mu\text{g l}^{-1}$.

4.6.1. Performance of the integral pumping tests

A total of 10 integral pumping tests were performed to investigate the groundwater downstream of the suspected source zones. Well locations are shown in Figure 4.37. About 40 days of pumping, with pumping durations of 5 to 7 days in each well were required. The pumping scheme is given in figure 4.38. To avoid the influence of previous integral pumping tests, wells were pumped from downstream first and then moving to the upstream direction.

As concentrations were expected to be low, i.e. near drinking water limits, the Austrian authorities gave permission to dispose of the pumped water directly into the sewage system. Thus no treatment of the pumped water was necessary.

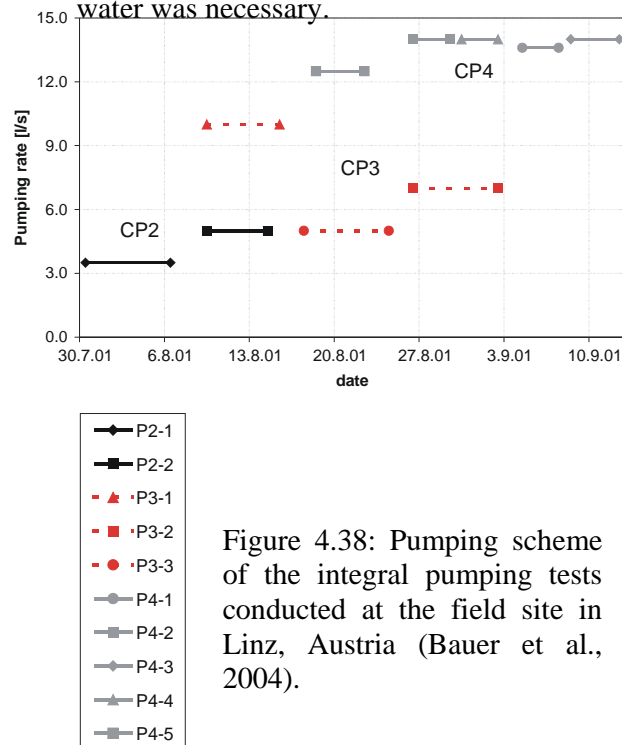


Figure 4.38: Pumping scheme of the integral pumping tests conducted at the field site in Linz, Austria (Bauer et al., 2004).

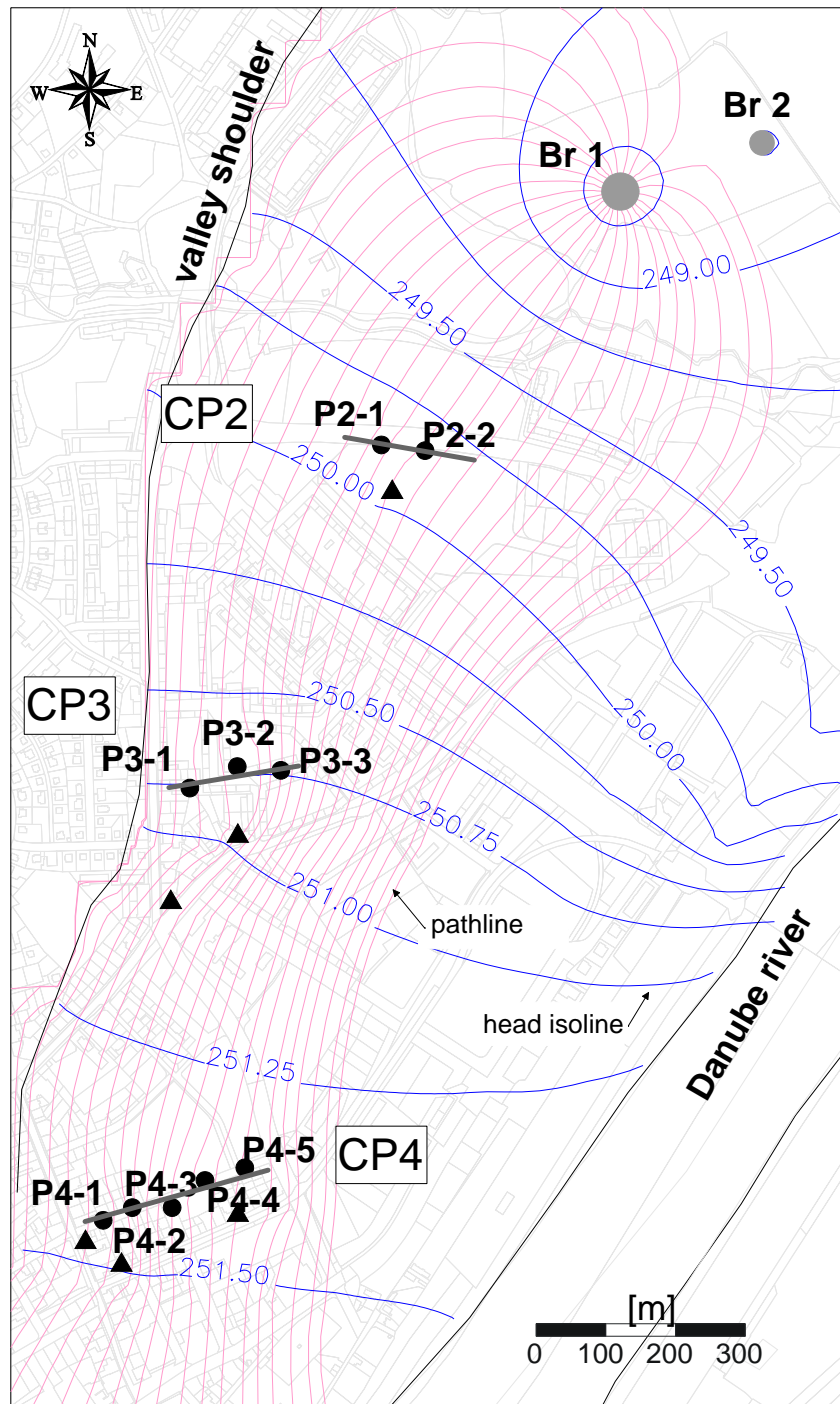


Figure 4.37: Field site in Linz, Austria. Shown is the Danube river to the south, piezometric heads, pathlines, locations of the wells, potential source zones and control planes. Black dots denote wells used for the integral pumping method, black triangles denote potential source zones, grey dots denote the wells BR 1 and BR 2 and bold grey lines indicate the control planes. Piezometric heads and pathlines are taken from the calibrated model, the pathlines represent the capture zone of BR 1. (after Bauer et al., 2004)

The measured concentration-time series are given in Figure 4.38.

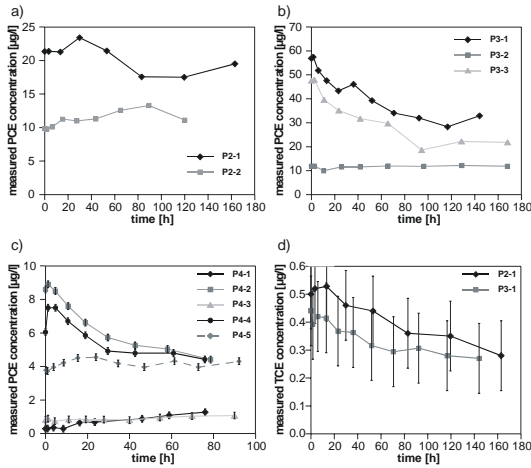


Figure 4.38: Measured PCE concentration time series: a) at CP2, b) at CP3 and c) at CP4. d) shows the concentration-time series measured for TCE at P2-1 and P3-1.

4.6.2. Interpretation of the integral pumping tests

The measured concentration time series shown in Figure 4.38 were used to perform the numerical inversion with the code CSTREAM. The numerical flow model was developed from a regional, coarse model of the whole “Linzer Bucht” (Gierlinger, 1999). The model area extends 3400 m in East-West and 3500 m in North-South direction and is represented by one model layer of varying thickness. Grid resolution varies from 50·50 m² cells down to 0.3·0.3 m² at the pumping wells. In the areas of the isochrones, the cell size is smaller than 5·5 m². The Danube river is represented by a river boundary with a river water level of 251.5 m and a leakage coefficient of $2 \cdot 10^{-5} \text{ m s}^{-1}$. Inflow from the hills to the North and West is modelled as a constant inflow boundary. The western boundary is the 248.8 m isoline taken from the regional flow model, set as a general head boundary. A drainage channel is also included in the model, which drains a large part of the infiltrating river water from the

aquifer. This channel runs parallel to the Danube river for about 1 km and serves to limit river infiltration to the aquifer along its length.

The code CSTREAM was used to perform the inversion at each control plane independently, i. e. the IPTs conducted at each CP are assumed not to affect the interpretation at the other CPs. Therefore, 3 different CSTREAM runs were used, one for each CP. The isochrones of each well at a CP influence the geometry of the isochrones of the other wells at the CP. Figure 4.39 shows the geometry of the isochrones at each CP, with the obtained average concentration from the numerical inversion. The pumping scheme shown in figure 4.38 influences the isochrone geometry, since the *interpretation time* is not at the beginning of pumping for each well, but at the start of the IPTs at each CP. In CP2, the well P2-1 was pumped first, therefore the second well P2-2 shows a deviation of the isochrone towards the upstream direction (note that the well location is outside the capture zone). This effect can be seen also in CP3, where the order of pumping was P3-1, P3-3 and finally P3-2, that is why the “centers” of isochrones are not at the well locations for wells P3-2 and P3-3. Finally, at CP4 the order of pumping was P4-5, P4-2, P4-4, P4-1 and P4-3. In figure 4.39 the isochrone geometry shows that the location of well P4-5 is at the “center” of the isochrone while for well P4-3 the isochrone is displaced to the upstream direction and the well is outside the capture zone.

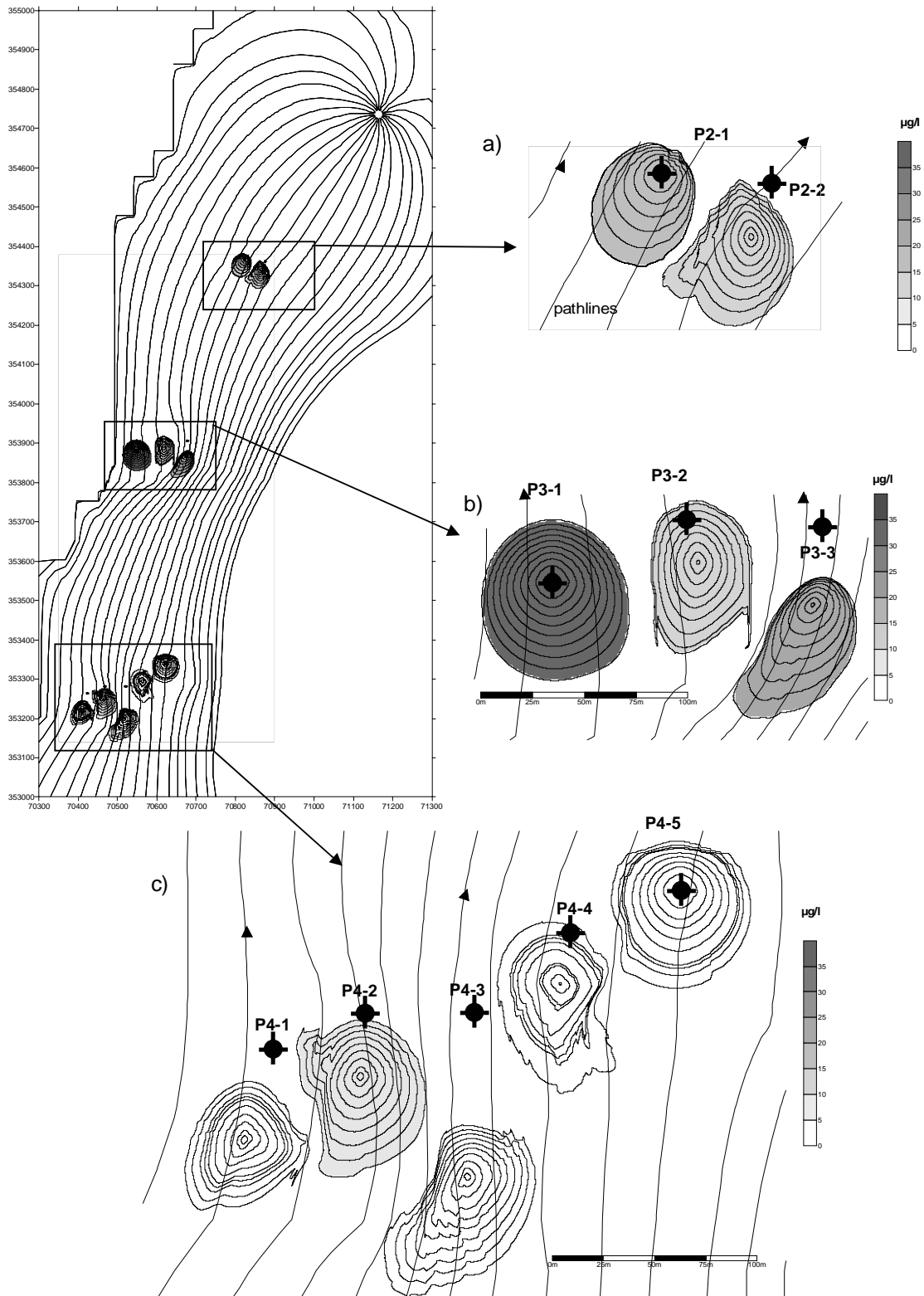


Figure 4.39: Well locations, isochrones and inverted mean concentration of PCE for control planes CP2, CP3 and CP4 (after Bauer et al., 2004) as determined by CSTREAM.

The average concentrations and mass flow rates were computed by using both the analytical solution based on the cylinder formula (Schwarz et al., 1998, see also chapter 3 for a detailed description) and the numerical inversion using CSTREAM (described at the beginning of this chapter).

A more detailed comparison of the analytical/numerical results is given in Bauer et al. (2004). Here I limit myself to show the final values of PCE and TCE average concentrations and mass flow rates in Tables 4.2 and 4.3.

In addition, Figure 4.40 shows a comparison of the isochrone geometry computed through the cylinder formula for control plane 2 (neglecting the influence of previous pumping for well P2-2) and using CSTREAM (accounting for both heterogeneity and influence of previous pumping). See also section 4.2.3. for a discussion on different ways of computing the isochrone geometry with CSTREAM. A detailed discussion on the practical results of the IPT application in Linz is given in Bauer et al. (2004)

Table 4.2: Results of the integral pumping tests for PCE (after Bauer et al., 2004) using CSTREAM.

Well	Maximum diameter [m]	Water flow across well capture zone [m ³ s ⁻¹]	Mean concentration [µg l ⁻¹]	Analytical over numerical mean concentration [-]	Maximum concentration [µg l ⁻¹]	Mass flow rate [g d ⁻¹]	Analytical over numerical mass flow rate [-]
P2-1	49.87	3.47E-03	19.50	0.99	25.34	5.84	0.54
P2-2	55.22	2.08E-03	10.90	1.08	15.70	1.96	1.72
P3-1	70.25	2.21E-03	34.30	1.01	57.59	6.55	0.84
P3-2	51.51	7.75E-04	11.80	1.00	12.82	0.79	1.64
P3-3	49.62	2.96E-03	24.90	1.03	48.12	6.36	1.06
P4-1	55.47	1.13E-03	1.02	0.97	1.62	0.10	1.28
P4-2	65.62	2.37E-03	5.37	0.98	9.04	1.10	1.74
P4-3	90.32	3.18E-03	1.02	0.95	1.68	0.28	0.96
P4-4	73.87	2.06E-03	4.43	1.12	8.00	0.79	0.58
P4-5	70.43	2.25E-03	4.27	0.99	6.94	0.83	2.09

Table 4.3: Results of the integral pumping tests for TCE (after Bauer et al., 2004) using CSTREAM.

Well	Maximum diameter [m]	Water flow across well capture zone [m ³ s ⁻¹]	Mean concentration [µg l ⁻¹]	Maximum concentration [µg l ⁻¹]	Mass flow rate [g d ⁻¹]	Analytical over numerical mass flow rate [-]
P2-1	49.87	3.47E-03	0.35	0.54	0.10	0.55
P3-1	70.25	2.21E-03	0.30	0.43	0.06	0.84

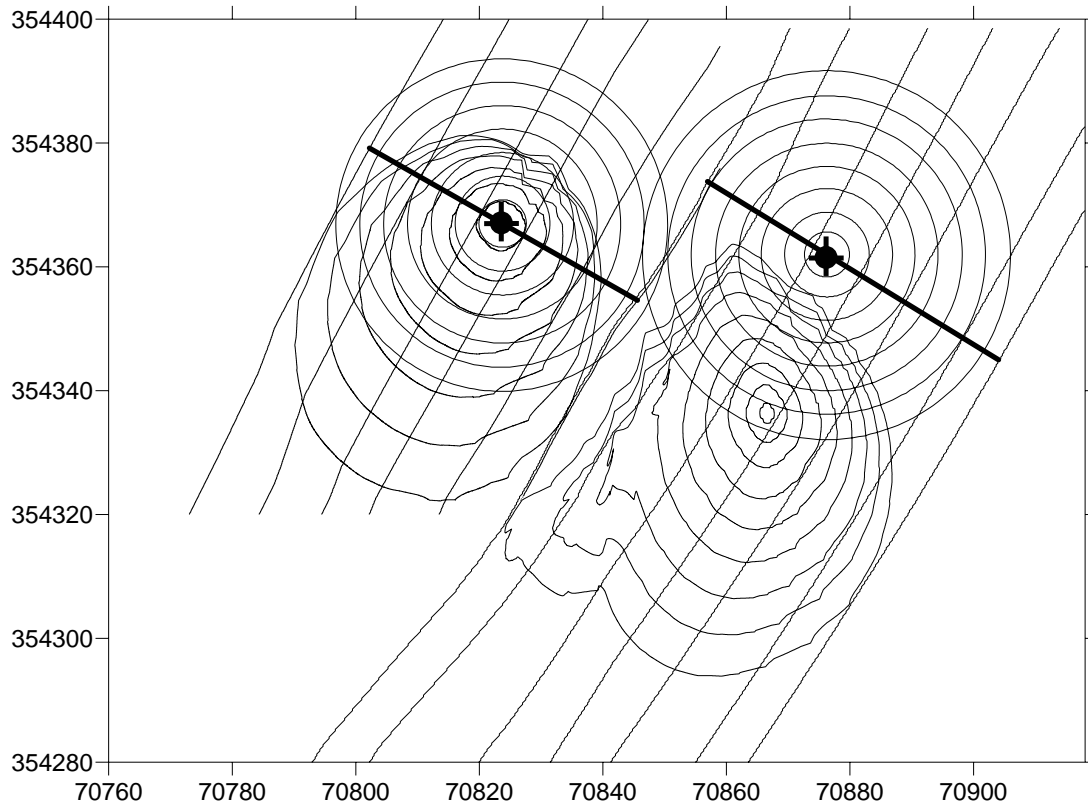


Figure 4.40: Comparison of isochrone geometry for the analytical and numerical approaches. Closed lines: Isochrones computed by particle back-tracking. Circles: Isochrones computed by the cylinder formula. Open lines: streamlines before pumping (natural uniform flow field towards NE). Black thick line: Control plane defined numerically (width of the captured streamtube)

4.7. Application example: Depth differentiated application in Bitterfeld, Germany.

This section provides the results of the interpretation of the multi-level integral pumping tests performed in the SAFIRA Bitterfeld test site, the first application of the integral approach with depth differentiated measurements. The numerical groundwater model was developed by Borkert (1999) and has been adapted to integrate specific information in the surroundings of the pumping wells and refine the discretization in the vertical and horizontal directions. The numerical interpretation was performed with the code CSTREAM.

4.7.1. Update and model cut of the regional SAFIRA MODFLOW model

The numerical interpretation of the integral pumping tests was done using a model cut of the regional model developed by Borkert (1999). The original model had 8-layers representing the regional geology of the Bitterfeld site, as shown in Figure 4.41.

For the numerical interpretation performed here we extracted the model cut shown in - figure 4.42.

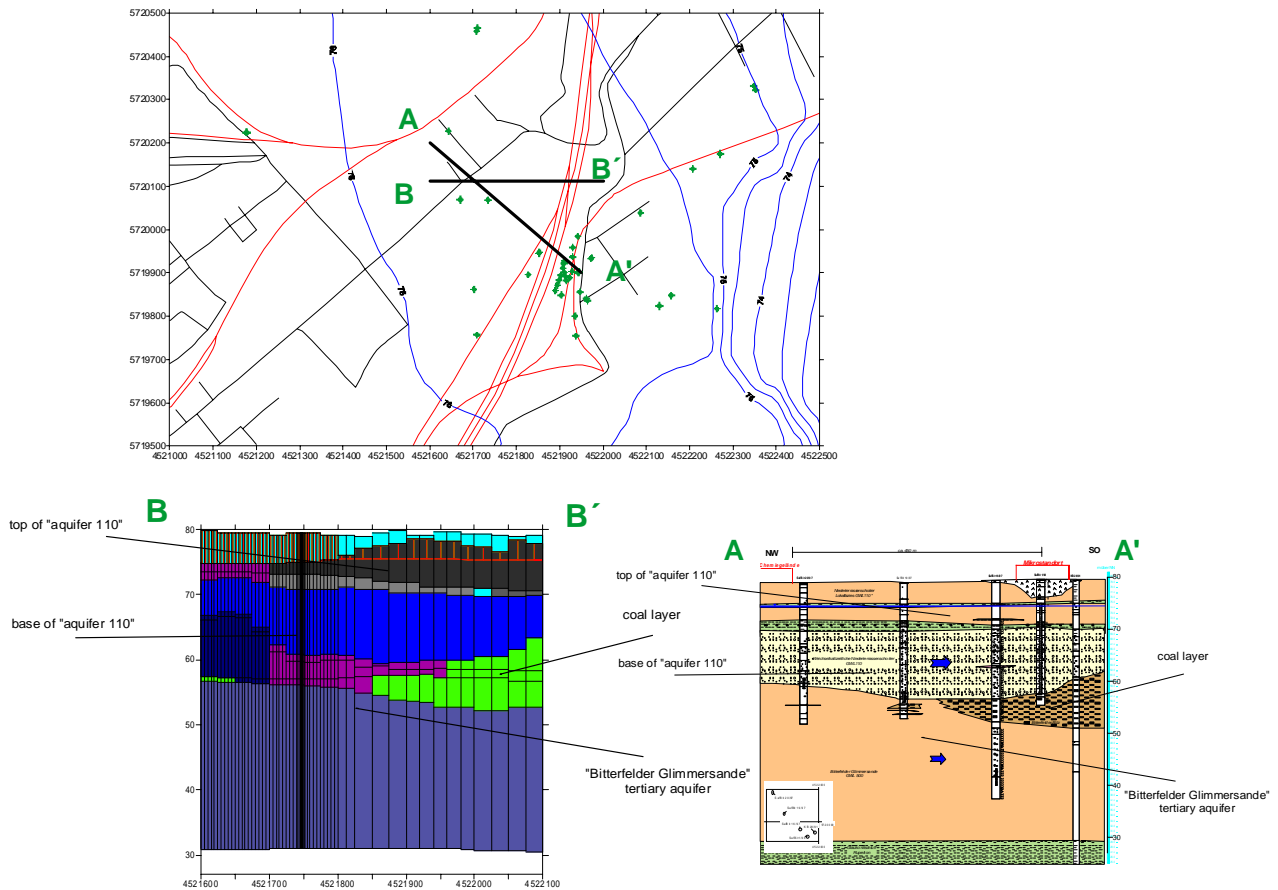


Figure 4.41. Vertical discretization of the Modflow model.

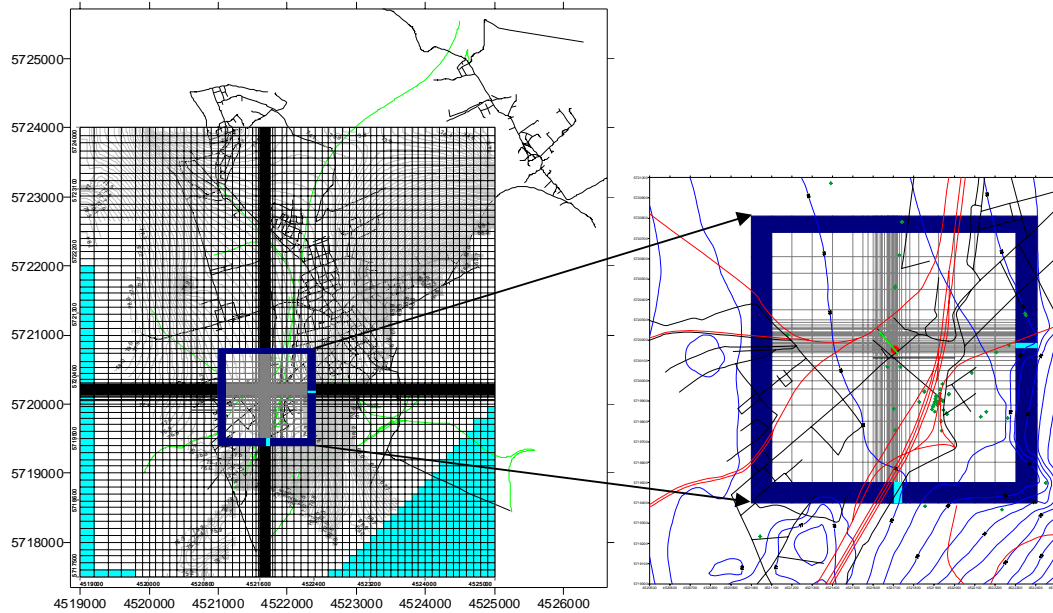


Figure 4.42. Model cut extracted from the regional model.

The discretization was refined in the horizontal and vertical directions. The horizontal grid was refined up to 2m within the surroundings of the pumping wells and the vertical discretization was refined from 8 to 14 layers. The flowmeter measurements obtained during the pumping tests provided new information on the variability in depth of the hydraulic conductivity. The hydraulic conductivities were modified in the surroundings of the wells in order to reproduce the depth-differentiated flow measured during the pumping tests. Figure 4.43 shows the refined vertical discretization up to 14 layers and figure 4.44 shows the values of hydraulic conductivity for the 14 layers.

For the validation of the modifications introduced in the model, the depth-differentiated flow during the pumping tests (obtained in the field using the flow meter measurements) is compared to the computed values extracted from the MODFLOW model as shown in figure 4.45.

The objective of the numerical model is to enable the numerical interpretation of the integral pumping tests, i. e. estimation of average concentrations and mass flow rates. Since the model can be considered homogeneous within each layer (in the vicinity of each well) and the isochrone geometry (as it will be shown below) displays a regular shape, the average concentration becomes independent of the aquifer parameters (i. e. hydraulic conductivity, thickness and porosity) and the mass flow rate is the product of average concentration and groundwater flow rate (i. e. linearly related to the hydraulic conductivity).

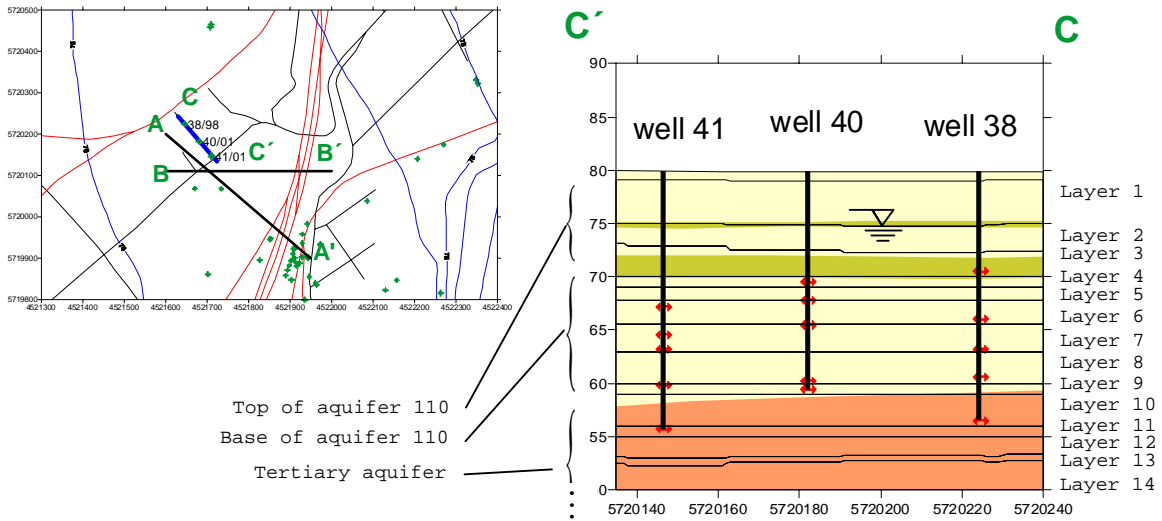


Figure 4.43: Model cut extracted from the regional model, position of the pumping wells and vertical discretization.

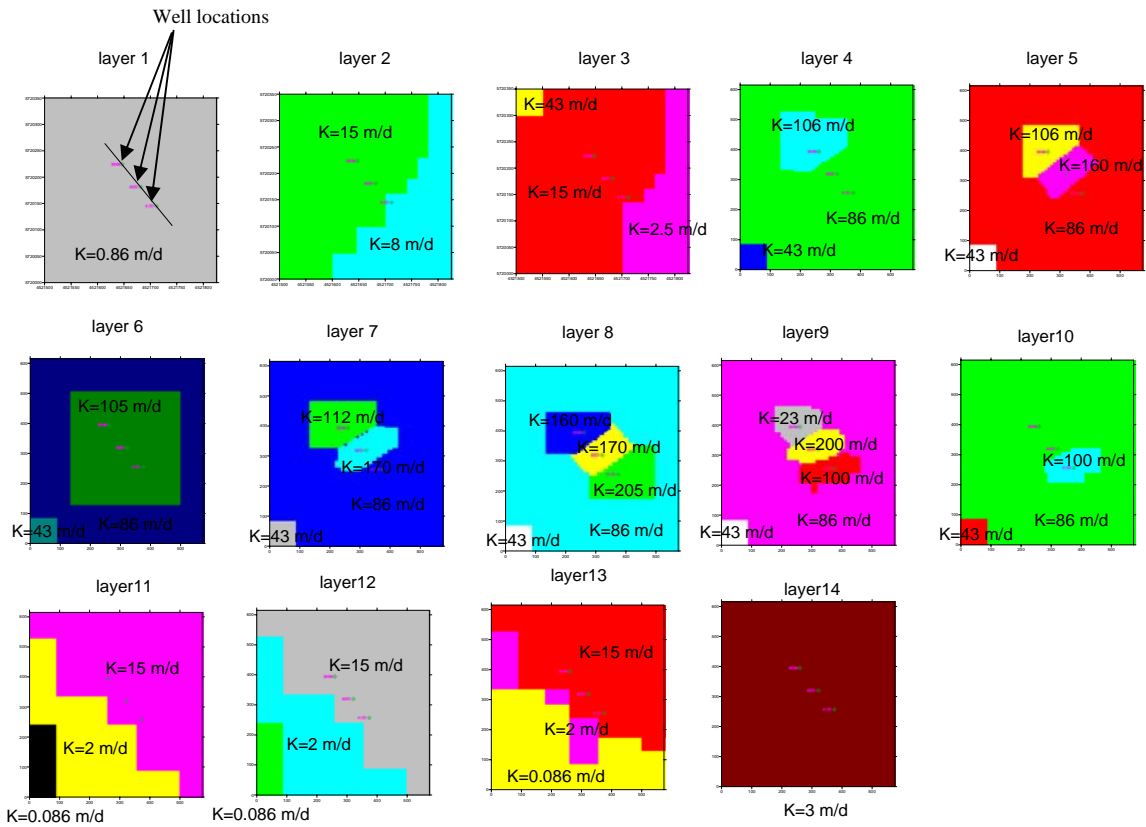


Figure 4.44: Values of hydraulic conductivity for the 14 layers of the model.

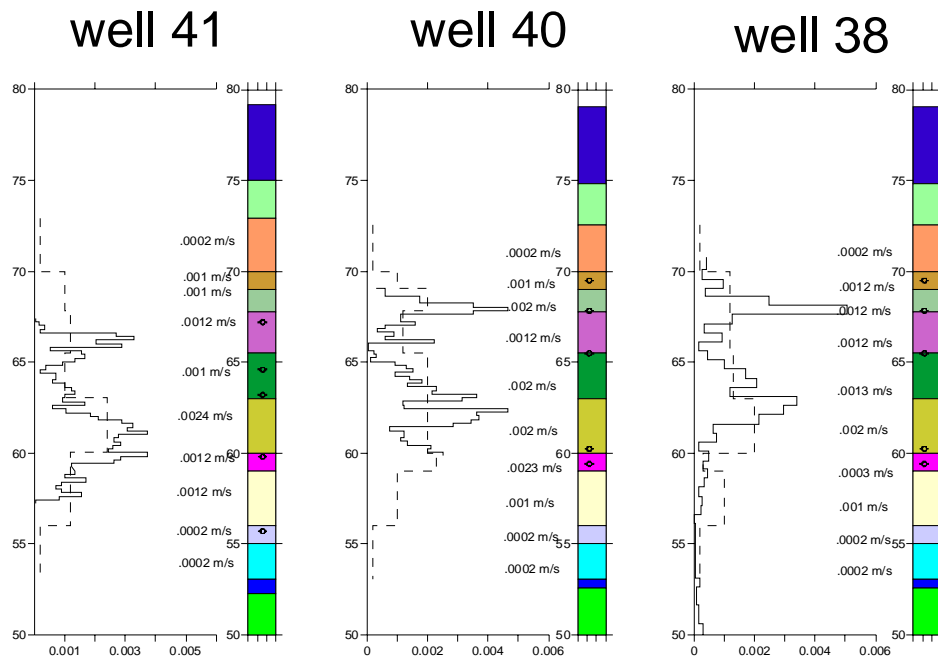


Figure 4.45. Measured and computed Darcy velocities at the pumping wells. Dotted line: modelled. Solid line: Flow meter measurement

4.7.2. Numerical evaluation of the integral pumping tests

The multi-level samplers used during the integral tests were located at the depths indicated in Figure 4.46. The numerical inversion was performed for model layers 4 to 10, using the concentration time series measured at each level, as indicated in Table 4.4

Table 4.4: Modflow layers for each depth level at the tree pumping wells

MODFLOW layer	w38	w40	w41
4	4		
5	4	4	
6	4	3	4
7	3	2	3
8	2	2	2
9	1	1	1
10	1		1

The code CSTREAM was used for the evaluation of the integral pumping tests in each layer. Figure 4.47 shows the head iso-lines under natural conditions (before the pumping tests). The groundwater flow direction is mainly towards east and the natural gradient is of the order of 0.0002, except for layer 4 where the flow direction is towards the northeast with a higher gradient of about 0.001.

Figure 4.48 and 4.49 show the isochrones obtained numerically in each layer. The influence of previous pumping tests leads to non-circular isochrones for wells 40 and 38; well 41 started pumping in the first place and has no influence of previous pumping tests.

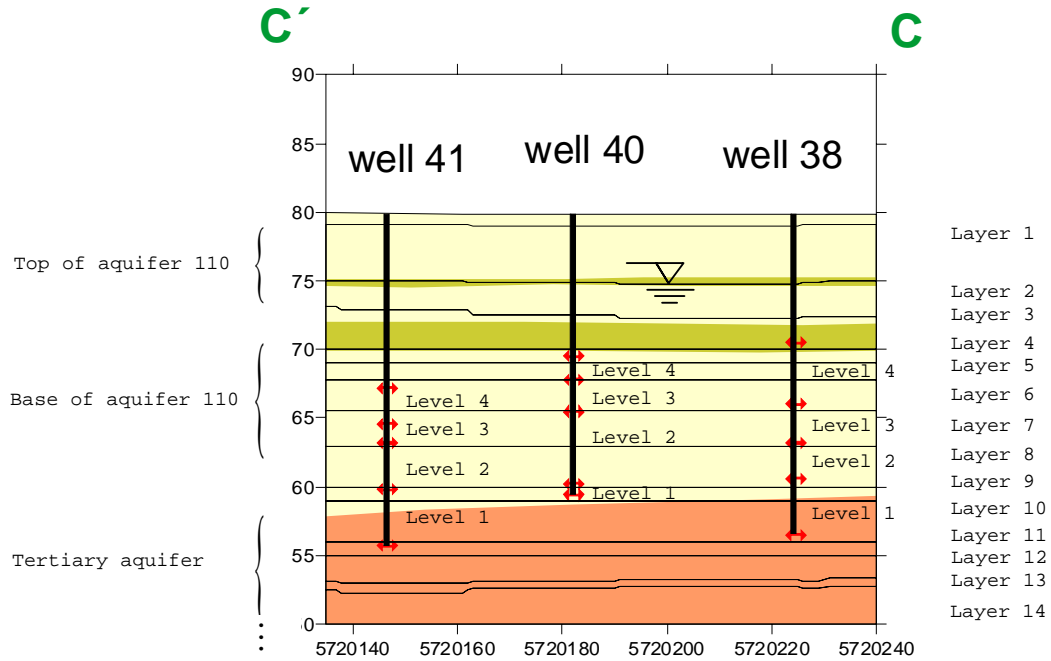


Figure 4.46: Location of the level separators (multi-level sampling) and layers of the Modflow model.

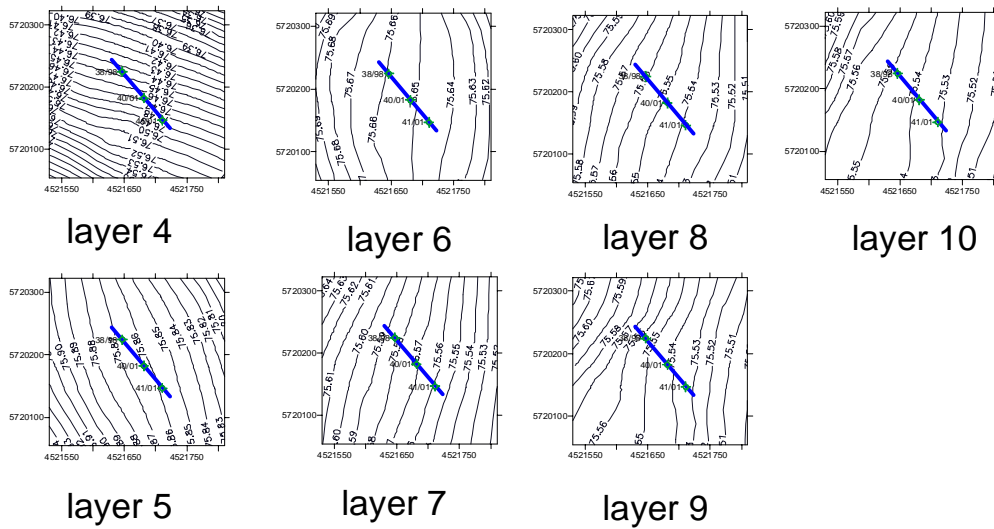


Figure 4.47: Head isolines under natural conditions (before the pumping tests) as computed in each layer of the MODFLOW model

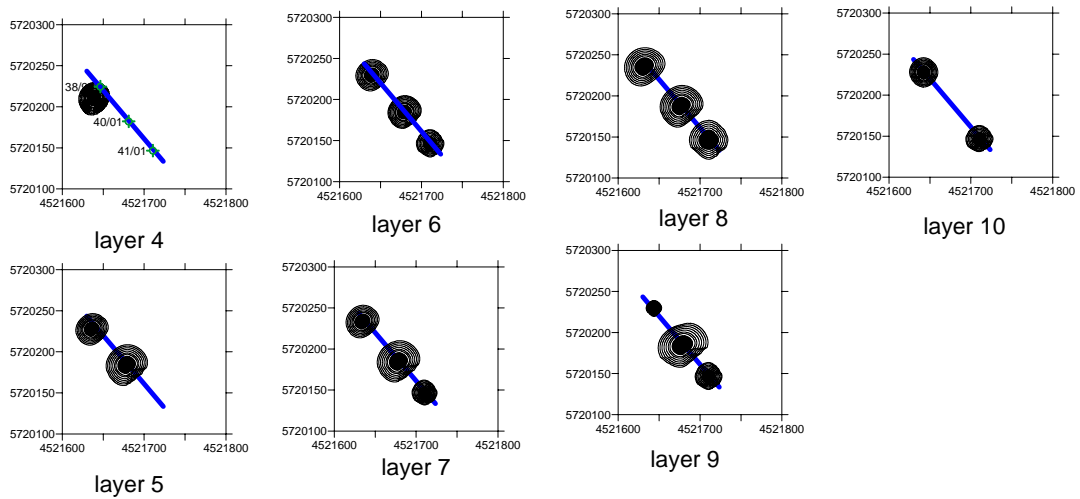


Figure 4.48. Capture zones of wells 38,40 and 41 for each layer of the modflow model

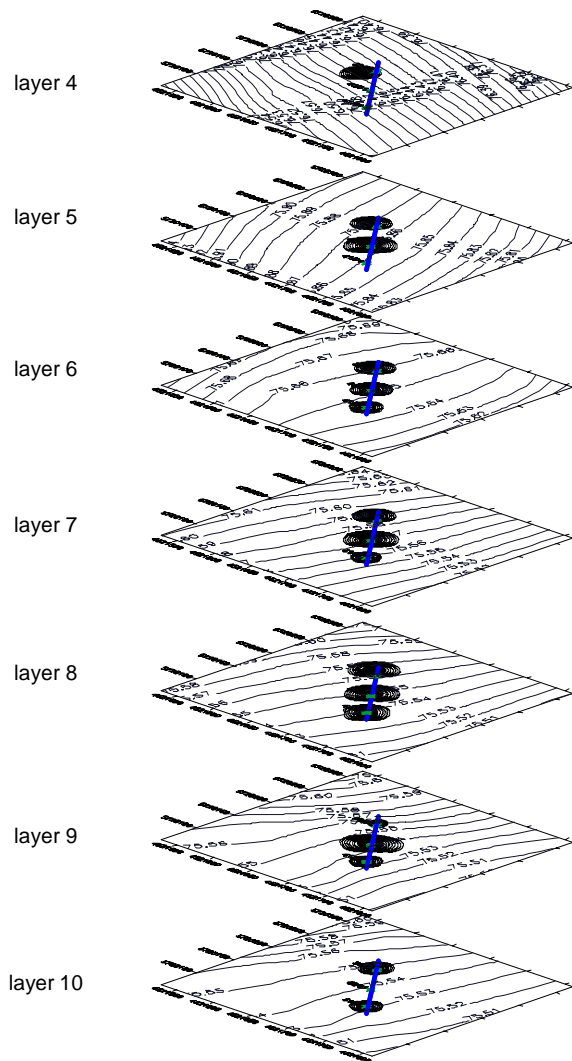
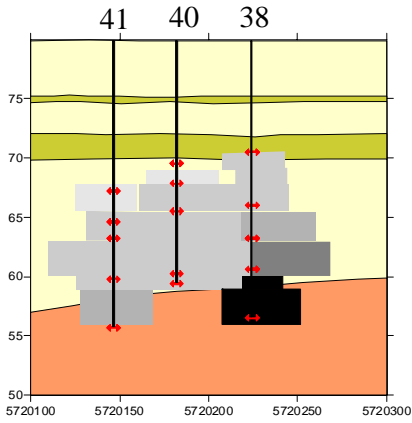
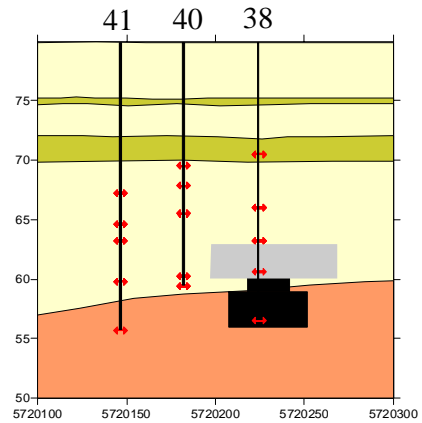


Figure 4.49: Isochrones in each layer, depth-differentiated

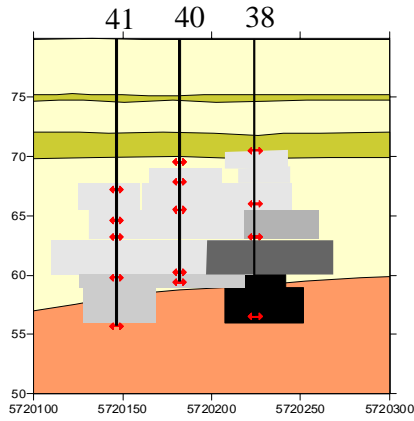
The inverse reconstruction of the initial concentration distribution from the measured concentration-time series leads to an estimation of the average concentration within each depth differentiated level. Using the data from the three wells and the 4 depth-levels it was possible to localize the contaminant distribution and identify changes in concentration in both vertical and horizontal directions for all the analysed contaminants (Benzene; Chlorobenzen; 2-C₆H₄ClCH₃; 1,2-DCB and 1,4-DCB). Figures 4.50 and 4.51 show the depth-differentiated results of the numerical inversion, in terms of average concentration.



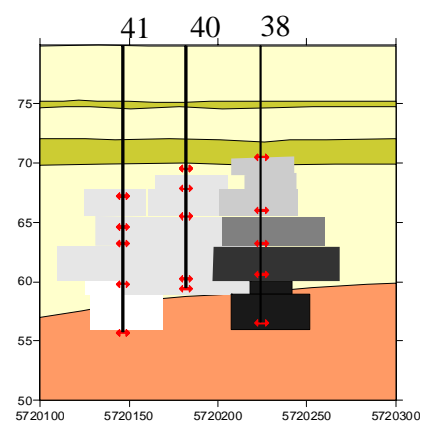
Benzene. BLACK=13 mg/L
EPA drinking water standard=0.005 mg/L



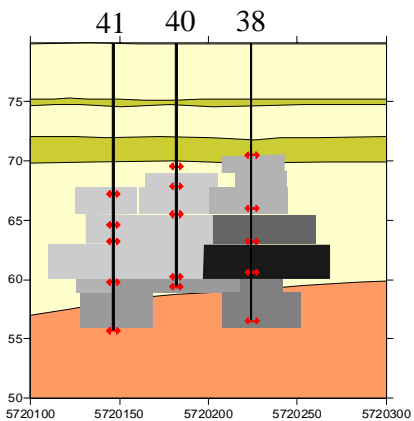
Monochlorobenzene. BLACK=40 mg/L
EPA drinking water standard=0.1 mg/L



2- C₆H₄ClCH₃. BLACK=0.5 mg/L
No EPA drinking water standard.



1,2-DCB. BLACK=2 mg/L
EPA drinking water standard=0.6 mg/L



1,4-DCB. BLACK=3.5 mg/L
EPA drinking water standard=0.075 mg/L

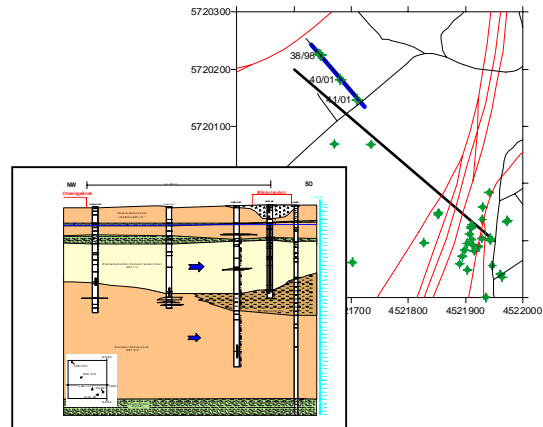


Figure 4.50: Depth differentiated contaminant distribution at the Control Plane

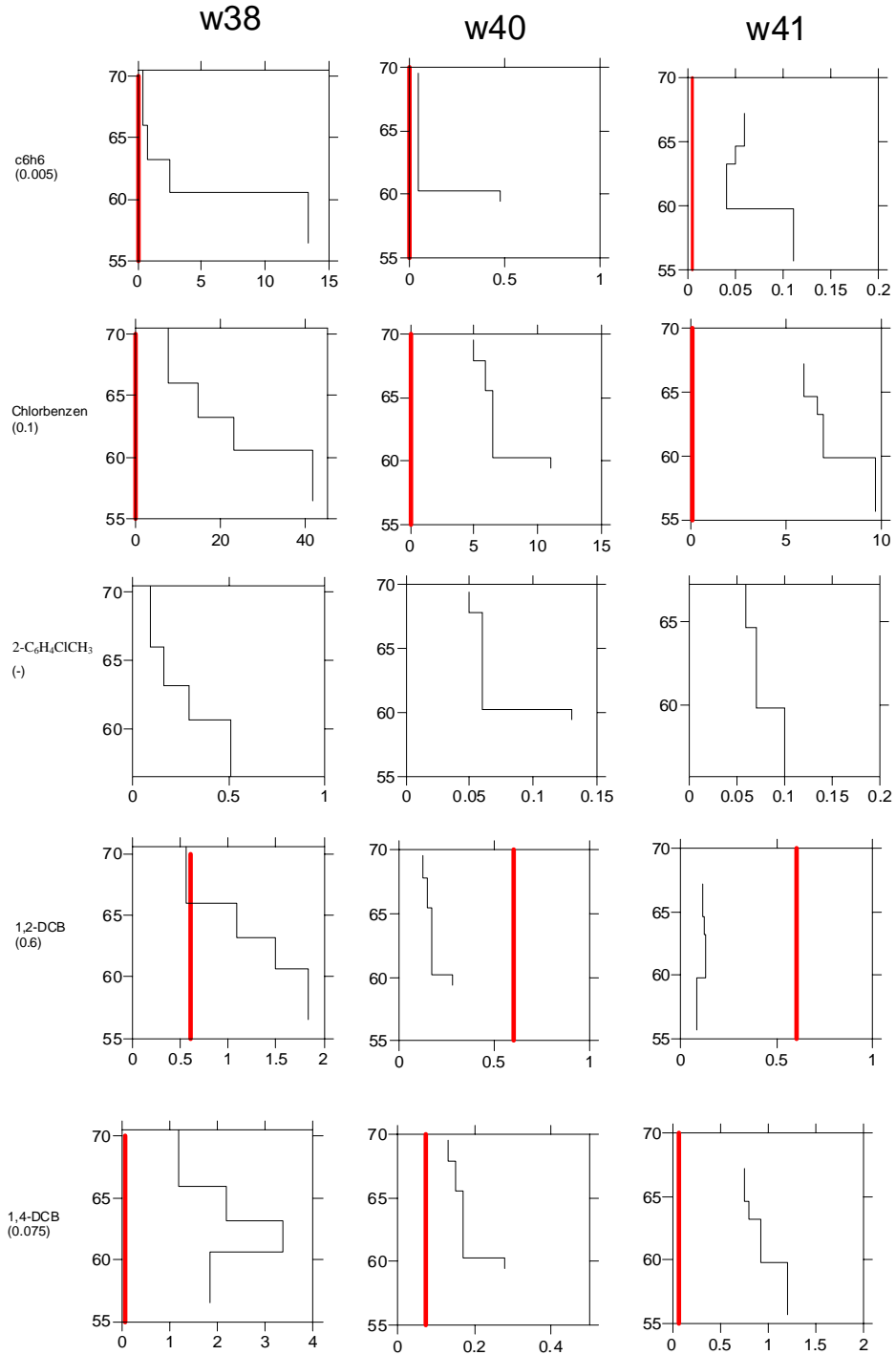


Figure 4.51: Average concentration [mg L^{-1}] at each depth level for wells 38,40 and 41. Vertical line: EPA drinking water standard July 2002 (value indicated in the parenthesis, in mg/l).

The total contaminant mass flow rate is obtained by integrating the contaminant mass flux along the control plane. Table 4.5 gives the output of the numerical

evaluation in terms of average concentration and mass flow rates.

	average concentration mg/l			mass flow rate g/day			
	W38	w40	w41	W38	w40	w41	TOTAL M
C_6H_6							
layer 4	0.35			0.98			
layer 5	0.35	0.05		0.54	0.12		
layer 6	0.35	0.06	0.06	0.73	0.11	0.09	
layer 7	0.72	0.05	0.05	3.34	0.32	0.15	
layer 8	2.49	0.05	0.04	18.84	0.37	0.27	
layer 9	13.62	0.47	0.12	3.54	1.20	0.15	
layer 10	13.33		0.12	28.77		0.27	
				56.74	2.12	0.92	59.77
Chlorbenzen							
layer 4	7.34			20.66			
layer 5	7.42	4.88		11.40	12.12		
layer 6	7.46	5.90	5.96	15.46	11.41	9.38	
layer 7	14.50	6.48	6.66	66.98	42.61	18.12	
layer 8	22.97	6.53	6.79	173.49	49.91	44.90	
layer 9	42.38	10.94	10.11	11.03	27.84	12.27	
layer 10	41.61		9.87	89.79		22.58	
				388.81	143.89	107.25	639.95
$2-C_6H_4ClCH_3$							
layer 4	0.09			0.24			
layer 5	0.09	0.05		0.13	0.13		
layer 6	0.09	0.06	0.06	0.18	0.12	0.10	
layer 7	0.16	0.06	0.07	0.72	0.37	0.18	
layer 8	0.29	0.06	0.07	2.16	0.43	0.45	
layer 9	0.52	0.13	0.10	0.13	0.32	0.12	
layer 10	0.51		0.10	1.11		0.22	
				4.68	1.37	1.08	7.13
1,2-DCB							
layer 4	0.55			1.55			
layer 5	0.56	0.13		0.85	0.32		
layer 6	0.56	0.15	0.11	1.16	0.30	0.17	
layer 7	1.08	0.16	0.12	5.01	1.08	0.34	
layer 8	1.48	0.17	0.13	11.20	1.27	0.84	
layer 9	1.86	0.28	0.08	0.49	0.71	0.10	
layer 10	1.83		0.08	3.94		0.18	
				24.20	3.68	1.63	29.51
1,4-DCB							
layer 4	1.17			3.30			
layer 5	1.18	0.72		1.82	1.80		
layer 6	1.19	0.83	0.77	2.46	1.60	1.21	
layer 7	2.17	0.76	0.80	10.00	5.01	2.18	
layer 8	3.34	0.76	0.86	25.26	5.83	5.71	
layer 9	1.88	1.46	1.30	0.49	3.71	1.58	
layer 10	1.84		1.25	3.96		2.86	
				47.29	17.94	13.53	78.77

Table 4.5: average concentration and mass flow rate computed with CSTREAM

The mass flow rate is an integrated quantity and therefore depends of the size of the considered control plane. Since each depth level represents its own control plane, we use the mass flux (mass flow per unit of area perpendicular to the flow) to compare the results for different levels.

The average mass flux representing the control plane defined by all wells can be computed by dividing the total mass flow rate by the total area of the control plane, estimated to be 1500 m² (length of the control plane = 100 m; thickness = 15 m). Using the values of Table 4.5 for the total mass flow rates, we obtain the average mass flux for each compound. To show the spatial variability within the control plane, minimum and maximum mass fluxes are also given.

Table 4.6 shows the overall results of the inversion, representing average values for the whole control plane. The most contaminated areas are at the lower part of well 38 and the cleanest zone is located at the upper part of well 41. The differences between maximum, minimum and average mass fluxes indicate that Benzene is mainly located at the highly contaminated area (mass fluxes being 3 orders of magnitude higher) while Chlorobenzene is more regularly distributed within the control plane surface. The distribution of 2-Chlorotoluene, 1,2 Dichlorobenzene and 1,4 Dichlorobenzene leads to mass fluxes that are one order of magnitude higher at the most contaminated area.

Table 4.6. Overall results of the numerical inversion for all 4 levels and 3 wells.

	Average Concentration [g/m ³]	Total Mass Flow Rate [g/day]	Average Mass Flux [g/day/m ²]	Max mass flux (well,layer) [g/day/m ²]	Min mass flux (well,level) [g/day/m ²]
Benzene	1.06	59.77	0.037	0.245 (38,1)	0.001 (40,3)
Monochlorobenzene	11.31	639.95	0.392	1.025 (38,2)	0.109 (41,4)
2-Chlorotoluene	0.13	7.13	0.004	0.013 (38,2)	0.001 (41,4)
1,2 Dichlorobenzene	0.52	29.51	0.018	0.066 (38,2)	0.002 (41,1)
1,4 Dichlorobenzene	1.39	78.77	0.048	0.149 (38,2)	0.014 (41,4)

Chapter 5

SUMMARY AND CONCLUSIONS

At many polluted sites, irregularly distributed source zone locations as well as preferential transport paths within the aquifer cause an irregular distribution of contaminants in the groundwater, which can be difficult to quantify using a limited number of monitoring wells. The Integral Pumping Test (IPT) method complements (and provides an alternative to) conventional monitoring grids, where the mass flow and concentration of contaminant plumes may be misinterpreted or even missed under certain conditions.

This method has been proved to be very useful at large scale contaminated sites in industrial and/or urban areas, where the presence of buildings constrain the density of the well monitoring network. Five large-scale applications of IPTs, in the context of the EU project INCORE, have been conducted in Stuttgart (Germany), Linz (Austria), Milano (Italy) and Strasbourg (France), reported in Ptak et al. (2003). In such sites, the separation between wells is typically tens of meters and the risk for contaminant plumes to remain unsampled between wells is avoided through pumping. The integral approach is capable of reaching aquifer regions that can not be investigated using conventional methods.

Further, in order to quantify natural attenuation (NA) processes, Griebler et al. (2004) revealed conclusive evidence for *in situ* biodegradation of benzene, toluene, o-xylene, m/p-xylene, naphthalene and 1-methylnaphthalene using $^{13}\text{C}/^{12}\text{C}$ fractionation data. Further, combination of the IA with such methods based on compound-specific isotope analysis has been applied to quantify field-scale biodegradation processes of BTEX compounds (Peter et al., 2004).

5.1. Integral approach, integral equation

The governing equation describing the relationship between measured data and estimated variables during an IPT is a Volterra integral equation of the first type. Such equations are not frequently used in subsurface hydrology. However, integral formulations of the flow equation have been used, recently, based of the Fourier transform (Vasco & Karaski, 2001) and on the Laplace transform (Ginn & Cushman, 1992). When studying transport, integral equations are applied in the context of probability theory to describe solute transport in the vertical direction through the unsaturated zone (Jury and Roth, 1990) using “Solute Transfer Functions” which give the probability density function of the BTC. Dagan & Cvetkovic (1996) presented a Lagrangian framework where the BTC under parallel heterogeneous flow is expressed as a Fredholm integral equation, with a kernel termed “reaction function”. Finkel (1999) extend the reaction function model to vertical transport for saturated conditions and Bold (2004) considered unsaturated media. Ginn (2001) expresses the BTC of a non reactive tracer under natural parallel flow as a flow-weighted sum using Volterra and Fredholm integral equations.

Integral equations are typically ill-posed, i. e., their solution is non-unique. For a long time mathematicians felt that ill-posed problems cannot describe real phenomena and objects. However, the class of ill-posed problems includes many classical mathematical problems and, most significantly, such problems have important applications (Tikhonov & Arsenin, 1977). A classical ill-posed

problem typically studied in hydrology is the inverse problem for parameter estimation (extensively discussed in the literature, e. g. Carrera & Neuman, 1986a; b ;c)

The derivation of the fundamental equations presented here partially follows the results given in previous work (equations 2.16 to 2.17, figures 2.2 and 2.3 in Schwarz, 2002). As described in chapter 2, the previous work is generalized through introducing the Reynolds transport theorem and building up the mathematical proof by accounting for 3-D heterogeneous conditions and advective (or linearly retarded) transport.

5.2. Analytical solutions: averaging measured data and dimensioning integral pumping tests.

The analytical framework developed in chapter 3 provides some novel relationships that are useful for both understanding the interpretation of IPTs and dimensioning the optimal pumping duration.

The analytical solution derived in Schwarz et al. (1998) (described also in chapter 3), written as a recursive equation, provided the first basic tool for the interpretation of IPTs. Theoretically, this solution is only valid for perfect radial flow during pumping (i. e. $q_0 = 0$). A new analytical solution for the general case of any q_0 was derived (after Bear & Jacobs, 1965) also as a recursive equation. This novel solution enables quantification of the influence of q_0 on the prediction, providing a range of applicability of the simplified approach (as discussed at the end of chapter 3). It is shown that radial flow is a reasonable approximation for pumping tests of duration $t < Q n_e / 2\pi b q_0^2$. Within the same comparison and using the general recursive solution (valid for any pumping

duration), it was found that IPTs of duration longer than $t_{\max} = 3 Q n_e / b q_0^2$ do not provide new information on the initial concentration distribution at the control plane, since after $t_{\max} = 3 Q n_e / b q_0^2$ the isochrone shape extends towards the upstream direction and does not significantly increase the width of the capture zone volume. Although this conclusion is drawn from a homogeneous conceptual model, it still applies to heterogeneous conditions, since long IPTs (i. e. duration close to $t_{\max} = 3 Q n_e / b q_0^2$) yield very elongated isochrone shapes (with a regular geometry in a homogeneous aquifer and with an irregular shape in heterogeneous media, but extending towards the upstream direction in any case and therefore not leading to new information).

Further, under the same assumptions as in Schwarz et al. (1998) a novel closed-form solution has been derived by means of Abel's integral transform (yielding a *non-recursive* solution). Although a more general numerical solution (non-radial flow) is now available, this solution brings fundamental knowledge on the representatives of samples, since it provides a weighting function for the measured data $C_w(t)$. The field-scale representative average concentration $C_{av}(t)$ is then expressed as a weighted average of $C_w(t)$ in an integral of the form

$$C_{av}(t) = \int_0^t C_w(\tau) f(\tau, t) d\tau \quad \text{where the}$$

weighting function $f(\tau, t)$ increases for increasing τ . Physically, this means that "late samples are more important", in the sense that they contain more information on the overall $C_{av}(t)$ average, compared to early samples. In other words, the IA provides a methodology for estimating an average concentration C_{av} , representative for a large aquifer volume. The estimate

C_{av} is just a weighted average of the measured concentrations at the pumping well $C_w(t)$. A simple formulation of the inversion problem is “how shall we average the measured $C_w(t)$ to obtain a representative estimate of C_{av} ?” or in other words “how does $f(\tau, t)$ depend on pumping time, heterogeneity, sorption, degradation, dispersion or linear retardation?”

Within a stochastic framework, the effects of heterogeneity can be accounted for in a systematic way, by introducing probabilities for spatial capture zone extents (van Leeuwen et al. 1998, 2000). Recently, methods for quantifying heterogeneity based on the analyses of draw-down observed in a pumping well have been proposed (Karami & Younger, 2002). Such methods provide a valuable tool for estimating uncertainty of the estimates of average concentration and mass flow rate.

5.3. Numerical algorithm: CSTREAM

The computer program CSTREAM has been developed, tested and applied within the context of this thesis, as described in chapter 4. It has been applied within several field scale studies for the interpretation of site-specific data in, for instance, Bayer-Raich et al. (2001), Jarsjö et al. (2002), Bauer et al. (2002), Tunturi (2003), Rügner et al. (2004) and Ptak et al. (2003).

In order to verify the accuracy of the algorithms, intensive testing has been made for both homogeneous conditions (by comparison of the output with the analytical solutions derived in chapter 3) and heterogeneous conditions (by performing virtual IPTs through numerical simulations of advective transport in heterogeneous models using the code MT3D (Zheng, 1990).

In general, CSTREAM may be used in two different ways: (1) dimensioning and evaluating real IPTs through measured data obtained in the field and (2) as a basic tool for performing theoretical studies in order to quantify, for instance, the influence of (unknown) heterogeneity (e. g. within a stochastic framework).

With regard to (1) (i. e., the practical usefulness), CSTREAM has been implemented under a wide range of different conditions. A highly heterogeneous model of the Neckar Valley was used for testing (Bayer-Raich et al., 2002) and quantifying uncertainties related to heterogeneous conditions and variability of boundary conditions (Jarsjö et al. 2002). In a more homogeneous model of the urban area in the city of Linz (Austria), Bauer et al., (2004) and Tunturi (2003) applied CSTREAM analyzing IPTs at several control planes by accounting for the actual sequence of pumping. In Osterhofen (Germany), difficult hydraulic conditions due to a steep slope of the aquifer bottom and very high Darcy velocities could be considered within CSTREAM leading to consistent results (Rügner et al., 2004).

The first field-scale application of IPTs in multi-layered aquifers was also evaluated by extending the numerical algorithms to consider depth-differentiated measurements of $C_w(t) = C_w(z_i, t)$. Using a new sampling technique, depth differentiated average concentration and mass flows were estimated in the industrial area of Bitterfeld (Germany), as described in section 4.7.

Using stochastic simulations within a geo statistical framework is a challenging field for future use of CSTREAM. Open questions that may be tackled using deterministic models or stochastic simulations are, for instance, “How do integral pumping tests influence each other when performing sequential or simultaneous pumping along series of

wells at a given CP?” “Which is the best order to pump the wells?” “How long shall we wait between successive pumping events?” “In what cases can we neglect the influence of successive/simultaneous pumping?” “In what cases is this influence critical?”

Future work for extending the numerical algorithms may be focused on considering 3-dimensional aquifers, without the restriction to multi-layered systems. Presently, the interpretation is based on the assumption that the vertical components of the flow field can be neglected, i. e. $\bar{q}_0(x, y, z)$ and $\bar{q}_w(x, y, z)$ are dependent on all (x, y, z) , but the vertical component is zero. In other words, no vertical mixing between layers is considered and the hydraulic conductivity field is assumed to be $K(x, y, z) = K(z)$. The multi-layered model implemented here is realistic and capable of accounting for the typical information available in field experiments: number of layers and hydraulic parameters of each layer (obtained in the field using, for instance, flow meter measurements yielding an estimate of the hydraulic conductivity $K(z)$ at the well). Actual 3D scenarios would be of interest mainly in the context of theoretical studies, i. e. by considering virtual aquifers where all aquifer parameters are known at all (x, y, z) locations of the aquifer.

References

[Abel, 1823] Abel. Solution de quelques problemes a l'aide d'integrales definies. Magazin for Naturvidenskaberne, Aargang I, Bind 2, Christiania 1823.

[Bauer et al., 2004] Bauer, S., Holder, T., Bayer-Raich, M., Ptak, T., Kolesar, C., Müller, D., 2004. Quantification of groundwater contamination in an urban area using integral pumping tests. *J. Contam. Hydrol.*, submitted.

[Bauer et al., 2002] Bauer, S., Bayer-Raich, M., Holder, T., Jarsjö, J., Ptak, T. and Teutsch, G., 2001. Inversion of concentration time series and field application at the INCORE Strasbourg site. Proceedings of the 1st IMAGE-TRAIN Cluster Meeting, Karlsruhe.

[Bayer-Raich et al., 2001] Bayer-Raich, M., Jarsjö, J. & Ptak, T. (2001) The Immission approach for quantifying contaminant mass fluxes in heterogeneous formations: numerical simulation and discussion of methodology. In: Las Caras del Agua Subterranea, Medina, A., Carrera, J. and Vives, L. (eds.), Instituto Geologico y Minero de España, Madrid, 863-869, ISBN 84-7840-426-0.

[Bayer-Raich et al. 2002b] Bayer-Raich M., Jarsjö J., Ptak T. & Holder T. (2002) Numerical estimations of contaminant mass flow rate based on concentration measurements in pumping wells. Calibration and Reliability in Groundwater Modelling: A Few Steps Closer to Reality (Proceedings of Modelcare'2002. Prague, Czech Republic, June 2002). IAHS Publ. no. 277, 2002.

[Bear, 1979] Bear, J. (1979). Hydraulics of Groundwater. McGraw-Hill International Book Company, 567 pp..

[Bear & Jacobs, 1965] Bear, J., and Jacobs, M., On the movement of water bodies injected into aquifers, *J. Hydrol.*, 3, 37-57, 1965.

[Béland-Pelletier et al. (2001)] Béland-Pelletier, C., Barker, J. F., Bockelmann, A. and Ptak, T., 2001. Evaluation of two techniques to estimate the mass flux of contaminants in groundwater. Joint Can. Geotech. Soc./Internat. Assoc. Hydrogeologists Conference, Calgary, AB, Sept. 16-19, 2001.

[Bockelmann et al., 2001] Bockelmann, A., Ptak, T. and Teutsch, G., 2001. An analytical quantification of mass fluxes and natural attenuation rate constants at a former gasworks site. *Journal of Contaminant Hydrology*, 53(3-4): 429-453.

[Bold, 2004] Bold, S. (2004) Process-based prediction of the long-term risk of groundwater pollution by organic non-volatile contaminants. PhD Thesis, Tübingen University.

[Borkert, M., 1999] Borkert, M. (1999): Instationäre mesoskalige hydraulische Modellierung des Standortes SAFIRA. Simulation der Flutung des Tagebaurestlochsystems Goitsche, GFE GmbH Halle, 1999. (in German).

[Carrera & Neuman, 1986a] Carrera, J., Neuman, S.P., 1986a, Estimation of aquifer parameter under transient and steady state conditions : 1. Maximum likelihood method incorporating prior information. *Water Resources Research*, v. 22, 2, p. 199-210.

[Carrera & Neuman, 1986b] Carrera, J., Neuman, S.P., 1986b, Estimation of aquifer parameter under transient and steady state conditions : 2. Uniqueness, stability, and solution algorithms. *Water Resources Research*, v. 22, 2, p. 211-227.

[Carrera & Neuman, 1986c] Carrera, J., Neuman, S.P., 1986c, Estimation of aquifer parameter under transient and steady state conditions : 3. Application to synthetic and field data. *Water Resources Research*, v. 22, 2, p. 228-242.

[Cooper & Jacob, 1946] Cooper, H. H., Jr., and C. E. Jacob (1946) A generalized graphical method for evaluating formation constants and summarizing well-field history, *Eos Trans. AGU*, 27(4), 526-534

[Dagan & Cvetkovic, 1996] Dagan G. & Cvetkovic V.. Reactive transport and immiscible flow in geological media. I. General Theory. *Proc. R. Soc. Lond.* 452, 285-301 (1996)

[EPA OSWER Directive, 1999] EPA, 1999. OSWER Directive: Use of monitored natural attenuation at superfund, RCRA corrective action and underground storage tank sites. Directive number 9200.4-17P. Washington, D.C.

[Finkel, 1999] Finkel, M. (1999). Quantitative Beschreibung des Transports von polyzyklischen aromatischen Kohlenwasserstoffen (PAK) und Tensiden in porösen Medien. PhD Thesis, Tübingen University.

[Frind and Molson, 2002] Frind, E.O. and Molson, J.W. (2002). Well vulnerability mapping: a new approach to wellhead protection. In: *Proceedings, 55th Canadian Geotech. Conference*, Niagara Falls, Oct. 2002.

[Ginn, 2001] Ginn, T. R. Stochastic-convective transport with nonlinear reactions and mixing: Finite streamtube ensemble formulation for multicomponent reaction systems with intra-streamtube dispersion, *J. Contaminant Hydrology*, 47:1-28, 2001.

[Holder et al., 1998] Holder, T., Teutsch, G., Ptak, T., Schwarz, R., (1998). A new approach for source zone characterization: the Neckar Valley study. In: M. Herbert and K. Kovar (Eds.): *GQ'98 Groundwater Quality: Remediation and Protection*. IAHS Publication, 250, 68-71.

[Holder & Teutsch, 1999] Holder, Th. and Teutsch, G., 1999. Prinzip des neuen Immissionsmessverfahrens, Anwendung der Immissionsmessung im Neckartal. In: *Integrale Altlastenerkundung im Stuttgarter Neckartal*, Schriftenreihe des Amtes für Umweltschutz, 4/1999, Stuttgart.

[International Water and Sanitation Centre, 2003] <http://www.irc.nl/>

[Jarsjö et al., 2003] Jarsjö J., Ptak T., Bayer-Raich M. & Holder T. Uncertainties in contaminant plume charectarizations based on concentration measurements in pumping wells: The Stuttgart-Nekartalue site. *ModelCare2002*, 4th International Conference on Calibration and Reliability in Groundwater Modelling, Prague, 17 – 20 June 2002

- [Jarsjö et al., 2004] Jarsjö J., Bayer-Raich M. & Ptak T. Monitoring groundwater contamination and delineating source zones at industrial sites: Uncertainty analyses using integral pump tests. *J. Contam. Hydrol.*, submitted.
- [Jury and Roth, 1990] Jury, W.A., and K. Roth. 1990. Transfer functions and solute transport through soil: Theory and applications. Birkhaeuser Publ., Basel, Switzerland.
- [Karami and Younger, 2002] Karami G.H. and Younger P. L. (2002): Analysing step-drawdown test in heterogeneous aquifers. *Quarterly Journal of Engineering Geology and Hydrogeology*, 35, 295-303.
- [Kolditz, 2001] Kolditz, O., (2001): Computational Methods in Environmental Fluid Mechanics. Springer-Verlag, 406pp.
- [LfU, 1996] Hnadbuch Altlasten und Grunwasserschadensfaelle, Leitfaden Erkundungsstrategie Grunwasser, Zentraler Fachdienst Wasser – Boden – Abfall – Altlasten bei der Landesanstalt fuer Umweltschutz Baden-Wuerttemberg.
- [Maier and Grathwohl, in preparation] Maier, U. and P. Grathwohl (2004). The Size of Steady State Plumes: numerical experiments. *Ground Water* in preparation
- [McDonald & Harbaugh, 1988] McDonald, M. & Harbaugh, W. (1988): MODFLOW – A Modular 3-dimensional Finite-Difference Groundwater Flow Model. – U. S. Geological Survey, 1988.
- [Moragas, 1896] Moragas, G. 1896. Corrientes subálveas, Estudio General sobre el Régimen de las Aguas contenidas en Terrenos Permeables e Influencias que ejercen los Alumbramientos por Galerías o Pozos, y Especial, del Regimen o Corriente Subterránea del Delta Aquifero del Besós. *Anales de la Revista de Obras Públicas*, 133 p.
- [Neupauer and Wilson, 1999] Neupauer R.M. and Wilson, J.L. (1999). Adjoint Method for Obtaining Backward-in-time Location and Travel Probabilities of a Conservative Groundwater Contaminant. *Water Resources Research*, 35(11), 3389-3398.
- [Peter et al., 2004] Peter, A.; Steinbach, A.; Liedl, R.; Ptak, T.; Michaelis, W.; Teutsch, G.: "Assessing microbial degradation of o-xylene at field-scale from the reduction in mass flow rate combined with compound-specific isotope analyses" (accepted for publication in *JCH*)
- [Ptak et al., 2000] Ptak, T., Schwarz, R., Holder, T. and Teutsch, G., 2000. Ein neues integrales Verfahren zur Quantifizierung der Grundwasserimmission: II. Numerische Lösung und Anwendung in Eppelheim, *Grundwasser*, 4(5): 176-183.
- [Ptak et al., 2003] Ptak, T., Alberti, L., Bauer, S., Bayer-Raich, M., Ceccon, S., Elsass, P., Holder, T., Kolesar, Ch., Müller, D., Padovani, C., Rinck, G., Schäfer, G., Tanda, M., Teutsch, G., Zanini, A., 2003. Integral investigation of groundwater quality. In: *Integrated Concept for Groundwater Remediation – INCORE. Final Report on CD-ROM*. UW Umweltwirtschaft Stuttgart, May 2003, ISBN 3-00-0111706-7.
- [Polyanin & Manzhirov, 1998] Polyanin A. D. & Manzhirov A. V. Handbook of integral equations CRC Press, Boca Raton, 1998.

[Pollock, 1994] Pollock, D.W. (1994), User's Guide for MODPATH/MODPATH-PLOT, Version 3: A particle tracking post-processing package for MODFLOW, the U.S. Geological Survey finite- difference ground-water flow model: U.S. Geological Survey

[Porter & Stirling, (1990)] David Porter and David S. G. Stirling, *Integral Equations*, Cambridge University Press, 1990

[Rivett et al., 2001] Rivett, M., Feenstra, S., Cherry, J., 2001. A controlled field experiment on groundwater contamination by a multicomponent DNAPL: creation of the emplaced-source and overview of dissolved plume development. *Journal of Contaminant Hydrology* 49 2001 111–149

[Schwarz, 2002] Schwarz, R., 2002. Grundwasser-Gefährdungsabschätzung durch Emissions- und Immissionsmessungen an Deponien und Altlasten. PhD-Thesis, Center of Applied Geosciences, University of Tübingen.

[Schwarz et al., 1997] Schwarz, R., Ptak, T., and Teutsch, G., Grundwasser-Gefährdungsabschätzung durch Emissions- und Immissionsmessungen an Deponien und Altlasten: Numerische Untersuchungen zur Anwendung und Auswertung. Report, PWAB Baden-Württemberg, Project-Nr. PD 96 181, Center of Applied Geosciences, University of Tübingen.

[Schwarz et al., 1998] Schwarz, R., Ptak, T., Holder, T., Teutsch, G., 1998. Groundwater risk assessment at contaminated sites: A new investigation approach. In: M. Herbert and K. Kovar (Eds.): *GQ'98 Groundwater Quality: Remediation and Protection*. IAHS Publication, 250, 68-71.

[Teutsch et al., 2000] Teutsch, G., Ptak, T., Schwarz, R. and Holder, T., 2000. Ein neues integrales Verfahren zur Quantifizierung der Grundwasserimmission: I. Beschreibung der Grundlagen. *Grundwasser*, 4(5): 170-175.

[Teutsch et al., 2000] Teutsch, G., Ptak, T., Schwarz, R. and Holder, T., 2000. Ein neues integrales Verfahren zur Quantifizierung der Grundwasserimmission: I. Beschreibung der Grundlagen. *Grundwasser*, 4(5): 170-175.

[Thiem, G. 1906] *Hydrologische Methoden*. Gebhardt, Leipzig, 1906, 56 pages.

[Tikhonov & Arsenin, 1977] Tikhonov A.N. & Arsenin, V. Y. (1977) *Solutions of Ill-Posed Problems*, Scripta Series in Mathematics, John Wiley & Sons, New York.

[Tunturi, 2003] Tunturi, Miikka. Quantification of groundwater contamination at field scale in heterogeneous aquifers considering parameter uncertainty. MsC Thesis, Center for applied Geosciences. Tübingen University.

[United Nations Environment Programme, 2002] <http://www.unep.org>

[Van Leeuwen et al., 1998] Van Leeuwen, M., te Stroet, C.B.M, Butler, A.P. and Tompkins, J.A. (1998). Stochastic determination of well capture zones. *Water Resources Research*, 34(9), 2215-2224.

[Van Leeuwen et al., 2000] Van Leeuwen, M., Butler, A.P., te Stroet, C.B.M, and Tompkins, J.A. (2000). Stochastic determination of well capture zones conditioned on regular grids of transmissivity measurements. *Water Resources Research*, 34(9), 2215-2224.

[Vasco-D.W.; Karasaki-K., 2001] Vasco-D.W.; Karasaki-K., (2001). Inversion of pressure observations: An integral formulation. *Journal of Hydrology*. 253(1-4): 27-40

[Volterra, 1894] Volterra, 1894. *Esercizi di fisica matematica*. "Rivista di Matematica", vol IV, 1894 pp.1-14.

[Zheng, C., 1990] Zheng, C. (1990). MT3D, A modular three-dimensional transport model for simulation of advection, dispersion and chemical reactions of contaminants in groundwater systems, Report to the U.S. Environmental Protection Agency, 170 p.

Lebenslauf

Martí Bayer-Raich

Born on 14-3-1973 in Barcelona

University studies

Sep. 1992- Sep. 1995	Bachelor's Degree in Mining Engineering. Universitat Politecnica de Catalunya (UPC)
Sep. 1995- Feb. 1999	Master's Degree in Geological Engineering. Universitat Politecnica de Catalunya (UPC) and Universitat de Barcelona (UB)
Apr. 2000- Apr. 2004	Promotion auf Zentrum für Angewandte Geowissenschaften Eberhard-Karls-Universität, Tübingen